Charles University in Prague

Faculty of Science

Biomedicine PhD Study Programmes

Molecular and Cellular Biology, Genetics and Virology

Mgr. Vendula Strádalová

STRUCTURAL AND FUNCTIONAL CHARACTERIZATION OF YEAST PLASMA MEMBRANE DOMAINS

PhD Thesis

Supervisor: **RNDr. Jan Malínský, PhD**

Institute of Experimental Medicine

Academy of Sciences of the Czech Republic

Prague, 2012

I declare that all sources and literature are properly cited and that the entire contents of this thesis or its major part was not previously utilized for obtaining of the same or other academic degree.

Prague, 11.05.2012 Vendula Strádalová

I confirm that the contribution of Vendula Strádalová to the presented results, as stated in chapter 4.3., is true.

Prague, 11.05.2012 RNDr. Jan Malínský, PhD, supervisor

Acknowledgements / Poděkování

I am very grateful to my supervisor Jan Malínský for all his enthusiasm, generous support, shared knowledge and wisdom and for creation of a pleasant atmosphere in the laboratory. I also greatly appreciate the excellent biophysical cooperation of my nice colleague Míša Blažíková. My many thanks next belong to Mirka Opekarová for her perfect biochemical guidance and to Guido Grossmann for plenty of his useful and ready advice. I am also glad that I had the opportunity to meet Prof. Widmar Tanner and to spend at least some time in his laboratory.

I am further very much obliged to Petra Veselá and Lenka Hlavínová for their excellent technical help with endless optimization of immunogold labeling and image evaluation. I am equally thankful to Ingrid Fuchs for her willing assistance during my stay in Regensburg.

I would also like to thank Prof. Pavel Hozák for giving me the opportunity to learn the high pressure freezing technique in his laboratory. And I do not want to miss the chance to thank Katka Gaplovská-Kyselá for the pleasant time we spent together during the HPF protocol establishment.

Můj velký dík pak v neposlední řadě patří mým milým rodičům, kteří mě podporovali a podporují na cestě, kterou jsem si zvolila, i když jim určitě mnohdy není jasné, čím se to vlastně zabývám a jaký je smysl mého počínání. Martinovi děkuji za psychickou podporu i rozptylování během sepisování tohoto díla vyprávěním pohádky o zmačkaných buňkách, proteinu, který Pil, vlastnil BAR, a kamarádil se s proteinem, co bral Lsd(p).

Contents

ABSTRACT

Plasma membrane (PM) of living cells hosts variety of important cellular functions that must be precisely coordinated in space and time. Recent research shows that the plasma membrane is organized into specific domains to accomplish all these tasks. Our laboratory is focused on the organization of the plasma membrane in *Saccharomyces cerevisiae* where several distinct lateral compartments were identified at the fluorescence microscopy level. One of them is the Membrane Compartment occupied by arginine transporter Can1 (MCC) which consists of isolated, highly stable, ergosterol enriched, 300nm patches containing specific proton symporters and proteins of unknown function (Sur7- and Nce102-like). These membrane domains are organized by cytosolic protein complexes called eisosomes, composed mainly of proteins Pil1 and Lsp1.

This work is a continuation of studies that tried to elucidate the composition, structure and function of MCC. In the first section of this work we concentrated on ultrastructural characterization of MCC domains. Foremost, we developed a protocol preserving the plasma membrane ultrastructure. The comparison of cryofixed and chemically crosslinked cells clearly showed that cryofixation by high pressure freezing together with freeze substitution and low temperature resin embedding leads to superior sample structure preservation and significantly increased labeling density as compared to conventional aldehyde fixation. We took advantage of these findings in the main part of the thesis that proved that MCC domains correspond to furrow-like plasma membrane invaginations, reported by freeze fracture studies in early sixties. We showed that the plasma membranes of *nce102Δ* and *pil1Δ* strains, defective in segregation of MCC-specific proteins, lacked the characteristic furrow-like invaginations. Conversely, mutants exhibiting elongated MCC patches in confocal microscope possessed accordingly elongated invaginations under electron microscope. And last but not least, the immunolocalization of Sur7-GFP and Pil1-GFP proteins on ultrathin resin sections confirmed the localization of both markers to furrow-like invaginations.

We showed that Nce102p is an important MCC constituent. Therefore, we next focused on the elucidation of its role in MCC formation. Determination of the Nce102p membrane topology suggested that this protein does not span the membrane four times as predicted but that it rather adopts a hairpin conformation which could contribute to furrow formation. We also demonstrated that close and distant Nce102 homologs can substitute this protein in tethering Can1p to MCC and concluded that the function of Nce102-like proteins was conserved in *Ascomycota*. Our data suggested that the C-terminus is necessary for the Nce102p function.

The last part of this work was stimulated by our observations that MCC does not colocalize with the cortical ER network occupying a substantial part of the plasma membrane in yeast. We showed that the deletion of the main MCC organizer, Pil1p, leads to an aberrant redistribution of cortical ER network. As we also found that cortical ER redirects the vesicular transport into distinct, ER-free, plasma membrane areas it is obvious that: 1) cortical ER contributes to a functional compartmentalization of the yeast plasma membrane and 2) MCC is also involved in this functional partitioning of the plasma membrane.

In summary, this work has brought new crucial details on the organization of the plasma membrane in budding yeast, with apparent general consequences for other organisms. We ascribed a specific structure to MCC domain which helped to clarify its unusual stability and led to a discovery of eisosome structure. The analysis of Nce102p then suggested how this protein directly affects MCC formation and shaping. And the investigation of cortical ER network showed that its distribution beneath PM is regulated by MCC presence and that this organelle is involved in positioning of various dynamic processes in PM.

ABSTRAKT

Plazmatická membrána (PM) všech buněk hostí celou řadu důležitých buněčných funkcí. Tyto funkce musí být pečlivě koordinovány, a jak současný výzkum ukazuje, plazmatická membrána je za tímto účelem uspořádána do specializovaných domén. Naše laboratoř se zabývá výzkumem způsobu organizace plazmatické membrány u kvasinky pivní, kde bylo za použití fluorescenční mikroskopie popsáno několik nepřekrývajících se domén. Jednou takovou doménou je MCC (*Membrane Compartment occupied by transporter Can1*), která je tvořena stabilními izolovanými oblastmi PM o velikosti asi 300 nm. MCC domény obsahují několik přenašečů a proteinů o neznámé funkci (proteiny příbuzné Sur7 a Nce102) a jejich formování je organizováno z cytosolu proteinovými komplexy zvanými eisosomy, jež jsou tvořeny především proteiny Pil1 a Lsp1.

Tato práce navazuje na studie, které měly za cíl objasnit složení, strukturu a funkci MCC. V první části práce jsme se zaměřili na ultrastrukturální analýzu MCC, přičemž jsme nejdříve vyvinuli protokol pro transmisní elektronovou mikroskopii (TEM), který dobře zachovává strukturu PM. Zjistili jsme, že mrazová fixace pomocí vysokotlakého zamražení, kombinovaná s mrazovou substitucí a zalitím vzorku do pryskyřice za nízké teploty, vede k výrazně lepšímu zachování buněčné struktury a vyššímu signálu při imunoznačení než při použití chemických fixativ. Tyto poznatky jsme využili v hlavní části práce, která prokázala, že MCC domény odpovídají žlábkovým invaginacím v plazmatické membráně kvasinek, tedy strukturám pozorovaným již před téměř 50 lety pomocí mrazového lámání. My jsme ukázali, že kmeny *nce102Δ* a *pil1Δ*, ve kterých jsou MCC domény poškozené či chybí, tyto žlábkové invaginace postrádají. A naopak, kmen *mak3Δ*, ve kterém jsme pozorovali abnormálně prodloužené MCC domény, měl odpovídajícím způsobem prodloužené žlábkové invaginace. Detekce proteinů Sur7 a Pil1 pomocí protilátek pro TEM pak jednoznačně prokázala lokalizaci obou proteinů do oblastí žlábkových invaginací.

Jelikož jsme ukázali, že protein Nce102 je důležitý regulátor MCC domén, zaměřili jsme se dále na objasnění jeho role v upořádání MCC. Naše analýza nepotvrdila předpoklad, že Nce102 vlastní 4 transmembránové domény, ale spíše ukázala, že Nce102 zaujímá v membráně konformaci tzv. vlásenky (*hairpin*). Toto uspořádání by mohlo pomoci objasnit způsob zapojení Nce102 do tvorby žlábkové invaginace. Ukázali jsme rovněž, že blízcí i vzdálení příbuzní proteinu Nce102 mohou zastoupit Nce102 v jeho roli při umisťování proteinu Can1 do MCC, což nás vedlo k závěru, že proteiny podobné Nce102 mají pravděpodobně stejnou funkci u všech druhů v kmeni *Ascomycota*.

Poslední část této disertační práce byla inspirovaná naším pozorováním, že MCC se nepřekrývá s hustou sítí kortikálního ER, jež se rozprostírá v těsné blízkosti plazmatické membrány. Delece Pil1, hlavního organizátoru MCC/eisosome, vedla k abnormálnímu rozmístění kortikálního ER pod membránou. Jelikož jsme zároveň zjistili, že kortikální ER přesměrovává vezikulární transport do oblastí plazmatické membrány nepokryté ER, je jasné, že: 1) kortikální ER přispívá k funkční organizaci plazmatické membrány a 2) MCC se tohoto funkčního rozdělení PM také účastní díky svému vlivu na distribuci kortikálního ER.

V souhrnu tato práce odkryla další podstatné detaily uspořádání plazmatické membrány kvasinek. Ukázali jsme, že MCC zaujímá specifickou trojrozměrnou strukturu, což pomohlo vysvětlit neobvyklou stabilitu této domény a zároveň vedlo k objasnění struktury eisosomu. Analýza Nce102 pak odhalila způsob, kterým tento protein může přispívat k formování MCC. A v neposlední řadě jsme ukázali, že MCC ovlivňuje rozprostření kortikálního ER pod membránou, což má vliv i na rozmístění dynamických procesů v plazmatické membráně.

LIST OF ABBREVIATIONS

ANTH	Ap180-N- terminal-homology
BAR	Bin-amphiphysin-Rvs
CIE	clathrin independent endocytosis
CME	clathrin mediated endocytosis
CW	cell wall
DRM	detergent resistant membrane
ENTH	epsin-N-terminal-homology
ER	endoplasmic reticulum
ERMES	ER-mitochondria encounter structures
FF	freeze fracture
FS	freeze substitution
GPI	glycosyl-phosphatidyl-inositol
HPF	high pressure freezing
L_d	liquid disordered
L_o	liquid ordered
MCC	membrane compartment occupied by Can1
MCP	membrane compartment occupied by Pma1
MCS	membrane contact site
MCT	membrane compartment of TORC2
PC	phosphatidylcholine
PCR	polymerase chain reaction
PE	phosphatidylethanolamine
PH	plekstrin homology
PI	phosphatidylinositol
$PI(4,5)P_2$	phosphatidyl- inositol-4,5-bis-phosphate
PM	plasma membrane
PS	phosphatidylserine
PSF	point spread function
SNARE	N-ethylmaleimide-sensitive factor attachment protein receptor
SM	sphingomyelin
S_o	solid-ordered, gel
TEM	transmission electron microscopy
TM	transmembrane
TMD	transmembrane domain
TORC2	target of rapamycin complex 2
WT	wild type

1. GENERAL INTRODUCTION

1.1. STRUCTURE AND FUNCTION OF PLASMA MEMBRANE

Plasma membrane (PM) is an important organelle that separates the internal cellular components from the surroundings. It is far from being a simple semi-permeable physical barrier as it dynamically regulates what is transported into and out from the cell and maintains the communication of the cell with the external medium. In eukaryotes, additional membranes compartmentalize also the intracellular space by forming various organelles that segregate specific chemical reactions and regulate the distribution of their products. To coordinate and serve all the cellular functions in various situations, all membranes need to be precisely organized in space and time.

Biological membranes are heterogeneous assemblies of lipids and proteins. The basic membrane structure is determined by amphipatic lipids that spontaneously selfassemble to form bilayers with their hydrophilic parts exposed to the water environment and hydrophobic chains hidden inside the bilayer (see Figures 2 and 3). The first complex model of cellular membranes that became accepted by a wide scientific community was developed by Singer and Nicolson in 1972. It described the lipid bilayer as a two-dimensional fluid matrix in which the embedded or attached proteins are arranged randomly and move freely (Singer & Nicolson, 1972). Further research then showed that both lipidic and preoteinaceous membrane components are not distributed randomly and that the membranes are compartmentalized laterally and also vertically and this order is actively maintained by the cell.

1.1.1. Membrane lipids

Based on the Singer and Nicolson model, the lipidic component was overlooked for some time as a simple fluid solvent in which the proteins perform their functions and the research concentrated more to membrane proteins. However, cellular membranes contain much more lipid species than it is necessary for a bilayer formation. Eukaryotic cells produce thousands of different lipids (Sud et al, 2007) which must have some functional relevance but this has not been clarified so far. Recent advances in mass spectrometry could help to solve this issue as new techniques allow analyzing the lipidomes from small amount of samples and

are able to identify the individual lipid species, not only the lipid classes (Ejsing et al, 2009; Shevchenko & Simons, 2010).

There are three main structural lipid classes in eukaryotic membranes: glycerophospholipids, sphingolipids, and sterols (Figure 1). Glycerolipids are composed from glycerol linked to two fatty acids of various lengths and one phosphate that can bear different hydrophilic head groups like choline (phosphatidycholine, PC), ethanolamine (phosphatidylethanolamine, PE), serine (phosphatidylserine, PS) or inositol (phosphatidylinositol, PI). One or both of the fatty acyl chains in glycerophospholipids are usually cis-unsaturated which causes kink(s) in the hydrophobic parts of the lipid molecules. Sphingolipids are composed of a C18 sphingoid base with an amide-linked C16-26 fatty acid, which together form a ceramide. The hydrophobic tails are usually longer than those at glycerolipids and they are saturated or trans-unsaturated (i.e. straight), so that sphingolipids are able to pack more densely in the membrane. Many of the sphingolipid species are glycosylated (glycosphingolipids), their head group can also be a phosphocholine (sphingomyelin, SM, in mammals) or phosphoinositol (inositolphosphorylceramide, IPC, in yeast). Sterols are planar non-polar lipids whose structure is composed of four rings. The main membrane sterol in mammalian cells is cholesterol, whereas yeast use ergosterol (Holthuis & Levine, 2005; van Meer et al, 2008).

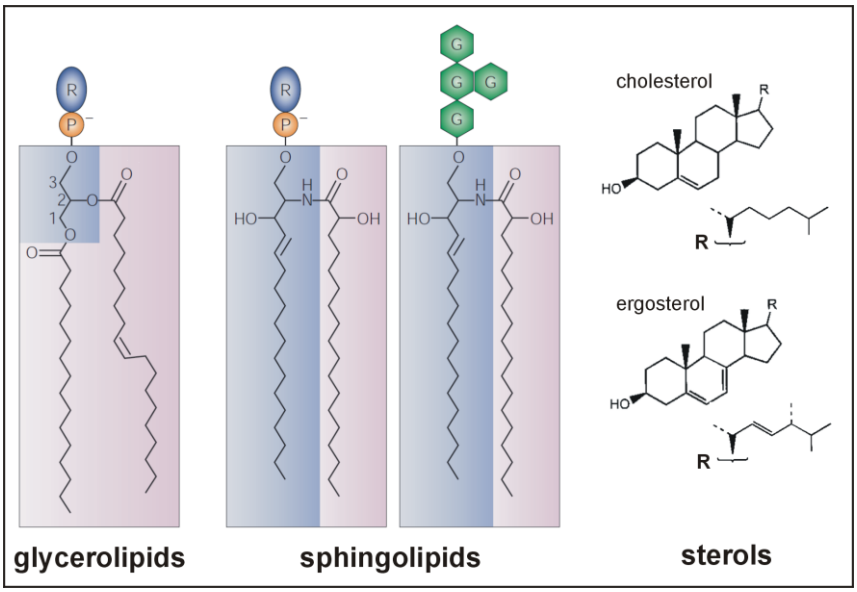

Figure 1. Three main lipid classes in eukaryotic membranes.

Basic chemical structure of glycerophospholipids, sphingolipids and sterols is depicted. The glycerol backbone in glycerolipids (left) and sphingosine in sphingolipids (middle) are highlighted in blue. The main sterols of mammalian (cholesterol) and yeast (ergosterol) membranes are shown. P^-: phosphate, R: head group, G: saccharide.

Image adapted from Holthuis & Levine (2005) and Xu et al (2001)

The different lipid species are not distributed homogenously throughout the cellular organelles. The endoplasmic reticulum (ER) which is the main lipid biosynthesizing organelle in the cell contains very low amounts of sterols and sphingolipids even though it significantly contributes to their synthesis. Sterols and sphingolipids, whose biosynthesis continues in Golgi, are predominantly designated to travel to plasma membrane. Trans-Golgi and plasma membrane are thus specifically enriched in these two lipid classes. The production of sphingolipids in Golgi system can help to sort membrane proteins and the higher packing density of these two lipid species probably contributes to the plasma membrane rigidity and resistance to various stresses (van Meer et al, 2008). In addition, even the distribution of lipid species between the two membrane leaflets of Golgi, plasma membrane and endosomal compartments is asymmetric. This transbilayer lipid asymmetry is actively maintained so that sphingolipids and highly glycosylated lipids are accumulated in extracellular/luminal membrane leaflet whereas PS, PE and PI and its phosphorylated variants are enriched in cytosolic leaflet (Figure 2). Sterols are present in both leaflets of the PM but due to their supposed preferential packing with sphingolipids they are probably more enriched in the exoplasmic membrane leaflet (Holthuis & Levine, 2005; van Meer et al, 2008; Kiessling et al, 2009).

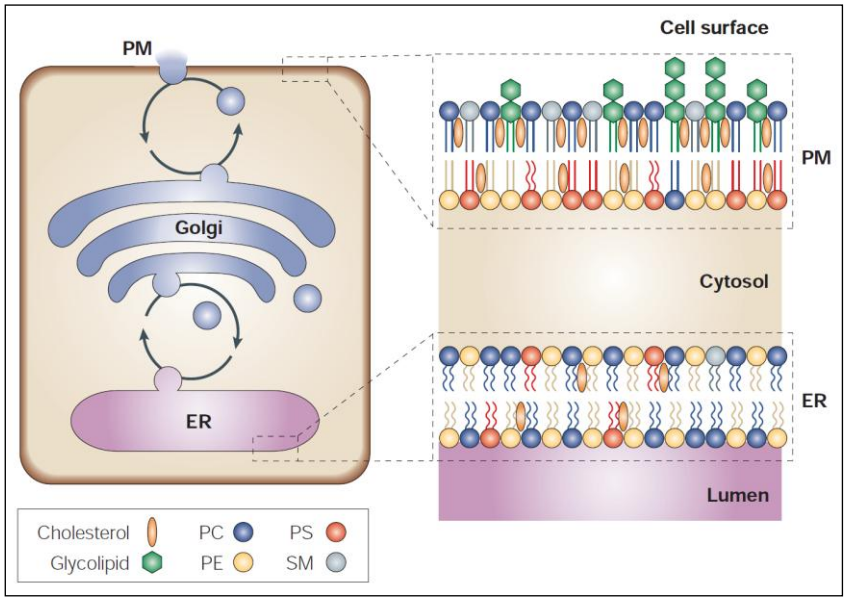

Figure 2. Asymmetric lipid distribution.

Plasma membrane is rich in sterols, sphingolipids and saturated glycerolipids. It has also an asymmetric transbilayer lipid arrangement with sphingolipids enriched in exoplasmic leaflet and aminophospholipids in inner leaflet. ER membrane is specifically enriched in unsaturated glycerolipids and shows a symmetric lipid distribution. Reproduced from Holthuis & Levine (2005).

1.1.2. Membrane proteins – molecular crowding in membrane planes

The extensive study of the membrane protein palette showed that there is a huge variability of membrane protein structure. Proteins can be either integral to the membrane or associated with the membrane via various lipidic anchors. Integral membrane proteins are either spanning the lipid bilayer completely with their transmembrane domains (Rapoport et al, 2004) or they are only partially embedded within the lipid bilayer forming there a so called "hairpin loop" (Bauer & Pelkmans, 2006). Numerous cytosolic proteins can be also posttranslationally modified with a great variety of lipophilic moieties for example with glycosylphosphatidylinositol (GPI) anchor (Paulick & Bertozzi, 2008) that brings the modified proteins into the exoplasmic PM leaflet and/or with various fatty acids (myristoylation, palmitoylation), or isoprenoids (farnesylation) that ensure the association of the proteins with cytosolic membrane leaflet (Resh, 2006; Aicart-Ramos et al, 2011). The Singer and Nicolson view of the membrane supposed that apart from being distributed randomly as monomers, the membrane proteins were not very abundant in the lipid matrix and did not extend much beyond the lipid bilayer. Further research then showed that the opposite is the truth – membranes are very crowded with proteins and lots of them can possess large ectodomains covering a substantial part of the membrane surface (especially GPI and acylated proteins) (Figure 3). This fact and the notion that proteins usually tend to function in oligomerized state led to a modified concept of a membrane being more mosaic than fluid (Engelman, 2005). Measurements of protein-lipid ratio in the plasma membrane revealed that transmembrane domains can occupy about 30% of the membrane area (Dupuy & Engelman, 2008). Other transmembrane protein density estimations calculated the number of some membrane proteins to be about 30,000 molecules per μm (Jacobson et al, 2007). In addition, many cytosolic proteins

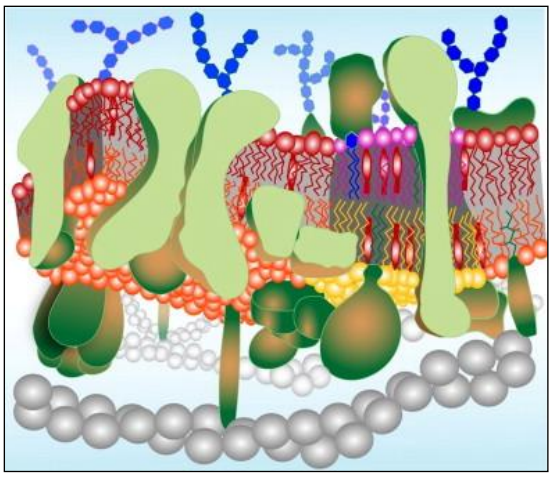

Figure 3.
Protein crowding in cellular membranes.

Visualization of plasma membrane: lipids of outer leaflet are in purple and red, lipids of inner leaflet are shown in orange and yellow, embedded or anchored proteins are depicted in green. Blue hexagons represent glycosylation and gray beads symbolize cytoskeleton. Reproduced from Kiessling et al (2009).

can be associated with membranes based on their affinity towards membrane lipids or membrane proteins. It is thus clear that there is not much space left for the unperturbed lipid area in the biological membranes and that the membranes might be less fluid and more rigid.

1.1.3. Interactions between membrane constituents

1.1.3.1. Phase separation of lipids

Apart from the asymmetric transbilayer and interorganelle distribution of lipids in biological membranes lateral lipid heterogeneity has been also described, at least in model membranes which helped to clarify some characteristic features of lipid phase behavior. Lipids can adopt different phases, mainly according to the temperature, that are characterized by a certain order of the lipid acyl chains. In gel or solid ordered (S_o) phase the lipid chains are highly ordered and tightly packed, whereas in the liquid (L) phase the chain order is lower and lipids can move more freely in the membrane plane. Cholesterol appeared to be a very important regulator of lipid phase behavior. When cholesterol or its analog is present at an adequate concentration, two types of liquid phases can coexist in the membrane – liquid disordered (L_d; cholesterol poor) and liquid ordered (L_o; cholesterol enriched). The L_o phase is based on the ability of the flat and rigid cholesterol molecule to impose a more ordered and straight conformation on the adjacent phospholipid chains without reducing drastically their lateral mobility (Ipsen et al, 1987) (Figure 4). Cholesterol preferentially interacts with lipids that have saturated acyl chains. This is the reason why it interacts more favorably with sphingolipids that possess rather long and saturated aliphatic chains. Thus, in complex lipid mixtures the L_o phase is preferentially formed from cholesterol together with sphingolipids or fully saturated phospholipids (Simons & Vaz, 2004). The coexistence of L_o and L_d phases has been documented in lipid mixtures mimicking the composition of the outer plasma membrane leaflet or in lipid mixture extracted from real plasma membrane and under certain conditions the different separated domains were also resolvable

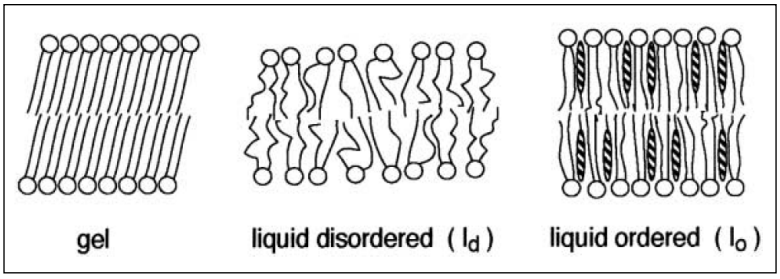

Figure 4. Lipid phases. Lipids below their melting temperature (T_m) form a solidified gel phase. At temperatures above T_m, lipids are present in a liquid disordered state. In the presence of cholesterol (hatched ovals) the liquid ordered phase can be formed. Reproduced from Munro (2003).

under the light microscope (Simons & Vaz, 2004). The model membrane systems simulating the asymmetric distribution of lipids between the two plasma membrane leaflets also showed that the ordered domains formed in the outer leaflet can induce formation of ordered domains in the inner leaflet (Kiessling et al, 2009).

1.1.3.2. Contribution of proteins to membrane structure

In contrast to model systems, cellular membranes are never at equilibrium, they are very complex and dynamic and even more importantly, they contain a great amount of proteins. Proteins in the membranes bring another level of complexity to the whole system and it is therefore still not clear whether the real L_o phase exists in the plasma membrane containing proteins (Bagatolli et al, 2010; Mouritsen, 2010).

Most proteins exhibit numerous specific protein-protein interactions that drive self-organization of functional clusters. This plausible protein-driven biological mechanism is also involved in membrane organization, though the principles underlying the formation of most membrane protein clusters are largely unknown. Nice examples are proteins from a large family of tetraspanins that regulate formation of a great palette of specific membrane microdomains via numerous combinations of homophilic and heterophilic protein interactions (Levy & Shoham, 2005; Yanez-Mo et al, 2009). Syntaxins were also shown to selforganize into functional clusters in the membrane via homophilic interactions of their SNARE motifs. These interactions caused tight packing of the syntaxin1 molecules that restricted the mobility of the resulting clusters and also sterically regulated their size (Sieber et al, 2007). Such mechanism could represent a more general principle of the membrane domain formation.

It is evident that membrane proteins interact with lipids and affect their movement/diffusion and behavior. The membrane spanning surface of intrinsic membrane proteins is surrounded by a lipid shell with restricted mobility that is called lipid annulus. Apart from the relatively non-specific protein-annular lipid interactions there were described also some “hot-spots” on the membrane proteins where certain lipids bind with higher specificities (Lee, 2011). Atomistic molecular dynamic simulations also showed that membrane proteins diffuse together with numerous lipids surrounding them regardless whether they are associated with the lipids specifically or not (Niemela et al, 2010). Lipids are important for incorporation of membrane proteins into the lipid bilayer and participate on their folding and function, too. Lipids are found specifically incorporated between the

transmembrane α-helices or at protein-protein interfaces in oligomerized protein complexes. Some proteins might even require specific interactions with certain lipids as cofactors to perform their functions (Lee, 2011). Moreover, a great variety of lipid-binding motifs exists in various cytosolic proteins that can further modify the organization of membranes. Well known examples of such domains are PH (pleckstrin homology) and ENTH/ANTH (epsin/AP180 N-terminal homology) domains that bind phosphoinositides or BAR (Bin-amphiphysin-Rvs) domains that interact with acidic lipids in the membranes (Lemmon, 2008) (Figure 5). It is thus clear that lipids and proteins both cooperate on membrane lateral heterogeneity and must be studied together.

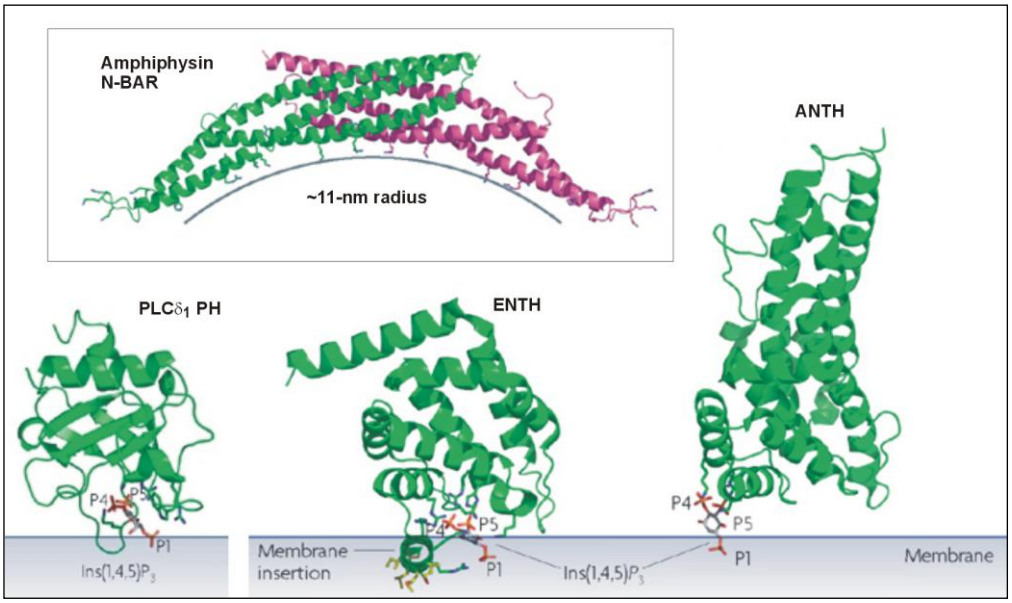

Figure 5. Structures of selected lipid binding (protein) domains. Pleckstrin homology (PH) domain of phospholipase Cδ1 (PLCδ$_1$), ANTH and ENTH domains of AP180/CALM and epsin (respectively) are examples of protein motifs binding phosphorylated inositides in the membrane. BAR domain family members can sense or promote membrane curvature; one BAR dimer of *Drosophila melanogaster* amphiphysin is shown. Adapted from Lemmon (2008).

1.1.4 Membrane architecture – models of plasma membrane organization

In the last 15 years, the research of the plasma membrane has been dominated by a so called "lipid raft" hypothesis which revitalized the role of lipids in the membrane lateral organization. This hypothesis tried to explain findings that epithelial cells are polarized with apical part of the plasma membrane being highly enriched in sphingolipids if compared to the basolateral membrane (Simons & van Meer, 1988). The original concept of lipid raft

hypothesis, postulated by Simons and Ikonen in 1997, suggested that the preferential packing of sphingolipids and cholesterol helped to sort proteins in the Golgi as the two lipid species formed specific L_o platforms, "rafts", which then floated in the L_d lipid plane in the exoplasmic leaflet of the PM (Simons & Ikonen, 1997). They supposed that certain proteins could be specifically attracted to the rafts while others were excluded and that this would help to organize the functional heterogeneity of the plasma membrane. The fact that sphingolipids and sterols are resistant to extraction by non-ionic detergents (like Triton X-100) at 4°C and that some proteins can follow this detergent insoluble lipid moiety into low-density fraction during sucrose gradient centrifugation (Brown & Rose, 1992) led to a hunting for "raft" proteins based on their presence in detergent resistant membrane (DRM) fraction. Lipid rafts were postulated to be involved in organization of caveolae, signaling complexes, endocytosis and sorting and trafficking in secretory pathway (Brown & London, 1998). The inaccurate biochemical definition of lipid rafts together with the protocol variations, involvement of different detergents and impossibility to observe rafts under microscope, however, caused a big confusion in the field. The existence of rafts started to be questioned and criticized and it continuously became clear that detergent resistance does not reflect the real arrangement of lipids and proteins in the plasma membrane (Munro, 2003; Shaw, 2006; Mishra & Joshi, 2007). The only unifying fact about lipid rafts was their postulated relative enrichment in sterols and sphingolipids. The recent view of lipid rafts, based on modern super-resolution microscopy techniques (Eggeling et al, 2009; He & Marguet, 2011), is that they represent dynamic, short-lived (tens of ms) nanodomains (< 20 nm) heterogeneous in protein composition, that can merge and be stabilized into larger raft platforms by lipid-protein and protein-protein interactions upon some specific stimuli. This sphingolipid-cholesterol potential to aggregate was postulated to form an important "lipid raft connectivity" in the plasma membrane that can be regulated by protein specificities (Lingwood & Simons, 2010).

The raft existence, however, has never been unequivocally proven and rafts have not been isolated so far. The major skepticism about lipid rafts stems mainly from their vaguely defined size, composition and lifetime criteria and from the passive way by which the lipids should induce order in the plasma membrane giving too little space for proteins (Leslie, 2011). The lipid connectivity of sphingolipid-sterol nanoassemblies *per se* cannot explain the formation of all observed plasma membrane domains. The extent of protein-protein and lipid-protein interactions involved in membrane domains formation was not yet clarified enough but as already mentioned in the previous chapter, it is evident that some membrane domain

types like tetraspanin enriched microdomains or syntaxin clusters are highly reliant on protein-protein interactions (Sieber et al, 2007; Yanez-Mo et al, 2009). Also the formation of signaling clusters is driven to a high extent by protein specificities and interactions with actin cytoskeleton (Hartman & Groves, 2011).

Other organizing principles have been already shown to be also involved in the functional lateral compartmentalization of the plasma membrane. Diverse plasma membrane domains are organized from cytosol by recruited factors, like fences or scaffolds. It was shown that the whole plasma membrane is associated with various types of cytoskeleton subdividing the membrane like a fence into domains in which proteins and lipids are transiently confined. Some transmembrane proteins probably interact with the skeleton, temporally aligning along the filaments and impeding the free diffusion of other molecules in both leaflets like pickets (Kusumi et al, 2010; Kusumi et al, 2011). Apart from this cytoskeleton-based fence model other types of fences can be distinguished that restrict diffusion in the plasma membrane. Well known examples of such membrane barriers are septin GTPases that can be found in yeast bud necks (Oh & Bi, 2011), at the base of primary cilia (Hu et al, 2010) and at the branch-points in dendrites (Tada et al, 2007) or tight junctions which separate the apical and basolateral parts of the plasma membrane in epithelial cells (Furuse, 2010).

Distinct types of membrane domains can be generated by an action of specific proteins that interact with certain lipids or proteins in the membrane, assemble into a scaffold and organize specifically the associated membrane region. Examples of such domains can be caveolae that are organized by a cholesterol-interacting protein caveolin (Parton et al, 2006; Parton & Simons, 2007) or endocytic clathrin coated pits that are generated by a coordinated action of adaptor proteins and clathrin molecules (see chapter 1.3.). Main known mechanisms involved in membrane compartmentalization are summarized in Figure 6.

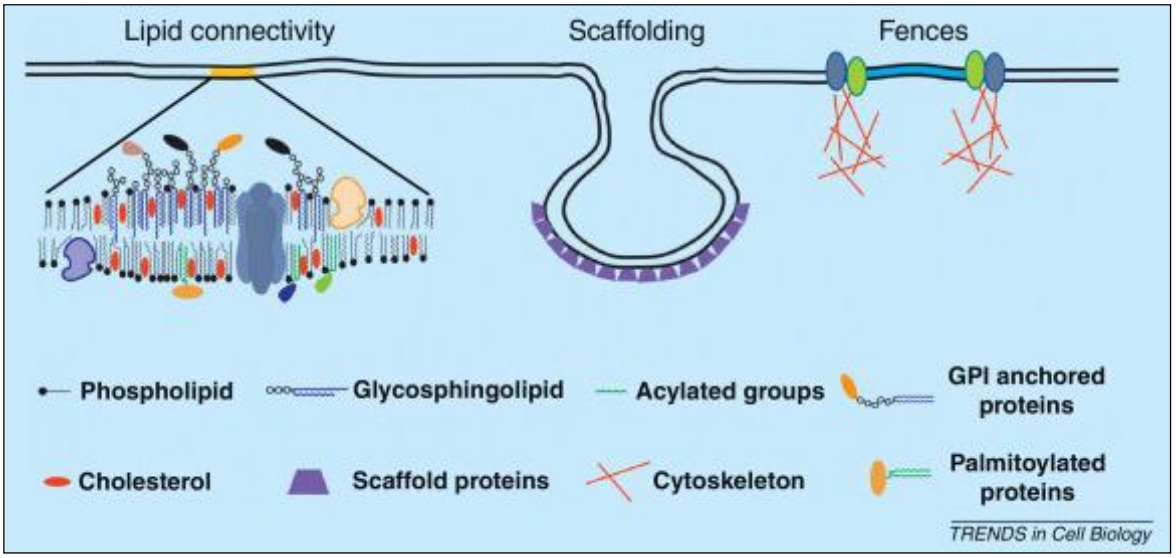

Figure 6. Principles involved in lateral organization of plasma membrane: Lipid connectivity of sterol-sphingolipid assemblage potential; protein scaffolds organizing associated membrane areas; and protein fences defining domains with restricted movement of membrane components. Reproduced from Ziolkowska et al (2012).

1.2. YEAST PLASMA MEMBRANE

The yeast plasma membrane is different from the mammalian one. It is more rigid (Valdez-Taubas & Pelham, 2003) probably due to a higher sterol and sphingolipid contents (Ejsing et al, 2009). The main yeast sterol is ergosterol which was also shown to be able to phase separate with saturated lipids (Xu et al, 2001) and the yeast sphingolipids differ from their mammalian counterparts, too: they have usually longer acyl chains and possess different head groups (Dickson & Lester, 2002). Combination of all these factors is probably the reason for the fact that all the yeast plasma membrane proteins studied so far were detected in the detergent insoluble fraction after the TritonX100 extraction (Bagnat et al, 2000; Lauwers & André, 2006). Recently, it was suggested that even gel phase domains enriched in sphingolipids and free of ergosterol could exist in the yeast plasma membrane (Aresta-Branco et al, 2011).

1.2.1. Yeast plasma membrane contains several non-overlapping compartments

With the advent of fluorescent protein tagging and live cell imaging it turned out that some proteins are not distributed homogenously in the yeast plasma membrane. Young and

coworkers (2002) showed that the integral membrane proteins from the Sur7 family, Sur7, Fmp45 and Ydl194c, are localized in patchy cortical domains that are very stable in time. Similar stable patchy plasma membrane distribution was documented independently for the arginine transporter Can1 at the same time. There were about 40-80 Can1-GFP dots per cell and based on their appearance in confocal microscope the size of individual patches was assessed to be about 300nm (Malinska et al, 2003). Moreover, the Can1 domains were mutually exclusive with the regions occupied by the H^+-ATPase Pma1 which seemed to fill the rest of the plasma membrane (Figure 7). Some proteins like the hexose transporter Hxt1 or amino acid permease Gap1 localized evenly in the plasma membrane (Malinska et al, 2003; Lauwers & André, 2006). The Can1 patches were subsequently shown to be identical with the Sur7 domains (Malinska et al, 2004) and named "Membrane Compartment occupied by Can1" (MCC). The membrane compartment outside the MCC patches containing Pma1 protein was accordingly named MCP. As constituents of both the MCC and MCP were classified as detergent-insoluble proteins (Bagnat et al, 2000; Dupré & Haguenauer-Tsapis, 2003; Malinska et al, 2003; Malinska et al, 2004) it became clear that simple detergent extraction classification is not sufficient method to describe the proper partitioning of the yeast plasma membrane proteins into lateral membrane domains in vivo.

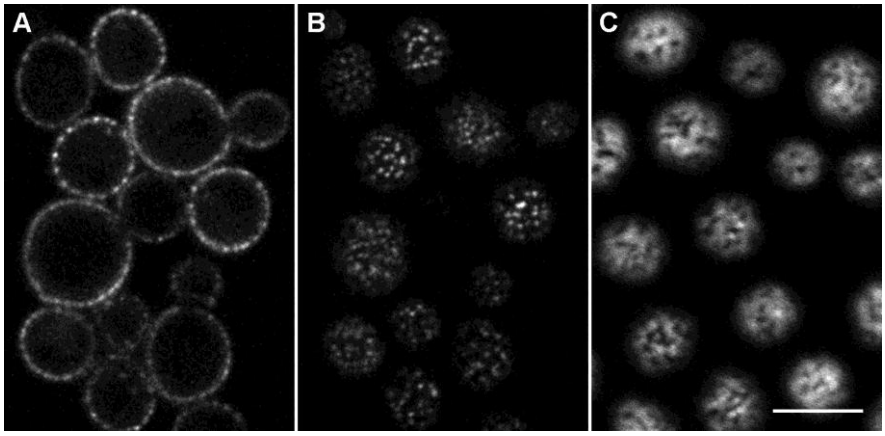

Figure 7.
MCC and MCP in yeast plasma membrane.

A, B) Distribution of MCC marked by Can1-GFP on the transversal (A) and surface (B) confocal sections. **C)** MCP pattern visualized by Pma1-GFP on surface optical section. Bar 5μm. Reproduced from Malinsky et al (2010).

Based on the early colocalization studies, the network-like membrane area occupied by Pma1, MCP, appeared to fill the rest of the plasma membrane around MCC and all the dynamic processes were supposed to happen there (Malinska et al, 2003; Brach et al, 2011). However, this is probably not the case as plasma membrane patchy domains containing the TORC2 signaling complexes were localized to a distinct highly dynamic membrane compartment that did not possess either MCC or MCP markers. This membrane domain was

therefore named MCT (Membrane Compartment occupied by TORC2). The plasma membrane localization of this protein complex depends on the Avo1 subunit and its PH domain which binds $PI(4,5)P_2$ in the cytoplasmic leaflet of PM (Berchtold & Walther, 2009).

1.2.2. Membrane compartment of Can1 and eisosome

1.2.2.1. Structure and composition of MCC/eisosome

Few years after the MCC discovery, a cytosolic protein complex called eisosome was found to underlie the MCC patches (Walther et al, 2006). The eisosome is composed mainly of two highly related abundant cytoplasmic proteins Pil1 and Lsp1 that were originally found in a complex with Pkh1/2 kinases, yeast homologs of mammalian 3'-phosphoinositide-dependent protein kinase PDK1 (Ho et al, 2002) and described as the negative regulators of these kinases (Zhang et al, 2004). The presence of Pil1p is important for the MCC/eisosome integrity because upon PIL1 deletion the normal punctate pattern of all MCC/eisosome constituents is lost and the whole structure collapses into 1 to 2 big eisosome remnants per cell (Walther et al, 2006; Grossmann et al, 2007). Deletion of Lsp1 does not have any apparent effect on localization of other constituents. Further work on characterization of MCC and eisosomes identified new members and there are described altogether nine transmembrane proteins accumulating in MCC and about 20 cytosolic proteins associated with the eisosome (Grossmann et al, 2007; Walther et al, 2007; Grossmann et al, 2008; Deng et al, 2009; Frohlich et al, 2009). They are summarized in Table 1.

Apart from accumulation of specific proteins in MCC, this domain also exhibits a specific lipid composition. Staining with filipin revealed that ergosterol is either enriched in this membrane compartment or it is more accessible for binding of this dye (Grossmann et al, 2007). Consistent with the involvement of lipids in the plasma membrane compartmentalization, MCC structure is affected in lipid biosynthesis mutants and in mutants with impaired vesicle transport (Grossmann et al, 2008).

1.2.2.2. Biogenesis and maintenance of MCC/eisosome

The MCC/eisosome is a very stable cortical structure that retains its position during the whole cell cycle (Young et al, 2002; Malinska et al, 2003; Walther et al, 2006). In dividing cells, MCC/eisosomes are formed de novo in the growing bud, gradually colonizing

the plasma membrane from the bud neck. Once they are nucleated, they do not move at standard conditions. The expression of Pil1p is cell-cycle regulated and is thus synchronized with the bud growth (Moreira et al, 2009). Pil1 protein is probably the establishing constituent and other components then follow Pil1 to form a mature MCC/eisosome complex (Malinsky et al, 2010).

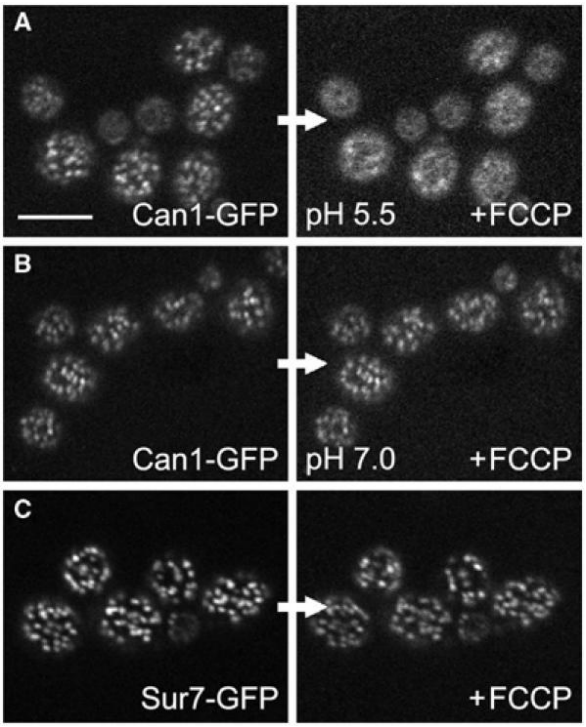

Figure 8. Some MCC proteins are affected by PM depolarization. A) Can1-GFP was released from MCC after depolarization of PM with FCCP. **B)** When the depolarization of PM was prevented by using a buffer of pH 7.0 no release of Can1p was observed. **C)** Sur7-GFP localization into MCC was not affected by membrane potential. Adapted from Grossmann et al (2007).

The integrity of MCC partially depends on membrane potential. After membrane depolarization the transporters Can1, Fur4 and Tat2 are released from MCC, become homogenously distributed in the plasma membrane and return back after the membrane potential is re-established (Figure 8). On the other hand, Sur7 and Nce102 proteins are not sensitive to such changes in membrane potential as they probably form structural elements of MCC (Grossmann et al, 2007; Grossmann et al, 2008).

Moreover, the formation of eisosomes is regulated by phosphorylation of Pil1p and Lsp1p via Pkh1/2 kinases (Zhang et al, 2004; Walther et al, 2007; Luo et al, 2008; Deng et al, 2009). The exact phosphorylation mechanism is not clear and it seems to be rather complex because two independent groups described not completely overlapping set of phosphorylation sites on Pil1p (Walther et al, 2007; Luo et al, 2008). Pil1p is getting hyperphosphorylated and eisosomes are probably partially disassembled during mating as judged from analysis of MATa cells treated with α-factor (Deng et al, 2009). Pkh1/2 kinases were shown to be regulated by sphingolipids (lcb) (Friant et al, 2001; Zhang et al, 2004) and except Pil1 and Lsp1 they further phosphorylate Pkc1 (protein kinase C), Ypk1/2 and Sch9 Ser/Thr kinases. Pkc1 and Ypk1/2 kinases are involved in cell wall integrity pathway, endocytosis, flippases regulation and cell growth (Zhang et al, 2004; and references therein) and also in mRNA

decay and P-body assembly on nutrient poor media (Luo et al, 2011). Ypk1/2 kinases were also reported to be involved in eisosome regulation as their inactivation leads to eisosome disassembly (Luo et al, 2008). Moreover, it seems that Pil1 and Lsp1 proteins themselves also (negatively) regulate the downstream signaling of Pkh1/2 kinases via Pkc1 and Ypk1/2 because the deletion of PIL1/LSP1 led to an increased activation of the kinase pathway and resistance to heat stress (Zhang et al, 2004).

Another important regulator of MCC/eisosome complex (in addition to Pil1) is the integral membrane protein Nce102 whose deletion causes two-fold decrease of MCC/eisosome number and increase of the Pil1p cytosolic pool (Grossmann et al, 2008; Frohlich et al, 2009). Nce102 was shown to negatively regulate Pkh1/2 kinases and prevent hyperphosphorylation of Pil1 and subsequent disassembly of eisosomes. Sphingolipids promote the accumulation of Nce102p within MCC and this way they regulate Pkh1/2 kinases; Nce102 was therefore described as a sphingolipid sensor in the membrane (Frohlich et al, 2009). Moreover, the presence of Nce102 is also required for the targeting of proton transporters Can1, Fur4 and Tat2 into MCC (Grossmann et al, 2008).

1.2.2.3. Function of MCC/eisosome

Colocalization experiments of MCC/eisosomes with accepted markers of clathrin-mediated endocytosis, Ede1, Rvs161/167 and Abp1 (see chapter 1.3.), showed that the highly dynamic process of canonical endocytosis happens in the plasma membrane outside MCC domains (Grossmann et al, 2008; Brach et al, 2011) and thus disproved the original idea of Walther and coworkers that eisosomes could be static sites of endocytosis (Walther et al, 2006). The same has been recently shown also for exocytosis (Brach et al, 2011). Just in contrast, it was shown that Can1 is first released from the MCC before it is endocytosed. This observation led to an idea that MCC could function as a protective area to slow down the turnover of certain proteins. The accelerated degradation of several transporters in MCC mutants, *nce102Δ* and *pil1Δ*, seemed to support this hypothesis (Grossmann et al, 2008). Recent experiments of a different group, however, challenged this suggested MCC function (Brach et al, 2011).

Elucidation of the connection between MCC/eisosomes and the endocytic process is still a hot topic as it was shown recently that the dynamics and/or localization of some endocytic factors are affected in *PIL1* deletion mutant (Murphy et al, 2011). The authors

suggested that this defect might arise from the mislocalized Slm1/2 proteins that are important for regulation of sphingolipid level whereas proper sphingolipid level is crucial for endocytosis. Importantly, the essential Slm1/2 protein pair was also shown to be involved in eisosome integrity regulation (Kamble et al, 2011).

Protein	ORF	Location	Description	Localization references
Sur7	Yml052w	MCC	Sur7 family, 4TMDs	Young et al, 2002; Malinska et al, 2004
Fmp45	Ydl222c	MCC	Sur7 family, 4TMDs	Young et al, 2002
Pun1	Ylr414c	MCC	Sur7 family, 4TMDs	Alvarez et al, 2008; Grossmann et al, 2008
Ynl194c	Ynl194c	MCC	Sur7 family, 4TMDs	Young et al, 2002
Can1	Yel063c	MCC	H^+-arginine transporter	Malinska et al, 2003
Fur4	Ybr021w	MCC	H^+-uracil transporter	Malinska et al, 2004
Tat2	Yol020w	MCC	H^+-tryptophan transporter	Grossmann et al, 2007
Nce102	Ypr149w	MCC	Nce102 family	Grossmann et al, 2008
Fhn1	Ygr131w	MCC	Nce102 family	Grossmann et al, 2008
Pil1	Ygr086c	Eisosome	BAR domain	Walther et al, 2006
Lsp1	Ypl004c	Eisosome	BAR domain	Walther et al, 2006
Pkh1	Ydr490c	Eisosome	Ser/Thr protein kinase	Walther et al, 2007
Pkh2	Yol100w	Eisosome	Ser/Thr protein kinase	Walther et al, 2007
Slm1	Yil105c	Eisosome	BAR and PH domains	Grossmann et al, 2008
Slm2	Ynl047c	Eisosome	BAR and PH domains	Grossmann et al, 2008
Seg1	Ymr086w	Eisosome	unknown	Deng et al, 2009; Frohlich et al, 2009
Eis1	Ymr031c	Eisosome	unknown	Grossmann et al, 2008
Ygr130c	Ygr130c	Eisosome	unknown	Grossmann et al, 2008
Mdg1	Ynl173c	Eisosome	unknown	Grossmann et al, 2008
Pst2	Ydr032c	Eisosome	Similar to flavodoxin-like proteins	Grossmann et al, 2008
Rfs1	Ybr052c	Eisosome	Similar to flavodoxin-like proteins	Grossmann et al, 2008
Ycp4	Ycr004c	Eisosome	Similar to flavodoxin-like proteins	Grossmann et al, 2008
Rgc1	Ypr115w	Eisosome	PH domain	Olivera-Couto et al, 2011 and refs. therein
Aim3	Ybr108w	Eisosome	unknown	Olivera-Couto et al, 2011 and refs. therein
Mrp8	Ykl142w	Eisosome	unknown	Olivera-Couto et al, 2011 and refs. therein
Sap1	Yer047c	Eisosome	Putative AAA family ATPase	Olivera-Couto et al, 2011 and refs. therein
Yta6	Ypl074w	Eisosome	Putative AAA family ATPase	Olivera-Couto et al, 2011 and refs. therein
Msc3	Ylr219w	Eisosome	unknown	Olivera-Couto et al, 2011 and refs. therein

Table 1. Known MCC and eisosome constituents.

1.3. CLATHRIN MEDIATED ENDOCYTOSIS

Endocytosis is a process by which cells internalize plasma membrane and extracellular material. Together with exocytosis it enables the turnover of plasma membrane components and regulates the composition of the plasma membrane in response to cellular needs; it is also involved in nutrient uptake and in control of signaling events. All these functions are very important so that cells evolved several endocytic routes. The most extensively studied and precisely described is the clathrin-mediated endocytosis (CME). Other pathways are collectively grouped under the term clathrin-independent endocytosis (CIE) and they are still awaiting a more detailed investigation. Multiple CIE pathways were described in mammals such as internalization via caveolae, phagocytosis, macropinocytosis, RhoA and Arf6 regulated pathways or CLIC/GEEC endocytosis of GPI-anchored membrane proteins (Doherty & McMahon, 2009; Howes et al, 2010). In contrast to mammals, only CME has been described in plants and for a long time also in yeast. The first yeast CIE pathway involving the action of Rho1 and formins has been published only very recently (Prosser et al, 2011).

The term clathrin-mediated endocytosis is derived from the fact that the internalization of plasma membrane material in this pathway occurs via membrane vesicles coated with a protein called clathrin that assembles into higher order lattice around the forming vesicle. The process of CME begins when a cargo at the PM is selected by various adaptor proteins. The complex protein-protein interaction network results in the formation of so called clathrin coated pit that further matures, invaginates and is subsequently cut off as a clathrin coated vesicle. The newly formed endocytic vesicles are rapidly uncoated and transported along actin cables to early endosomes where the cargo is further sorted (Grant & Donaldson, 2009; McMahon & Boucrot, 2011; Weinberg & Drubin, 2012)). (see Figure 9 for endocytosis overview).

It is now obvious that the formation of an endocytic vesicle involves a highly coordinated sequence of assembly and disassembly of numerous proteins (about 60 in yeast) each of which is recruited to the endocytic spot with a precise dynamics to accomplish its function in the right moment. Analysis of many endocytic protein dynamics revealed that the endocytic factors can be grouped into several modules according to their similar behavior during the vesicle formation. At least four modules were described in yeast (Kaksonen et al,

2005; Stimpson et al, 2009) and similar modular design of endocytosis was recently described also in mammalian cells (Taylor et al, 2011)

Early stages of endocytosis involve the selection of a place at the PM where the vesicle will form, selection of the cargo and coat formation. Little is known about the endocytic site selection mechanism. Some experiments suggest that the endocytic sites could be nucleated before the cargo recruitment and that some adaptor proteins from the early/coat module can play a role in this process, namely yeast proteins Syp1 and Ede1 and their mammalian homologs FCHo1/2 and Eps15/intersectins1/2 (Toshima et al, 2006; Reider et al, 2009; Stimpson et al, 2009; Henne et al, 2010; Weinberg & Drubin, 2012). It is highly probable that additional factors are involved in this process. The situation in mammalian system is even more complicated because different types of clathrin coated structures with different dynamics were described on their PM. Apart from canonical endocytic clathrin pits, also flat clathrin coated plaques were observed in some mammalian cells on their coverslip-attached surface (Kirchhausen, 2009; Saffarian et al, 2009). There are also numerous observations of so called endocytic hot-spots, where the clathrin vesicles seem to initiate repeatedly from one place on the PM (Gaidarov et al, 1999; Kirchhausen, 2009; Henne et al, 2010; Taylor et al, 2011), although some authors polemize with such a concept of specialized PM endocytic domains (Ehrlich et al, 2004).

The cargo selection and coat formation/maturation is a complex process that involves numerous interactions of cargo, adaptor proteins, PM lipids (especially $PI(4,5)P_2$) and clathrin. Clathrin does not have the ability to directly bind cargo and/or lipids so that this linkage is accomplished by adaptor proteins that differ in their specificity to bind various cargo and other associated factors and regulators (McMahon & Boucrot, 2011; Reider & Wendland, 2011). Adaptor proteins recognize the cargo designed for internalization by specific signals on cargo molecules like phosphorylation, ubiquitination or intrinsic linear peptide sequences (Bonifacino & Traub, 2003; Traub, 2009; Conibear, 2010; Reider & Wendland, 2011). The cargo-adaptors-lipid complexes recruit clathrin which stabilizes the forming pit. It is thought that it is not clathrin but rather some of the adaptor molecules that are directly involved in the membrane curvature generation as some of the adaptors possess F-BAR domains (Syp1, FCHo1/2) and/or bind $PI(4,5)P_2$ (ANTH or ENTH domain containing proteins like AP180 and epsins/Ent1,2) (Reider et al, 2009; Robertson et al, 2009; Henne et al, 2010; McMahon & Boucrot, 2011). During the coat formation, regulators of the actin nucleation factor Arp2/3 are recruited to the spot, for example Las17 in yeast, N-WASP in

mammals. It seems that they are negatively regulated in the initial phases of the vesicle formation to prevent a premature actin polymerization (Boettner et al, 2009; Galletta et al, 2010). At a certain moment this blocation of actin nucleation is released by other factors and actin polymerization starts. Many actin regulating proteins are involved in this process, including also type-I myosins or Abp1 protein (Kaksonen et al, 2006; Robertson et al, 2009; Weinberg & Drubin, 2012). It seems that actin is more important for yeast endocytosis where its polymerization probably helps to overcome the high turgor pressure inside the cell (Kaksonen et al, 2006; Aghamohammadzadeh & Ayscough, 2009). The exact role of actin during mammalian endocytosis is a matter of recent research as it seems that different cell types and different clathrin structures differ in their actin requirement (Kirchhausen, 2009). While actin polymerizes it drives the invagination of the clathrin pit further into the cytoplasm and it probably also assists during vesicle fission (Kaksonen et al, 2006; Ferguson et al, 2009). The forming membrane neck is quickly occupied by other factors, mainly BAR domain containing proteins (amphiphysins) and dynamin (in mammals) that are involved in the scission of the vesicle. The scission process in mammals depends on the action of the GTPase dynamin whereas yeast probably relies only on amphiphysins (Rvs161/167), the involvement of a dynamin-like protein Vps1 during yeast endocytosis is still controversial (Conibear, 2010; Weinberg & Drubin, 2012). The driving force for the vesicle pinch-off probably also originates from the tension generated by differential distribution of $PI(4,5)P_2$ at the tubular neck which is protected against hydrolysis by BAR domain proteins and the coated vesicle that is accessible to synaptojanin-like $PI(4,5)P_2$ phosphatases (Liu et al, 2006). These $PI(4,5)P_2$ phosphatases are activated in the late stages of endocytosis and are also involved in the coat disassembly after vesicle internalization. Uncoating is a complex post-scission process that involves action of many factors like kinases (GAK, Prk1, Ark1), phosphatases, ATPases (Hsc70 and auxilin) or GTPases (Arf). This step is important for the recycling of coat factors that can be then reused in another endocytic round (Toret et al, 2008; Weinberg & Drubin, 2012).

Despite some differences between yeast and mammalian CME, the recent research shows that the basic principle of clathrin-mediated endocytosis might be conserved throughout *Eukaryota*. Plants also posses many homologs of mammalian/yeast endocytic machinery proteins and it is thus highly probable that the plant CME proceeds by a mechanism similar to that described in yeast and mammals (Chen et al, 2011).

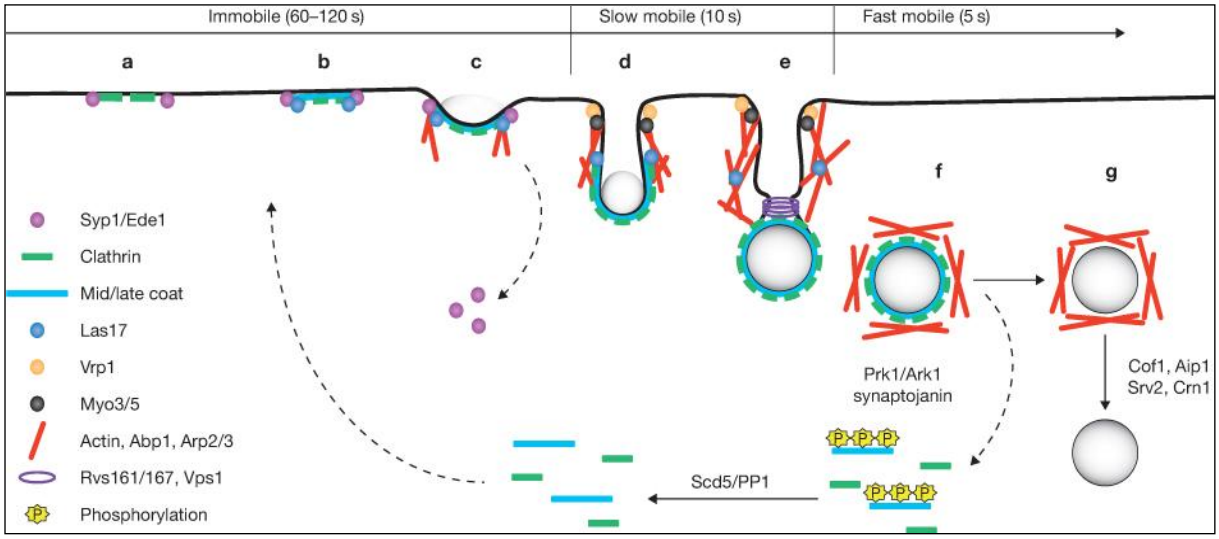

Figure 9. Clathrin mediated endocytosis in yeast. a, b) recruitment of early factors and coat assembly; **c, d)** Syp1 and Ede1 departure and WASP/myosin/actin slow mobile invagination phase; **e)** invagination, vesicle scission machinery assembly and scission; **f)** vesicle release and uncoating; **g)** inward transport of the vesicle, reactivation of coat factors. Reproduced from Boettner et al (2012).

1.4. YEAST CORTICAL ENDOPLASMIC RETICULUM

A significant part of the yeast plasma membrane is associated with the network of endoplasmic reticulum (ER). As this association is quite close, it is highly probable that this so called cortical ER might influence the processes taking place in the plasma membrane. In this chapter I will therefore briefly review what is known about this important membranous organelle with the emphasis on the yeast cortical ER.

1.4.1. Basic facts about endoplasmic reticulum

The endoplasmic reticulum in all eukaryotic cells consists of the nuclear envelope and the dynamic peripheral network of cisternae and tubules spreading in the cytoplasm and sharing one continuous lumen. It is a very important multifunctional organelle that is involved in a variety of cellular functions like production and modification of secreted and membrane proteins, synthesis of phospholipids and steroids, detoxification and regulation of intracellular calcium levels (Baumann & Walz, 2001; Estrada de Martin et al, 2005b).

Most of the processes carried out by ER are probably not distributed homogenously in the ER network and ER is rather sub-divided into specialized domains. The most traditional

classification of ER to nuclear envelope, ribosome-studded rough ER and ribosome-free smooth ER is based on morphological observations and can be also extended for transitional ER (tER) which are specialized cup-shaped ER sites dedicated to exit of newly synthesized proteins along the secretory pathway via COPII vesicles (Estrada de Martin et al, 2005b; Levine & Rabouille, 2005). The compartmentalization of ER into specialized subdomains goes probably far beyond this rough classification (Baumann & Walz, 2001). According to the cellular needs or specialization (in multicellular organisms), some of the ER subcompartments can predominate and the ratio of specific compartments can be dynamically modified.

The ER sheets and tubules are continuously rearranged. In animal cells the ER dynamics relies mostly on microtubules (Terasaki et al, 1986; Lee & Chen, 1988; Lee et al, 1989; Terasaki, 2000; Friedman et al, 2010), even though actin can be also involved in some cases (Levine & Rabouille, 2005). The rearrangement of yeast and plant ER, on the other hand, is mediated predominantly by actin cytoskeleton (Prinz et al, 2000; Fehrenbacher et al, 2002).

1.4.2. Membrane contact sites

Apart from the well described role of ER in vesicular transport of lipids and trans-membrane and secreted proteins, this organelle is connected with all other cellular membranous organelles via numerous close membrane appositions called membrane contact sites (MCS). It is supposed that MCS mediate specific non-vesicular intermembrane transport of small molecules and ions like lipids and calcium between ER and mitochondria, plastids, vacuole/lysosome, endosomes, Golgi, peroxisomes and plasma membrane (Levine, 2004; Holthuis & Levine, 2005; Levine & Rabouille, 2005; Levine & Loewen, 2006; Wu et al, 2006; Lebiedzinska et al, 2009; Schulz et al, 2009). The best characterized MCS so far are probably the nucleus-vacuole junctions that are established by interactions of the vacuolar protein Vac8p and the outer-nuclear membrane protein Nvj1p. These structures are involved in a process called “piecemeal microautophagy of the nucleus” that happens upon the nutrient depletion conditions (Pan et al, 2000; Kvam & Goldfarb, 2007). There has also been a considerable recent progress in characterization of yeast ER-mitochondria encounter structures (ERMES) that link the ER and the outer mitochondrial membrane. The ERMES core constituents are heterotetrameric protein complexes composed of one ER protein

(Mmm1), one soluble protein (Mdm12) and two outer-mitochondrial-membrane proteins (Mdm34 and Mdm10) that physically tether both organelles together (Kornmann et al, 2009; Kornmann & Walter, 2010) and could possibly ensure a lipid exchange between these organelles as well (Kopec et al, 2010). A small Ca^{2+}-binding Miro (mitochondrial rho-like) GTPase Gem1 has been shown to regulate the ERMES sites in yeast (Kornmann et al, 2011). However, less is known about the composition and regulation of other MCS, including the ER-PM contact sites.

1.4.3. Cortical endoplasmic reticulum

A significant part of the cytosolic ER network in animals, plants and fungi is always associated with the plasma membrane (Prinz et al, 2000; Levine & Rabouille, 2005; Orci et al, 2009; Sparkes et al, 2009), forming there a dynamic meshwork of cortical ER. In yeast and plants the cortical ER forms a substantial part of the peripheral ER network (Prinz et al, 2000; Pichler et al, 2001; Perktold et al, 2007; Sparkes et al, 2009; West et al, 2011) (schematically shown in Figure 10). Yeast cortical ER is connected with the nuclear envelope by several ER tubules under normal conditions (Koning et al, 1993; Prinz et al, 2000) and recently also the existence of a large ER cisterna in the yeast cytoplasm was described (West et al, 2011).

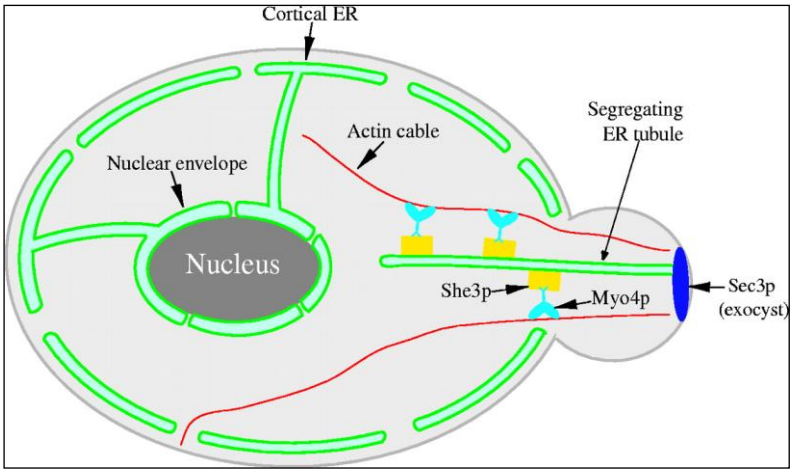

Figure 10. Model of the yeast endoplasmic reticulum network.

Most of yeast peripheral ER network is formed by cortical ER beneath PM that is connected with nuclear envelope by several tubules. Cortical ER is inherited by transportation of ER membranes along actin cables into bud. The special cytoplasmic cisterna involved in the inheritance process is not depicted here. Reproduced from Du et al (2004).

A very interesting issue is how large proportion of the cortical ER in yeast is directly involved in the ER-PM contact sites establishment. Pichler and coworkers defined the upper distance limit for ER-PM MCS in yeast to 30 nm and identified more than 1000 ER-PM contact sites per one yeast cell in transmission electron microscope micrographs (Pichler et al, 2001). Recently, West and colleagues measured the ER-PM spacing more precisely in cryofixed cells and showed that the distance between these two organelles varies from 16 to

59 nm with the mean value of about 33nm (West et al, 2011). It means that the majority of the cortical ER in yeast can be in the position suitable for MCS establishment. Biochemical isolation and analysis of the ER membranes associated with PM showed that they are enriched in enzymes involved in lipid synthesis, especially PS- and PI-synthases (Pichler et al, 2001) suggesting that proximity of ER may define specific sub-domains of the plasma membrane. In agreement with this assumption, several yeast oxysterol binding protein homologs (Osh proteins) have been found to localize to ER domains near PM using live cell imaging of fluorescently labeled proteins (Schulz et al, 2009). However, whether they really transport sterols between ER and PM still remains controversial (Georgiev et al, 2011).

Proper formation and maintenance of the peripheral/cortical ER in yeast is controlled by a largely unknown mechanism. The inheritance of the peripheral ER in the bud depends on exocyst (Wiederkehr et al, 2003; Reinke et al, 2004) and several other factors like She3, actin, Myo5, Ice2, Ptc1, Scs2, Aux1 (Du et al, 2001; Fehrenbacher et al, 2002; Estrada et al, 2003; Estrada de Martin et al, 2005a; Du et al, 2006; Loewen et al, 2007). Recently, West et al. (2011) showed that the ER associated with the plasma membrane in mother cell does not contribute to the formation of peripheral ER in the daughter. Instead, a special cytoplasmic ER cisterna in the mother is formed that is involved in the inheritance process.

Some of the above mentioned factors, like Ice2, Scs2 and actin, are important not only for the inheritance process but also for a correct formation/maintenance of the cortical ER network pattern beneath the plasma membrane in yeast (Fehrenbacher et al, 2002; Estrada de Martin et al, 2005a; Loewen et al, 2007). Some other integral ER proteins are enriched in the cortical ER and missing in the perinuclear ER, like reticulons (Rtn1,2), Yop1 and Ist2. Reticulons/Yop1 are responsible for shaping and/or maintenance of the highly curved ER tubules and egdes of cisternae and upon their deletion the ER gains less tubular and more sheet-like morphology (De Craene et al, 2006; Voeltz et al, 2006; Shibata et al, 2010; West et al, 2011). Ist2 belongs to TMEM16 protein family of calcium activated chloride channels and its retention in cortical ER/PM zones depends on its C-terminus (Fischer et al, 2009; Maass et al, 2009). This C-terminal part of Ist2 has the capacity to redirect other proteins to cortical ER domains and induce formation of junctional PM-ER in mammalian cells (Ercan et al, 2009; Lavieu et al, 2010). The deletion of Ist2 protein in yeast, however, has no obvious influence on the cortical ER morphology, at least on the fluorescence microscopy level (Fischer et al, 2009).

2. AIMS OF THE WORK

This thesis focuses on lateral organization of the plasma membrane in budding yeast, mainly on the structural and functional description of Membrane Compartment of Can1, MCC. This work was preceded by a comprehensive analysis of the MCC mainly with the use of advanced fluorescence microscopy techniques that revealed its protein and lipid composition and some basic facts about its biogenesis and dynamics (mainly its striking stability in time).

The specific scopes of my PhD project were:

1) To establish a reliable protocol for morphological and immunological preservation of yeast cells for transmission electron microscopy and to perform a detailed ultrastructural analysis of MCC domain.
2) To explore the role of specific proteins in MCC organization.
3) To examine the role of MCC in the functional organization of plasma membrane and cell cortex.

3. USED METHODS

3.1. CONSTRUCTION OF FLUORESCENT PROTEIN MARKERS

In our studies of membrane organization we broadly used fluorescence microscopy, mainly confocal imaging. To follow proteins of interest under confocal microscope in living yeast cells, we tagged them with fluorescent markers derived from GFP or dsRed in integrative or extrachromosomal expression plasmids. For visualization of the endoplasmic reticulum network we used an artificial ER luminal reporter composed of ER-targeting signal sequence fused to GFP or dsRed and a C-terminal ER retention peptide His-Asp-Glu-Leu (ss-GFP/dsRed-HDEL) (Prinz et al, 2000; Bevis et al, 2002). The plasmids were constructed by standard cloning techniques based on PCR, restriction enzyme digestion and ligation. Lithium acetate transformation was then used to deliver the plasmids into various yeast strains.

3.2. FLUORESCENCE MICROSCOPY

Yeast strains expressing fluorescent markers were observed under the confocal laser scanning microscope (Zeiss LSM 5 DUO) in our laboratory. For longer time-lapse experiments we took advantage of spinning disk confocal microscopes (Zeiss Cell Observer SD) in Göttingen, Carl Zeiss Light Microscopy Application Center, and in Brno, Centre for Biomedical Image Analysis. In our case, the spinning disk microscope was suited better for live cell imaging than the scanning confocal microscope due to a lower photobleaching and phototoxicity and faster image acquisition. All microscopic observations were performed on living yeast cells. For this purpose we used special gentle immobilization of the cells on the cover glass by a thin slice of 1% agarose diluted in 50mM phosphate buffer (pH 6.3) or in growth medium which ensures a proper environment for the growing cells (humidity, nutrients).

3.3. ELECTRON MICROSCOPY

Transmission electron microscopy (TEM) was used to study membrane organization at high resolution. In contrast to light microscopy imaging, it is not possible to observe a living sample in TEM as it requires a special treatment due to a high vacuum inside the microscope.

Thus, the key question is the close-to-native preservation of the studied sample during its processing for TEM. We used several different approaches for sample preparation and subsequent observation under the transmission electron microscope: 1) plastic embedding following chemical fixation or cryofixation combined with freeze substitution and 2) freeze fracture/freeze etching.

3.3.1. Plastic embedding

During plastic embedding the samples are fixed, dehydrated in organic solvents, infiltrated with various (water immiscible) resins, polymerized and sliced to thin sections. Contrast for observation in TEM is added by heavy metal salts applied either during embedding procedure or on-section.

There are two basic ways how to fix a living sample for plastic embedding. The original, still widely used, is a chemical crosslinking of (mostly) proteins with aldehydes (formaladehyde or glutaraldehyde). The second is the physical fixation by rapid freezing of the sample (cryofixation) under the conditions when amorphous ice is formed (so called vitrification). Chemical fixation is more accessible for use in every laboratory; cryofixation in contrast requires special, rather expensive, equipment. Main disadvantage of chemical crosslinking, however, is its susceptibility to artifacts generation. The chemical reaction is slow in comparison with lots of cellular events so that the fast cellular processes cannot be monitored. Moreover, it requires a specific buffer system which is never optimal for all cellular compartments. The slow course of the reaction allows for redistribution of various cellular components which is further combined with the cellular shrinkage and extraction of non-fixed components during the subsequent dehydration and resin infiltration steps.

3.3.2. High pressure freezing and freeze substitution

In contrast to chemical crosslinking, cryofixation is very fast and almost simultaneous in the whole cell. The cells can be usually frozen in the medium and thus no buffer system is needed. There are several methods of cryofixation including slam freezing, plunge freezing or high pressure freezing. The most versatile from the above mentioned methods is probably the high pressure freezing (HPF). The HPF principle is based on the fact that at high pressure of about 2000 bar (200 MPa) the vitrification of water is easier to reach. The HPF machine first

pressurizes a sample and immediately freezes it in liquid nitrogen (Studer et al, 2001). This set-up allows vitrifying samples up to 200 μm thick which is more than ten times higher value compared to other cryofixation techniques. The frozen samples can be further processed for plastic embedding with the use of freeze substitution (FS) and low-temperature resin infiltration and embedding. During FS, the ice is replaced by an organic solvent at very low temperatures (usually about -90°C). This method can be even combined with the addition of chemical crosslinkers or contrasting agents into the FS medium. Because all reactions run at very low temperatures and after the physical fixation of the sample, the extraction and component redistribution is minimized. It is also believed that the effect of added chemicals is not as harsh as at ambient temperature. This leads to perfect ultrastructure and antigen preservation.

3.3.3. Immunogold labeling

Immunogold labeling in TEM is always a compromise between perfect sample structure and antigen preservation. Most of the chemical fixatives and contrasting agents destroy many epitopes in the sample and aggravate their subsequent detection with antibodies. They are therefore omitted (reduced) even if the resulting morphology is not perfect. Two basic immunolabeling techniques exist in TEM: pre-embedding and post-embedding approaches. During pre-embedding labeling, the sample is labeled before it is infiltrated with the resin. The detected antigens should not be thus influenced by the subsequent dehydration and embedding procedures which should result in increased labeling signal. This approach can be combined only with the conventional chemical fixation and usually requires membrane permeabilization with detergents. In yeast, the cell wall has to be also digested before labeling so that the final morphology is quite affected. In contrast to pre-embedding, antibody labeling is the last step in post-embedding approach – here the labeling reaction runs on the surface of the resin section of the sample. The secondary antibodies for TEM studies are linked to colloidal gold particles of a certain size that allow the detection of stained objects under the electron microscope.

3.3.4. Freeze fracture/freeze etching

Freeze fracture/freeze etching technique is especially useful for visualization of cellular membranes as it provides a unique view on membrane surface (plane) that cannot be obtained by resin thin-section technology.

The principle of this method lies in the quick freezing of a sample and its subsequent fracturing with a knife at low temperature. The fracture occurs more easily along the membranous organelles (along the hydrophobic planes of membranes) but straight breaks through the cellular interior are present as well. The fractured surface is then usually "etched": it means that a thin layer of ice is sublimated in high vacuum to uncover more details of the sample. The exposed cellular structures are shadowed with platinum vacuum vapors applied at a fixed angle of 45° which allows obtaining topological information about the sample. This thin metal layer is subsequently stabilized by a carbon film evaporated to the sample surface at a normal 90° angle. The metal/carbon replica is then cleaned by digestion of the biological material with a strong acid solution, transferred to a grid and observed in TEM.

3.4. MEMBRANE PROTEIN TOPOLOGY DETERMINATION

For determination of the membrane topology (orientation of a protein in membrane) of Nce102 and Sur7 trans-membrane proteins we used an assay based on a C-terminal dual Suc2/His4C reporter (Deak & Wolf, 2001; Kim et al, 2003a; Kim et al, 2003b).

The reporter consists of two parts, fragment of SUC2 gene and truncated HIS4 gene, fused to the C-terminus of a protein of interest (or its part). Suc2p is an invertase which is highly glycosylated in the ER lumen (contains eight glycosylation sites) and the HIS4C gene codes for histidinol dehydrogenase. This enzyme, when facing cytosol, is able to convert histidinol to histidine. In addition, it contains also several glycosylation sites (Strahl-Bolsinger & Scheinost, 1999).

The first step in the assay is to prepare (with the use of PCR and homologous recombination) a set of reporter plasmids containing parts of the tested gene that are 3'-truncated after each transmembrane domain (TMD). Each gene variant in the plasmid is then followed by the same reporter composed of three HA tags, SUC2 gene and HIS4C gene. Afterwards, all gene-reporter variants are expressed in a yeast strain that is deficient in

histidine production and they are tested for: 1) their ability to grow on a medium containing histidinol instead of histidine and 2) for the presence/absence of the glycosylated Suc2p.

The orientation of each transmembrane domain is determined according to the localization of the reporter. When the reporter is present in the ER lumen, the Suc2p is glycosylated and this can be visualized as a shift in protein mobility on the western blot (detected using anti-HA antibody) after the deglycosylation with the endonuclease H (EndoH) enzyme. At the same time, this strain is not able to grow in a medium containing histidinol as the converting enzyme is hidden in the ER lumen. In the opposite case the reporter is facing cytosol and the histidinol dehydrogenase enables the strain to grow on the histidinol medium but the Suc2p is not glycosylated and no mobility shift can be detected on the western blot.

4. RESULTS

4.1. LIST OF PRESENTED PUBLICATIONS

Research paper 1:

Stradalova V, Gaplovska-Kysela K, Hozak P. Ultrastructural and nuclear antigen preservation after high-pressure freezing/freeze-substitution and low-temperature LR White embedding of HeLa cells. Histochem Cell Biol **2008**, 130(5):1047-52.

IF_{2010} = 4.727 times cited: 4 (WoS)

Research paper 2:

Stradalova V, Stahlschmidt W, Grossmann G, Blazikova M, Rachel R, Tanner W, Malinsky J. Furrow-like invaginations of the yeast plasma membrane correspond to membrane compartment of Can1. J Cell Sci **2009**, 122 (16): 2887-94.

IF_{2010} = 6.290 times cited: 27 (WoS)

Research paper 3:

Loibl M, Grossmann G, Stradalova V, Klingl A, Rachel R, Tanner W, Malinsky J, Opekarová M. C terminus of Nce102 determines the structure and function of microdomains in the Saccharomyces cerevisiae plasma membrane. Eukaryotic Cell **2010**, 9(8):1184-92.

IF_{2010} = 3.395 times cited: 2 (WoS)

Research paper 4:

Stradalova V, Blazikova M, Grossmann G, Opekarová M, Tanner W, Malinsky J. Distribution of cortical endoplasmic reticulum determines positioning of endocytic events in yeast plasma membrane. PLoS ONE **2012**, 7(4): e35132. doi:10.1371/journal.pone.0035132.

IF_{2010} = 4.411

4.2. COMMENTS ON PRESENTED PUBLICATIONS

4.2.1. Research paper 1

Ultrastructural and nuclear antigen preservation after high-pressure freezing/freeze-substitution and low-temperature LR White embedding of HeLa cells

Transmission electron microscopy (TEM) is a powerful tool to observe cellular components in high resolution. However, the complicated sample processing for TEM is prone to artifacts generation, especially when the chemical fixation with aldehydes is applied (see also chapter 3.3.). Preservation of sample morphology and epitopes for immunogold labeling as close to native state as possible is crucial for correct interpretation of the biological data observed by TEM. Cryofixation of biological material together with low temperature resin embedding seem to be very promising in this regard.

We found a significant improvement of sample morphology when we applied high pressure freezing (HPF) followed by freeze substitution (FS) and low-temperature resin embedding instead of conventional chemical fixation. Moreover, we directly demonstrated the great positive impact of the HPF/FS method on epitope preservation for the on-section postembedding immunogold labeling. It was believed that the immunolabeling after cryofixation is in general higher than after chemical crosslinking. We performed a quantitative comparison of the immunolabeling signals resulting from chemical fixation and cryofixation-based protocols in the same resin for three different antigens. In all cases the labeling signal was several times higher in HPF/FS processed cells than in aldehyde crosslinked samples (Figure 11). The HPF/FS should be thus, if possible, the first method of choice in morphological as well as in immunolocalization studies. We took advantage of these findings in our next investigation of the yeast plasma membrane organization.

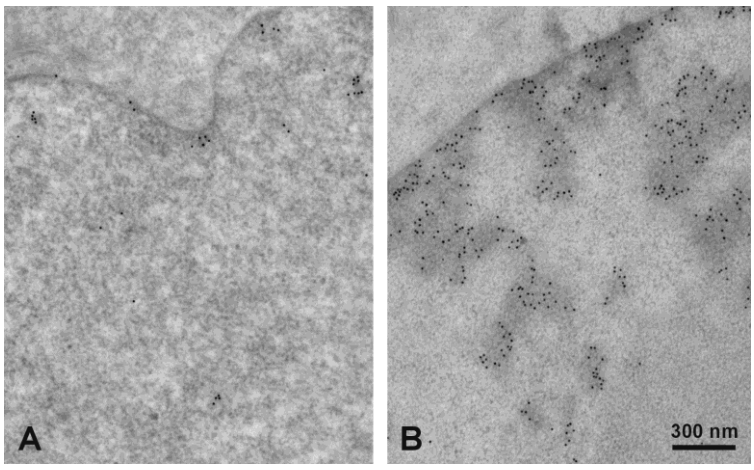

Figure 11. Elevated immunogold signal on HPF/FS cells.
Immunolocalization of DNA in HeLa cells embedded in LR White after chemical fixation **(A)** and after HPF and FS **(B)**. The increase in number of gold particles (black dots) on HPF/FS sample is evident. Note the difference in sample structure between HPF and chemically fixed cells.

4.2.2. Research paper 2

Furrow-like invaginations of the yeast plasma membrane correspond to membrane compartment of Can1

The membrane compartment occupied by Can1 (MCC) was the first stable lateral compartment described in the yeast plasma membrane that exhibited a specific protein and lipid composition. We were therefore interested whether this special plasma membrane domain was also connected with some specific membrane or cytosolic structure and decided to explore its ultrastructure using various TEM approaches.

By using a combination of freeze fracture/freeze etching and HPF/FS/ low temperature resin embedding we found that two yeast strains defective in MCC formation, *nce102Δ* and *pil1Δ*, lacked furrow-like plasma membrane invaginations. These membrane invaginations were known from early FF studies of WT yeast cells and remained uncharacterized for almost 50 years. As the distribution of the furrow-like invaginations resembled the pattern of MCC, except the density of MCC under confocal microscope being 2-fold lower, we tried to figure out whether MCC could be identical with the membrane furrows. At first, we wondered whether the lower density of MCC in confocal microscope as compared to density of furrows on FF replicas could be caused simply by confocal fluorescence imaging. With the help of computer modeling of furrow pattern blurred by confocal imaging (convolved with 2D PSF) we demonstrated that both densities were comparable. Next, we also noticed that on ultrathin resin sections the invaginations never overlapped with the cisternae of cortical endoplasmic reticulum (ER). When we co-expressed the MCC fluorescent marker Sur7-mRFP with the luminal ER marker ss-GFP-HDEL, we could say also the same for the MCC: MCC patches localized either to ER-free plasma membrane (PM) regions or to ER fluorescence minima. As a next step, we explored mutant yeast strains *ypr050cΔ* and *mak3Δ* (both lacking gene *MAK3*) in which the Sur7-GFP labeled MCC patches were abnormally elongated. The TEM analysis of the mutant cells showed that the furrow-like membrane invaginations were elongated to the same extent as the MCC patches observed under the confocal microscope (Figure 12). Finally, we also succeeded to localize the MCC and eisosome markers Sur7-GFP and Pil1-GFP, respectively, to furrow-like plasma membrane invaginations with the help of immunogold pre- and post-embedding labeling techniques. In addition, our results suggested that the positions of both immunodetected proteins along the invagination profile slightly differ. The eisosomal marker Pil1 appeared to localize only to the negatively curved bottom

part of the invagination whereas the transmembrane MCC marker Sur7 was observed more often at the positively curved rim of the furrow. Taken together, we could conclude that we finally characterized the mysterious furrow-like membrane invaginations as we unequivocally showed that they correspond to MCC plasma membrane domains. In other words, we showed that a stable lateral plasma membrane domain possesses a specific membrane structure. As membrane invaginations almost identical to the yeast furrows have been observed in many organisms including bacteria, other fungi, green algae and even higher plants, the described membrane arrangement can reflect a general principle of plasma membrane organization.

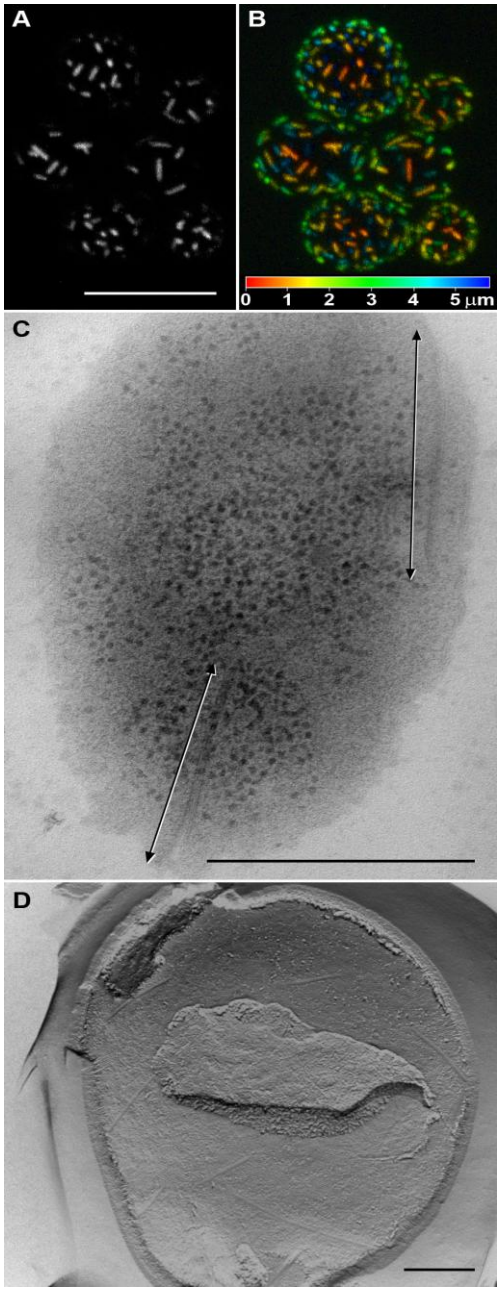

Figure 12. MCC pattern and furrow-like invaginations in *ypr050c*Δ cells. Comparison of cell surface distributions of MCC patches (labeled with Sur7-GFP; A,B) and the furrow-like invaginations of the plasma membrane (C,D) in *ypr050c*Δ mutant. Superposition of four consecutive confocal sections (A), depth-coded 3D stack covering whole confocally sectioned cells (B), tangential ultrathin section following HM20 embedding (C) and a view of a freeze-fracture face of the inner leaflet of the plasma membrane (P face; D) are presented. The position of two furrow-like invaginations is indicated in C (arrows). Scale bars: 5 µm (A,B), 500 nm (C,D).

4.2.3. Research paper 3

C terminus of Nce102 determines the structure and function of microdomains in the Saccharomyces cerevisiae plasma membrane

We showed that the *nce102Δ* cells are defective in segregation of specific MCC constituents and they also lack the furrow-like plasma membrane invaginations. Nce102p thus seemed to be an important MCC constituent and we therefore aimed to explore its molecular function.

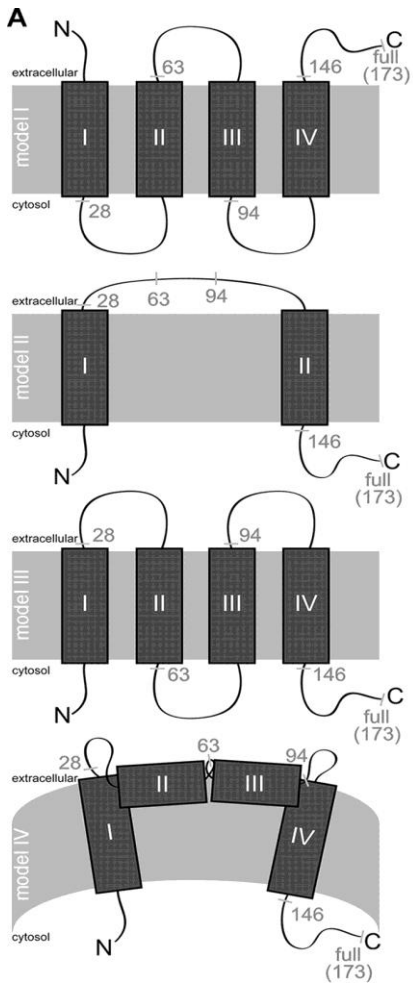

Figure 13. Nce102 topology.

Predicted (I) and experimentally determined (II, III, and IV) topology alternatives for the Nce102 molecule. Sites used for the synthesis of Nce102 truncated versions are depicted.

We found proteins sharing homology with the *S. cerevisiae* Nce102p throughout *Ascomycota* and as the first step we tested close and distant Nce102 homologs for their ability to localize to MCC and to substitute Nce102p in tethering Can1 transporter into MCC. The closest homolog of Nce102p present in *S. cerevisiae* genome, Ygr131w (we named it Fhn1: http://www.yeastgenome.org/cgi-bin/locus.fpl?locus=fhn1), was able to accumulate in MCC and also to redirect Can1-GFP protein back to MCC when overexpressed in *nce102 Δ* strain. The distant Nce102 ortholog from *Schizosaccharomyces pombe*, *Sp*Fhn1 (http://old.genedb.org/genedb/Search?submit=Search+for&name=fhn1&organism=pombe&desc=yes&wildcard=yes), behaved similarly. We therefore named both newly characterized proteins "Functional Homolog of Nce102" and concluded that the function of Nce102p in PM organization is probably conserved in *Ascomycota*.

As a substantial degree of conservation among Nce102 homologs can be found in highly hydrophobic regions of the protein we decided to determine the Nce102 membrane topology experimentally using the HA/Suc2/His4C reporter assay in order to have a better

idea how this protein functions in the membrane. Nce102p was predicted to posses 4 transmembrane domains (TMDs) with its N- and C-termini facing the cell exterior whereas another MCC predicted tetraspanner, Sur7p, should have an opposite orientation with both termini oriented towards the cytoplasm. Whilst the assay fully confirmed the predicted topology of Sur7p having four TMDs and both termini oriented towards the cytoplasm, the Nce102p behaved differently. Firstly, the assay showed that the N- and C-terminus of Nce102p are oriented towards cytosol and not outside the cell as predicted. At the same time the experiment suggested that the Nce102p possessed only 2 TM domains with the whole central region of the protein facing cell exterior. The topology reporter is quite bulky and the studied Nce102 protein rather small so we next performed additional analysis with insertion of shorter glycosylation sequences into the middle part of Nce102 protein to see whether this protein section is really exposed to ER lumen/cell exterior. This experiment suggested that the middle hydrophobic part of Nce102p was only partially immersed in the plane of the plasma membrane (Figure 13). Even though we cannot exclude the possibility that Nce102p possesses all four complete transmembrane domains, due to the method imperfection, we suggest that the Nce102 topological model with the middle section only partially embedded in the outer PM leaflet is physiologically relevant. This topology endows the protein with certain flexibility to fulfill its functions and in addition, our data show that the structure of the Nce102p could correspond to a so called “hairpin” structure that has been described at a variety of membrane-shaping proteins like reticulons, reggie/flotillin or caveolin (Bauer and Pelkmans, 2006).

We further revealed that the C-terminal part of Nce102p has an essential importance for the function of the Nce102p in the plasma membrane organization. Upon deletion of the whole C-terminal cytosolic region of Nce102p its accumulation in MCC was lost and Can1-GFP transporter was either no longer concentrated in this PM domain. The same phenotype was observed after deletion of only 6 amino acids from the very C-terminus of the Nce102p. Freeze fracture analysis of the strain expressing the C-terminally truncated Nce102 protein version then showed that the formation of furrow-like membrane invaginations was abolished as well. Notably, this part of the Nce102 protein is also highly conserved among Nce102 homologs.

4.2.4. Research paper 4

Distribution of cortical endoplasmic reticulum determines positioning of endocytic events in yeast plasma membrane

Our observation that MCC/eisosome and cortical ER do not overlap (see paper 2, chapter 4.2.2.) stimulated us to explore the situation in the yeast cell cortex more carefully.

Foremost, we wondered whether the close association of cortical ER with the plasma membrane could influence functional organization of the plasma membrane. We checked whether the whole MCP area is accessible for clathrin-mediated endocytosis or whether the cortical ER can act as a spatial hindrance for vesicular trafficking. Indeed, the coexpression of early endocytic marker Ede1-GFP with ER luminal marker ss-dsRed-HDEL revealed that endocytic sites originate preferentially in the PM areas that are not covered with the cortical ER. Control experiments and quantification of all colocalization data then showed that MCC/eisosome, endocytic sites and cortical ER occupy three distinct plasma membrane domains. As the cortical ER network continuously rearranges we were further interested how the ER dynamics influences the functional partitioning of the plasma membrane. Time-lapse experiments revealed the coexistence of micron-sized plasma membrane domains that differed in their association with cortical ER. Some parts of the plasma membrane were covered with the cortical ER network for a longer time and some were more often free of this coverage and thus more predisposed for vesicular transport. We concluded that cortical ER is involved in a functional compartmentalization of the plasma membrane as it delimits the regions of the PM where the communication with the cytosol can occur (Figure 14).

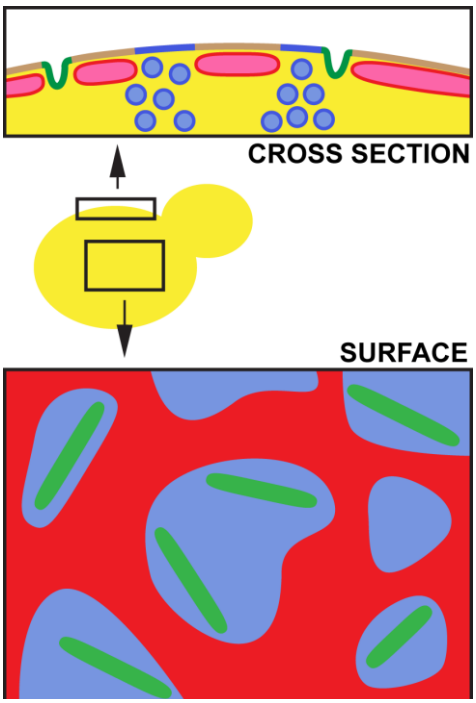

Figure 14.
Model of functional plasma membrane compartmentalization in yeast.

Three distinct domains can be distinguished in the yeast PM: stable MCC domains (green) surrounded by a membrane covered with a dynamic network of cortical ER (red) and the PM free of cortical ER coverage (blue). Vesicle transport can take place only in the ER-free PM.

The only stable parts of the plasma membrane in our study were the endocytosis-inactive MCC patches. As the MCC/eisosomes are invaginated and thus they extend to the space where also the cortical ER spreads we next asked whether the MCC/eisosomes have some influence on cortical ER distribution beneath the plasma membrane. To this end, we compared the cortical ER patterns in WT and in MCC/eisosome mutant strains *pil1Δ* and *nce102Δ*. The cortical ER network in *nce102Δ* strain, where the MCC/eisosome area is not invaginated, did not seem to be significantly affected. On the contrary, the disruption of the whole MCC/eisosome structure in *pil1Δ* strain led to a significant redistribution of the cortical ER. The cortical ER network in *pil1Δ* cells became more compact, less tubular and was broken with lower number of bigger holes. The observations from confocal microscope were confirmed by an ultrastructural TEM analysis. On the other hand, the overexpression of Pil1 protein that leads to more eisosomes formed on the plasma membrane resulted in more broken cortical ER pattern. It thus seems that the regular distribution of cortical ER along the cell periphery depends on the eisosome presence at the plasma membrane, irrespective of the fact how much the membrane area is invaginated. The sequestration of MCC marker Sur7, cortical ER and Ede1 into three distinct plasma membrane domains was preserved in both mutant strains and also the rate of cortical ER movement beneath the plasma membrane was not significantly changed in the MCC mutants. The proper formation of MCC/eisosome controlled by Pil1 protein thus regulates the distribution of the cortical ER network beneath the plasma membrane and this way it also controls the plasma membrane areas accessible for endocytosis.

4.3. MY CONTRIBUTION TO PRESENTED PUBLICATIONS

***Research paper 1**:*

I worked on the establishment of the HPF/FS protocol, processed the samples for TEM, performed the postembedding immunogold labeling with anti-lamin A and anti-LAP2α antibodies, analyzed the immunolabeling data, prepared all figures for publication, wrote the manuscript and participated on the article revision.

***Research paper 2**:*

I performed all the HPF/FS and low-temperature resin embedding experiments, including the serial sectioning, optimized and performed the postembedding immunogold labeling, analyzed the freeze fracture samples of the *ypr050cΔ* strain and participated on the confocal microscopic analysis of the *ypr050cΔ* and *mak3Δ* cells.

***Research paper 3**:*

I constructed some of the plasmids, performed and analyzed the overexpression experiments with the Nce102-homologs, determined the topology of Sur7 protein and participated on the assessment of the expression levels of truncated Nce102p variants.

***Research paper 4**:*

I prepared most of the plasmids and yeast strains, performed all the confocal laser scanning microscopy and data analysis, performed major part of the spinning disk confocal microscopy imaging, processed and analyzed the samples for TEM, wrote major part of the manuscript, prepared some of the figures and worked on the revision of the manuscript.

5. GENERAL DISCUSSION AND PERSPECTIVES

Elucidation of molecular principles that drive organization of the plasma membrane is a subject of an intensive recent research. We ascribed a specific ultrastructure to a well defined plasma membrane domain and finally solved the mystery of the yeast furrow-like plasma membrane invaginations:

The furrow-like invaginations remained uncharacterized for almost 50 years and even if it was predictable that they should contain specific lipid/protein composition, it was only our work which unraveled their identity as we unequivocally demonstrated that the furrows are equivalent with the Membrane Compartment occupied by Can1, MCC. Two years later, the fine structure of finger-like invaginations involved in clathrin-mediated endocytosis has been also solved with the use of cryofixation and freeze substitution (Kukulski et al, 2011) which together with our findings finally explained the difference between MCC and canonical endocytic sites even on ultrastructural level. The usage of cryofixation and freeze substitution turned out to be critical for preservation of the yeast plasma membrane for electron microscopy studies because chemically fixed yeast cells exhibited an altered fine structure of the plasma membrane. The identification of MCC with furrow-like invagiantions helped to clarify the striking stability of the MCC/eisosome patches as it was clear that such a big and complicated structure like 300 nm long membrane invagination would not be mobile. Our experiments further suggested how the Nce102p contributes to the MCC membrane curvature and furrow formation. Deletion of the Nce102p or its C-terminal part leads to flattening of the MCC membrane area and the topology determination assay showed that Nce102p could adopt a double-hairpin structure similar to reticulons that curve the membrane like a wedge (Shibata et al, 2009).

Our immunolocalization data that localized the main MCC/eisosome organizator Pil1p to the bottom tip of the furrow were recently confirmed by two groups that solved the 3D conformation of Pil1 and Lsp1 proteins and demonstrated that both main eisosomal constituents contain BAR domains (Olivera-Couto et al, 2011; Ziolkowska et al, 2011). Proteins possessing various types of BAR domains dimerize and these dimers further interact to form higher-order aggregates. They have the ability to bind curved membrane areas or even to impose curvature to the bound membrane (Masuda & Mochizuki, 2010). Indeed, Pil1 and Lsp1 were shown to bind and tubulate liposomes (Karotki et al, 2011; Olivera-Couto et al, 2011) and to form higher-order lattices on membranes (Karotki et al, 2011). The estimated

copy numbers of Pil1p and Lsp1p per cell are higher than those of tubulin or actin so that the self-assembled eisosomal protein scaffold was proposed to represent a new kind of membrane cytoskeleton that organizes the apposed MCC membrane area (Karotki et al, 2011). However, more work will be needed to elucidate the influence of the phosphorylation status on the conformation and function of Pil1 and Lsp1 proteins in eisosomes and to clarify the exact positioning and functional relevance of the Nce102p in MCC. Moreover, recently published data suggest that another eisosomal component, the essential protein pair Slm1/2, probably also contains a subtype of a BAR motif, the F-BAR domain, in addition to a PH domain. Both domains, PH and F-BAR, are necessary to target Slm proteins to eisosomes (Olivera-Couto et al, 2011). The Slm1/2 proteins were also shown to be important for eisosome integrity (Kamble et al, 2011) and it will be thus interesting to explore their involvement in the MCC/eisosome formation and function.

Freeze fracture studies showed that furrow-like membrane invaginations are present in many organisms which suggested that this type of cortical/ plasma membrane structure could be highly conserved. Consistently with this assumption, MCC/eisosome complexes were detected in other fungal species in the last few years including *Candida albicans* (Alvarez et al, 2008; Alvarez et al, 2009; Reijnst et al, 2011), *Aspergillus nidulans* (Vangelatos et al, 2010), *Ashbya gossypii* (Seger et al, 2011) and *Schizosaccharomyces pombe* (Kabeche et al, 2011). These fungi differ in some aspects from the MCC/eisosomes in *S. cerevisiae*, with most differences being found in the more distantly related species like Aspergilli (Vangelatos et al, 2010). Consistently with the situation in *S. cerevisiae*, homologs of Pil1p are important for proper formation of MCC/eisosomes in all studied fungi. The *A. gossypii* Pil1 regulates also the polar growth (Seger et al, 2011) and the *C. albicans* Pil1p is probably even essential for cell viability (Reijnst et al, 2011). In all the studied species the MCC/eisosomes were absent in the membrane areas exhibiting active membrane growth and turnover like bud and hyphae tips (Alvarez et al, 2008; Vangelatos et al, 2010; Reijnst et al, 2011; Seger et al, 2011) or growing ends and cytokinesis plane in *S. pombe* (Kabeche et al, 2011). They were also never colocalized with sites of canonical endocytosis. The MCC/eisosome presence seems to be important in spores because in both filamentous fungi, *A. nidulans* and *A. gossypii*, the MCC/eisosomal components were expressed more in spores than in hyphae (Vangelatos et al, 2010; Seger et al, 2011). In agreement with this, the Nce102 homolog in *Aspergillus fumigatus* has been shown to be important for normal sporulation (Khalaj et al, 2012). Also in *S. pombe*, a special variant of *Sp*Pil1 protein, *Sp*Pil2, is expressed only in spores and not in

vegetatively growing cells (Kabeche et al, 2011). In *S. cerevisiase*, the MCC/eisosome behavior during sporulation was not systematically explored so far but it was shown that the *sur7Δ* cells exhibited a reduced efficiency of sporulation. The Sur7-GFP signal was observed only in the ascus membrane but not in the membrane of spores (Young et al, 2002).

Our ultrastructural data propose that MCC/eisosomes should form special invaginated furrows in the plasma membrane. Even if the freeze fracture plasma membrane pattern is not available for all the fungal species where MCC/eisosomes were described (and *vice versa* – it is not known whether MCC/eisosomes are present in all organisms in which the furrows were observed) the recent research on the rod-shaped fission yeast *Schizosaccharomyces pombe* strongly supports this rule. The MCC/eisosomes in this organism are highly elongated (about 1μm long), they do not exhibit any preferred orientation in respect to the growth axis and are more abundant in stationary cells (Kabeche et al, 2011). All these features nicely correlate with the known pattern of furrow-like invaginations detected in this yeast (Walther et al, 1984; Takeo, 1985; Konomi et al, 2003; Osumi et al, 2006). Surprisingly, the length of the furrows seems to be regulated by the cellular context because the expression of budding yeast *Sc*Pil1 variant in the *pil1Δpil2Δ S. pombe* cells led to formation of long eisosomes and the expression of fission yeast *Sp*Pil1 variant in *S. cerevisiae* produced punctate eisosomal pattern (Kabeche et al, 2011). In this regard it will be interesting to explore the role of N-terminal protein acetylation in MCC/eisosome regulation as we detected significantly elongated MCC/eisosomes in S. cerevisiae *ypr050cΔ* or *mak3Δ* strains where the catalytic subunit of the N-terminal acetyltransferase C (NatC) complex is missing. This protein modification was shown to be necessary to target Arl3 GTPase to Golgi (Behnia et al, 2004; Setty et al, 2004) and N-terminal acetylation can also serve as a degradation signal (Hwang et al, 2010). The level of phosphoinositides in the plasma membrane and/or the phosphorylation status of Pil1p might also be important (Walther et al, 2007; Luo et al, 2008; Frohlich et al, 2009; Karotki et al, 2011).

The *S. pombe* MCC/eisosomes exhibit another nice parallel with their budding yeast counterparts and it is the behavior of the Nce102 homolog *Sp*Fhn1. Not only does the *Sp*Fhn1p colocalize with the *Sp*Pil1 protein in the furrows but it is also important for the MCC/eisosome formation as the *fhn1Δ* cells exhibit aberrant *Sp*Pil1 pattern, similarly to *S. cerevisiae* (Grossmann et al, 2008; Frohlich et al, 2009; Kabeche et al, 2011). These results clarify our observation that the *Sp*Fhn1p was able to substitute the Nce102p when

heterologously expressed in the *S. cerevisiae nce102Δ* strain. In addition, they also support our conclusion that the function of Nce102-like proteins might be conserved in *Ascomycota*. On the contrary, the deletion of *A. gossypii NCE102* gene did not have any obvious effect on the localization of the *Ag*Pil1p in hyphae (Seger et al, 2011).

In contrast to a (relatively) well established involvement of Pil1/Lsp1 and Nce102-like proteins in MCC/eisosome generation, the roles of the MCC members from the Sur7 family seem to be less clear. The most extreme example of the Sur7 family divergence is the *S. pombe* Sur7 protein homolog which does not colocalize with the *Sp*Pil1 decorated eisosomes at all and localizes to the growing ends of the fission yeast cells instead (Kabeche et al, 2011). There are at least four proteins from the Sur7 family in S. cerevisiae, Sur7, Fmp45, Pun1 and Ynl194c, all of which localize to MCC (Young et al, 2002; Alvarez et al, 2008; Grossmann et al, 2008) but triple *sur7Δ fmp45Δ ynl194cΔ* (Young et al, 2002) or quadruple *sur7Δ fmp45Δ ynl194cΔ pun1Δ* (Alvarez et al, 2008) deletion mutants did not have any strong phenotype, except the slightly more rounded cell morphology in the quadruple mutant cells. This effect is caused by the absence of Pun1p because this protein has been shown to be important for proper cell wall (CW) synthesis. The *pun1Δ* cells were smaller, exhibited more rounded shape and had thinner CW with reduced β-glucan layer and aberrant outer CW mannoprotein layer. The mutant cells were also more sensitive to metal ion stress (Hosiner et al, 2011) and were defective in pseudohyphal growth (Xu et al, 2010). However, the role of the Sur7p which is the most abundant protein from the Sur7 family in the vegetatively growing cells is still unclear. Our immunolocalization studies showed that the Sur7p could be localized on the upper rim of the furrow-like membrane invagination. It will be interesting to explore whether this feature has some functional relevance. In contrast to the rather minor effect of deletion of the Sur7-like proteins in *S. cerevisiae*, deletion of the Sur7 homolog in the pathogenic yeast *Candida albicans* has a far more pronounced effect on the cell morphology. Cells lacking the *Ca*Sur7p have delocalized septins and actin and abnormal cell wall protrusions penetrating deep into the cytoplasm (Alvarez et al, 2008), their cell wall contains decreased levels of β-glucan and the cells are thus more sensitive to various CW-targeted antifungal agents (Bernardo & Lee, 2010; Wang et al, 2011). The mutant cells also have a problem to switch to hyphal growth and to form biofilms (Alvarez et al, 2008; Bernardo & Lee, 2010) which is consistent with lower virulence of the *Ca*Sur7 deletion strain (Bernardo & Lee, 2010; Douglas et al, 2012). All these findings concerning the plasma

membrane organization in fungi are thus also very important for the development of new antifungal agents (Baxter et al, 2011).

There are still many questions concerning the functions of the MCC/eisosomes in the cell. We suggested one possible role for MCC/eisosome when we showed that MCC/eisosomes are involved in the distribution of cortical endoplasmic reticulum along the cell periphery. The deletion of the main eisosomal constituent Pil1p leads to an aberrant cortical ER morphology. This in turn has also an impact on the functional organization of the plasma membrane as we also demonstrated that the presence of the cortical ER in close vicinity to the plasma membrane influences the dynamic processes in the plasma membrane and its communication with the cytosol. Thus, we showed that the organization of the plasma membrane can be driven not only by protein scaffolds and fences but also by the whole cellular organelle like endoplasmic reticulum. Our findings nicely document how the cellular processes are all interconnected.

6. CONCLUSIONS

This work contributed to the knowledge about the organization of the yeast plasma membrane. Identification of the membrane compartment of Can1, MCC, with the furrow-like membrane invaginations was a major breakthrough in the understanding of the MCC/eisosome structure and stability. Elucidation of the Nce102p topology and reconciling its structural function then revealed a mechanism by which the Nce102 protein contributes to furrow formation. We showed that the function of Nce102p is conserved in other fungi and that this could reflect a general mechanism of membrane organization. We also suggested a role for the MCC/eisosomes in the functional compartmentalization of the plasma membrane via the regulation of the distribution of cortical endoplasmic reticulum along the cell periphery. Our findings already stimulated further research that helped to unravel additional details about MCC/eisosome formation and regulation.

7. REFERENCES

Aghamohammadzadeh S, Ayscough KR (2009) Differential requirements for actin during yeast and mammalian endocytosis. Nat Cell Biol 11(8): 1039-1042

Aicart-Ramos C, Valero RA, Rodriguez-Crespo I (2011) Protein palmitoylation and subcellular trafficking. Biochimica et Biophysica Acta (BBA) - Biomembranes 1808(12): 2981-2994

Alvarez FJ, Douglas LM, Konopka JB (2009) The Sur7 protein resides in punctate membrane subdomains and mediates spatial regulation of cell wall synthesis in Candida albicans. Communicative & Integrative Biology 2(2): 76-77

Alvarez FJ, Douglas LM, Rosebrock A, Konopka JB (2008) The Sur7 Protein Regulates Plasma Membrane Organization and Prevents Intracellular Cell Wall Growth in Candida albicans. Molecular Biology of the Cell 19(12): 5214-5225

Aresta-Branco F, Cordeiro AM, Marinho HS, Cyrne L, Antunes F, de Almeida RFM (2011) Gel Domains in the Plasma Membrane of Saccharomyces cerevisiae. Journal of Biological Chemistry 286(7): 5043-5054

Bagatolli LA, Ipsen JH, Simonsen AC, Mouritsen OG (2010) An outlook on organization of lipids in membranes: Searching for a realistic connection with the organization of biological membranes. Progress in Lipid Research 49(4): 378-389

Bagnat M, Keranen S, Shevchenko A, Shevchenko A, Simons K (2000) Lipid rafts function in biosynthetic delivery of proteins to the cell surface in yeast. Proceedings of the National Academy of Sciences 97(7): 3254-3259

Bauer M, Pelkmans L (2006) A new paradigm for membrane-organizing and -shaping scaffolds. FEBS Letters 580(23): 5559-5564

Baumann O, Walz B (2001) Endoplasmic reticulum of animal cells and its organization into structural and functional domains. Int Rev Cytol 205: 149-214

Baxter BK, DiDone L, Ogu D, Schor S, Krysan DJ (2011) Identification, in Vitro Activity and Mode of Action of Phosphoinositide-Dependent-1 Kinase Inhibitors as Antifungal Molecules. ACS Chemical Biology 6(5): 502-510

Behnia R, Panic B, Whyte JRC, Munro S (2004) Targeting of the Arf-like GTPase Arl3p to the Golgi requires N-terminal acetylation and the membrane protein Sys1p. Nat Cell Biol 6(5): 405-413

Berchtold D, Walther TC (2009) TORC2 plasma membrane localization is essential for cell viability and restricted to a distinct domain. Mol Biol Cell 20(5): 1565-1575

Bernardo S, Lee S (2010) Candida albicans SUR7 contributes to secretion, biofilm formation, and macrophage killing. BMC Microbiology 10(1): 133

Bevis BJ, Hammond AT, Reinke CA, Glick BS (2002) De novo formation of transitional ER sites and Golgi structures in Pichia pastoris. Nat Cell Biol 4(10): 750-756

Boettner DR, D'Agostino JL, Torres OT, Daugherty-Clarke K, Uygur A, Reider A, Wendland B, Lemmon SK, Goode BL (2009) The F-BAR Protein Syp1 Negatively Regulates WASp-Arp2/3 Complex Activity during Endocytic Patch Formation. Current Biology 19(23): 1979-1987

Boettner DR, Chi RJ, Lemmon SK (2012) Lessons from yeast for clathrin-mediated endocytosis. Nat Cell Biol 14(1): 2-10

Bonifacino JS, Traub LM (2003) Signals for sorting of transmembrane proteins to endosomes and lysosomes. Annual Review of Biochemistry 72(1): 395-447

Brach T, Specht T, Kaksonen M (2011) Reassessment of the role of plasma membrane domains in the regulation of vesicular traffic in yeast. J Cell Sci 124(Pt 3): 328-337

Brown DA, London E (1998) Functions of lipid rafts in biological membranes. Annual Review of Cell and Developmental Biology 14(1): 111-136

Brown DA, Rose JK (1992) Sorting of GPI-anchored proteins to glycolipid-enriched membrane subdomains during transport to the apical cell surface. Cell 68(3): 533-544

Conibear E (2010) Converging views of endocytosis in yeast and mammals. Current Opinion in Cell Biology 22(4): 513-518

De Craene JO, Coleman J, Estrada de Martin P, Pypaert M, Anderson S, Yates JR, 3rd, Ferro-Novick S, Novick P (2006) Rtn1p is involved in structuring the cortical endoplasmic reticulum. Mol Biol Cell 17(7): 3009-3020

Deak PM, Wolf DH (2001) Membrane Topology and Function of Der3/Hrd1p as a Ubiquitin-Protein Ligase (E3) Involved in Endoplasmic Reticulum Degradation. Journal of Biological Chemistry 276(14): 10663-10669

Deng C, Xiong X, Krutchinsky AN (2009) Unifying fluorescence microscopy and mass spectrometry for studying protein complexes in cells. Mol Cell Proteomics 8(6): 1413-1423

Dickson RC, Lester RL (2002) Sphingolipid functions in Saccharomyces cerevisiae. Biochimica et Biophysica Acta (BBA) - Molecular and Cell Biology of Lipids 1583(1): 13-25

Doherty GJ, McMahon HT (2009) Mechanisms of endocytosis. Annu Rev Biochem 78: 857-902

Douglas LM, Wang HX, Keppler-Ross S, Dean N, Konopka JB (2012) Sur7 Promotes Plasma Membrane Organization and Is Needed for Resistance to Stressful Conditions and to the Invasive Growth and Virulence of Candida albicans. mBio 3(1)

Du Y, Ferro-Novick S, Novick P (2004) Dynamics and inheritance of the endoplasmic reticulum. J Cell Sci 117(Pt 14): 2871-2878

Du Y, Pypaert M, Novick P, Ferro-Novick S (2001) Aux1p/Swa2p is required for cortical endoplasmic reticulum inheritance in Saccharomyces cerevisiae. Mol Biol Cell 12(9): 2614-2628

Du Y, Walker L, Novick P, Ferro-Novick S (2006) Ptc1p regulates cortical ER inheritance via Slt2p. EMBO J 25(19): 4413-4422

Dupré S, Haguenauer-Tsapis R (2003) Raft Partitioning of the Yeast Uracil Permease During Trafficking Along the Endocytic Pathway. Traffic 4(2): 83-96

Dupuy AD, Engelman DM (2008) Protein area occupancy at the center of the red blood cell membrane. Proceedings of the National Academy of Sciences 105(8): 2848-2852

Eggeling C, Ringemann C, Medda R, Schwarzmann G, Sandhoff K, Polyakova S, Belov VN, Hein B, von Middendorff C, Schonle A, Hell SW (2009) Direct observation of the nanoscale dynamics of membrane lipids in a living cell. Nature 457(7233): 1159-1162

Ehrlich M, Boll W, van Oijen A, Hariharan R, Chandran K, Nibert ML, Kirchhausen T (2004) Endocytosis by Random Initiation and Stabilization of Clathrin-Coated Pits. Cell 118(5): 591-605

Ejsing CS, Sampaio JL, Surendranath V, Duchoslav E, Ekroos K, Klemm RW, Simons K, Shevchenko A (2009) Global analysis of the yeast lipidome by quantitative shotgun mass spectrometry. Proceedings of the National Academy of Sciences 106(7): 2136-2141

Engelman DM (2005) Membranes are more mosaic than fluid. Nature 438(7068): 578-580

Ercan E, Momburg F, Engel U, Temmerman K, Nickel W, Seedorf M (2009) A conserved, lipid-mediated sorting mechanism of yeast Ist2 and mammalian STIM proteins to the peripheral ER. Traffic 10(12): 1802-1818

Estrada de Martin P, Du Y, Novick P, Ferro-Novick S (2005a) Ice2p is important for the distribution and structure of the cortical ER network in Saccharomyces cerevisiae. J Cell Sci 118(Pt 1): 65-77

Estrada de Martin P, Novick P, Ferro-Novick S (2005b) The organization, structure, and inheritance of the ER in higher and lower eukaryotes. Biochem Cell Biol 83(6): 752-761

Estrada P, Kim J, Coleman J, Walker L, Dunn B, Takizawa P, Novick P, Ferro-Novick S (2003) Myo4p and She3p are required for cortical ER inheritance in Saccharomyces cerevisiae. J Cell Biol 163(6): 1255-1266

Fehrenbacher KL, Davis D, Wu M, Boldogh I, Pon LA (2002) Endoplasmic reticulum dynamics, inheritance, and cytoskeletal interactions in budding yeast. Mol Biol Cell 13(3): 854-865

Ferguson S, Raimondi A, Paradise S, Shen H, Mesaki K, Ferguson A, Destaing O, Ko G, Takasaki J, Cremona O, O' Toole E, De Camilli P (2009) Coordinated Actions of Actin and BAR Proteins Upstream of Dynamin at Endocytic Clathrin-Coated Pits. Developmental Cell 17(6): 811-822

Fischer MA, Temmerman K, Ercan E, Nickel W, Seedorf M (2009) Binding of plasma membrane lipids recruits the yeast integral membrane protein Ist2 to the cortical ER. Traffic 10(8): 1084-1097

Friant S, Lombardi R, Schmelzle T, Hall MN, Riezman H (2001) Sphingoid base signaling via Pkh kinases is required for endocytosis in yeast. EMBO J 20(23): 6783-6792

Friedman JR, Webster BM, Mastronarde DN, Verhey KJ, Voeltz GK (2010) ER sliding dynamics and ER-mitochondrial contacts occur on acetylated microtubules. J Cell Biol 190(3): 363-375

Frohlich F, Moreira K, Aguilar PS, Hubner NC, Mann M, Walter P, Walther TC (2009) A genome-wide screen for genes affecting eisosomes reveals Nce102 function in sphingolipid signaling. J Cell Biol 185(7): 1227-1242

Furuse M (2010) Molecular Basis of the Core Structure of Tight Junctions. Cold Spring Harbor Perspectives in Biology 2(1)

Gaidarov I, Santini F, Warren RA, Keen JH (1999) Spatial control of coated-pit dynamics in living cells. Nat Cell Biol 1(1): 1-7

Galletta BJ, Mooren OL, Cooper JA (2010) Actin dynamics and endocytosis in yeast and mammals. Current Opinion in Biotechnology 21(5): 604-610

Georgiev AG, Sullivan DP, Kersting MC, Dittman JS, Beh CT, Menon AK (2011) Osh Proteins Regulate Membrane Sterol Organization but Are Not Required for Sterol Movement Between the ER and PM. Traffic 12(10): 1341-1355

Grant BD, Donaldson JG (2009) Pathways and mechanisms of endocytic recycling. Nat Rev Mol Cell Biol 10(9): 597-608

Grossmann G, Malinsky J, Stahlschmidt W, Loibl M, Weig-Meckl I, Frommer WB, Opekarova M, Tanner W (2008) Plasma membrane microdomains regulate turnover of transport proteins in yeast. J Cell Biol 183(6): 1075-1088

Grossmann G, Opekarova M, Malinsky J, Weig-Meckl I, Tanner W (2007) Membrane potential governs lateral segregation of plasma membrane proteins and lipids in yeast. EMBO J 26(1): 1-8

Hartman NaC, Groves JT (2011) Signaling clusters in the cell membrane. Current Opinion in Cell Biology 23(4): 370-376

He H-T, Marguet D (2011) Detecting Nanodomains in Living Cell Membrane by Fluorescence Correlation Spectroscopy. Annual Review of Physical Chemistry 62(1): 417-436

Henne WM, Boucrot E, Meinecke M, Evergren E, Vallis Y, Mittal R, McMahon HT (2010) FCHo Proteins Are Nucleators of Clathrin-Mediated Endocytosis. Science 328(5983): 1281-1284

Ho Y, Gruhler A, Heilbut A, Bader GD, Moore L, Adams S-L, Millar A, Taylor P, Bennett K, Boutilier K, Yang L, Wolting C, Donaldson I, Schandorff S, Shewnarane J, Vo M, Taggart J, Goudreault M, Muskat B, Alfarano C, Dewar D, Lin Z, Michalickova K, Willems AR, Sassi H, Nielsen PA, Rasmussen KJ, Andersen JR, Johansen LE, Hansen LH, Jespersen H, Podtelejnikov A, Nielsen E, Crawford J, Poulsen V, Sorensen BD, Matthiesen J, Hendrickson RC, Gleeson F, Pawson T, Moran MF, Durocher D, Mann M, Hogue CWV, Figeys D, Tyers M (2002) Systematic identification of protein complexes in Saccharomyces cerevisiae by mass spectrometry. Nature 415(6868): 180-183

Holthuis JC, Levine TP (2005) Lipid traffic: floppy drives and a superhighway. Nat Rev Mol Cell Biol 6(3): 209-220

Hosiner D, Sponder G, Graschopf A, Reipert S, Schweyen RJ, Schuller C, Aleschko M (2011) Pun1p is a metal ion-inducible, calcineurin/Crz1p-regulated plasma membrane protein required for cell wall integrity. Biochimica et Biophysica Acta (BBA) - Biomembranes 1808(4): 1108-1119

Howes MT, Mayor S, Parton RG (2010) Molecules, mechanisms, and cellular roles of clathrin-independent endocytosis. Current Opinion in Cell Biology 22(4): 519-527

Hu Q, Milenkovic L, Jin H, Scott MP, Nachury MV, Spiliotis ET, Nelson WJ (2010) A Septin Diffusion Barrier at the Base of the Primary Cilium Maintains Ciliary Membrane Protein Distribution. Science 329(5990): 436-439

Hwang C-S, Shemorry A, Varshavsky A (2010) N-Terminal Acetylation of Cellular Proteins Creates Specific Degradation Signals. Science 327(5968): 973-977

Chen X, Irani NG, Friml J (2011) Clathrin-mediated endocytosis: the gateway into plant cells. Current Opinion in Plant Biology 14(6): 674-682

Ipsen JH, Karlstrom G, Mouritsen OG, Wennerstrom H, Zuckermann MJ (1987) Phase equilibria in the phosphatidylcholine-cholesterol system. Biochim Biophys Acta 905(1): 162-172

Jacobson K, Mouritsen OG, Anderson RG (2007) Lipid rafts: at a crossroad between cell biology and physics. Nat Cell Biol 9(1): 7-14

Kabeche R, Baldissard S, Hammond J, Howard L, Moseley JB (2011) The filament-forming protein Pil1 assembles linear eisosomes in fission yeast. Molecular Biology of the Cell 22(21): 4059-4067

Kaksonen M, Toret CP, Drubin DG (2005) A modular design for the clathrin- and actin-mediated endocytosis machinery. Cell 123(2): 305-320

Kaksonen M, Toret CP, Drubin DG (2006) Harnessing actin dynamics for clathrin-mediated endocytosis. Nat Rev Mol Cell Biol 7(6): 404-414

Kamble C, Jain S, Murphy E, Kim K (2011) Requirements of Slm proteins for proper eisosome organization, endocytic trafficking and recycling in the yeast Saccharomyces cerevisiae. J Biosci 36(1): 79-96

Karotki L, Huiskonen JT, Stefan CJ, Ziolkowska NE, Roth R, Surma MA, Krogan NJ, Emr SD, Heuser J, GrĂĽnewald K, Walther TC (2011) Eisosome proteins assemble into a membrane scaffold. The Journal of Cell Biology 195(5): 889-902

Khalaj V, Azizi M, Enayati S, Khorasanizadeh D, Ardakani EM (2012) NCE102 homologue in Aspergillus fumigatus is required for normal sporulation, not hyphal growth or pathogenesis. FEMS Microbiology Letters 329(2): 138-145

Kiessling V, Wan C, Tamm LK (2009) Domain coupling in asymmetric lipid bilayers. Biochimica et Biophysica Acta (BBA) - Biomembranes 1788(1): 64-71

Kim H, Melen K, von Heijne G (2003a) Topology Models for 37 Saccharomyces cerevisiaeMembrane Proteins Based on C-terminal Reporter Fusions and Predictions. Journal of Biological Chemistry 278(12): 10208-10213

Kim H, Yan Q, von Heijne G, Caputo GA, Lennarz WJ (2003b) Determination of the membrane topology of Ost4p and its subunit interactions in the oligosaccharyltransferase complex in Saccharomyces cerevisiae. Proceedings of the National Academy of Sciences 100(13): 7460-7464

Kirchhausen T (2009) Imaging endocytic clathrin structures in living cells. Trends in Cell Biology 19(11): 596-605

Koning AJ, Lum PY, Williams JM, Wright R (1993) DiOC6 staining reveals organelle structure and dynamics in living yeast cells. Cell Motil Cytoskeleton 25(2): 111-128

Konomi M, Fujimoto K, Toda T, Osumi M (2003) Characterization and behaviour of α-glucan synthase in Schizosaccharomyces pombe as revealed by electron microscopy. Yeast 20(5): 427-438

Kopec KO, Alva V, Lupas AN (2010) Homology of SMP domains to the TULIP superfamily of lipid-binding proteins provides a structural basis for lipid exchange between ER and mitochondria. Bioinformatics 26(16): 1927-1931

Kornmann B, Currie E, Collins SR, Schuldiner M, Nunnari J, Weissman JS, Walter P (2009) An ER-mitochondria tethering complex revealed by a synthetic biology screen. Science 325(5939): 477-481

Kornmann Bt, Osman C, Walter P (2011) The conserved GTPase Gem1 regulates endoplasmic reticulumâ€“mitochondria connections. Proceedings of the National Academy of Sciences 108(34): 14151-14156

Kornmann Bt, Walter P (2010) ERMES-mediated ER-mitochondria contacts: molecular hubs for the regulation of mitochondrial biology. Journal of Cell Science 123(9): 1389-1393

Kukulski W, Schorb M, Welsch S, Picco A, Kaksonen M, Briggs JA (2011) Correlated fluorescence and 3D electron microscopy with high sensitivity and spatial precision. J Cell Biol 192(1): 111-119

Kusumi A, Shirai YM, Koyama-Honda I, Suzuki KGN, Fujiwara TK (2010) Hierarchical organization of the plasma membrane: Investigations by single-molecule tracking vs. fluorescence correlation spectroscopy. FEBS Letters 584(9): 1814-1823

Kusumi A, Suzuki KGN, Kasai RS, Ritchie K, Fujiwara TK (2011) Hierarchical mesoscale domain organization of the plasma membrane. Trends in Biochemical Sciences 36(11): 604-615

Kvam E, Goldfarb DS (2007) Nucleus-vacuole junctions and piecemeal microautophagy of the nucleus in S. cerevisiae. Autophagy 3(2): 85-92

Lauwers E, André B (2006) Association of Yeast Transporters with Detergent-Resistant Membranes Correlates with Their Cell-Surface Location. Traffic 7(8): 1045-1059

Lavieu G, Orci L, Shi L, Geiling M, Ravazzola M, Wieland F, Cosson P, Rothman JE (2010) Induction of cortical endoplasmic reticulum by dimerization of a coatomer-binding peptide anchored to endoplasmic reticulum membranes. Proc Natl Acad Sci U S A 107(15): 6876-6881

Lebiedzinska M, Szabadkai G, Jones AW, Duszynski J, Wieckowski MR (2009) Interactions between the endoplasmic reticulum, mitochondria, plasma membrane and other subcellular organelles. Int J Biochem Cell Biol 41(10): 1805-1816

Lee AG (2011) Biological membranes: the importance of molecular detail. Trends in Biochemical Sciences 36(9): 493-500

Lee C, Ferguson M, Chen LB (1989) Construction of the endoplasmic reticulum. J Cell Biol 109(5): 2045-2055

Lee C, Chen LB (1988) Dynamic behavior of endoplasmic reticulum in living cells. Cell 54(1): 37-46

Lemmon MA (2008) Membrane recognition by phospholipid-binding domains. Nat Rev Mol Cell Biol 9(2): 99-111

Leslie M (2011) Do Lipid Rafts Exist? Science 334(6059): 1046-1047

Levine T (2004) Short-range intracellular trafficking of small molecules across endoplasmic reticulum junctions. Trends Cell Biol 14(9): 483-490

Levine T, Loewen C (2006) Inter-organelle membrane contact sites: through a glass, darkly. Curr Opin Cell Biol 18(4): 371-378

Levine T, Rabouille C (2005) Endoplasmic reticulum: one continuous network compartmentalized by extrinsic cues. Curr Opin Cell Biol 17(4): 362-368

Levy S, Shoham T (2005) Protein-Protein Interactions in the Tetraspanin Web. Physiology 20(4): 218-224

Lingwood D, Simons K (2010) Lipid rafts as a membrane-organizing principle. Science 327(5961): 46-50

Liu J, Kaksonen M, Drubin DG, Oster G (2006) Endocytic vesicle scission by lipid phase boundary forces. Proc Natl Acad Sci U S A 103(27): 10277-10282

Loewen CJ, Young BP, Tavassoli S, Levine TP (2007) Inheritance of cortical ER in yeast is required for normal septin organization. J Cell Biol 179(3): 467-483

Luo G, Costanzo M, Boone C, Dickson RC (2011) Nutrients and the Pkh1/2 and Pkc1 Protein Kinases Control mRNA Decay and P-body Assembly in Yeast. Journal of Biological Chemistry 286(11): 8759-8770

Luo G, Gruhler A, Liu Y, Jensen ON, Dickson RC (2008) The sphingolipid long-chain base-Pkh1/2-Ypk1/2 signaling pathway regulates eisosome assembly and turnover. J Biol Chem 283(16): 10433-10444

Maass K, Fischer MA, Seiler M, Temmerman K, Nickel W, Seedorf M (2009) A signal comprising a basic cluster and an amphipathic alpha-helix interacts with lipids and is required for the transport of Ist2 to the yeast cortical ER. J Cell Sci 122(Pt 5): 625-635

Malinska K, Malinsky J, Opekarova M, Tanner W (2003) Visualization of protein compartmentation within the plasma membrane of living yeast cells. Mol Biol Cell 14(11): 4427-4436

Malinska K, Malinsky J, Opekarova M, Tanner W (2004) Distribution of Can1p into stable domains reflects lateral protein segregation within the plasma membrane of living S. cerevisiae cells. J Cell Sci 117(Pt 25): 6031-6041

Malinsky J, Opekarova M, Tanner W (2010) The lateral compartmentation of the yeast plasma membrane. Yeast 27(8): 473-478

Masuda M, Mochizuki N (2010) Structural characteristics of BAR domain superfamily to sculpt the membrane. Semin Cell Dev Biol 21(4): 391-398

McMahon HT, Boucrot E (2011) Molecular mechanism and physiological functions of clathrin-mediated endocytosis. Nat Rev Mol Cell Biol 12(8): 517-533

Mishra S, Joshi PG (2007) Lipid raft heterogeneity: an enigma. J Neurochem 103 Suppl 1: 135-142

Moreira KE, Walther TC, Aguilar PS, Walter P (2009) Pil1 controls eisosome biogenesis. Mol Biol Cell 20(3): 809-818

Mouritsen OG (2010) The liquid-ordered state comes of age. Biochimica et Biophysica Acta (BBA) - Biomembranes 1798(7): 1286-1288

Munro S (2003) Lipid rafts: elusive or illusive? Cell 115(4): 377-388

Murphy ER, Boxberger J, Colvin R, Lee SJ, Zahn G, Loor F, Kim K (2011) Pil1, an eisosome organizer, plays an important role in the recruitment of synaptojanins and amphiphysins to facilitate receptor-mediated endocytosis in yeast. Eur J Cell Biol 90(10): 825-833

Niemela PS, Miettinen MS, Monticelli L, Hammaren H, Bjelkmar P, Murtola T, Lindahl E, Vattulainen I (2010) Membrane proteins diffuse as dynamic complexes with lipids. J Am Chem Soc 132(22): 7574-7575

Oh Y, Bi E (2011) Septin structure and function in yeast and beyond. Trends in Cell Biology 21(3): 141-148

Olivera-Couto A, Grana M, Harispe L, Aguilar PS (2011) The eisosome core is composed of BAR domain proteins. Mol Biol Cell 22(13): 2360-2372

Orci L, Ravazzola M, Le Coadic M, Shen WW, Demaurex N, Cosson P (2009) From the Cover: STIM1-induced precortical and cortical subdomains of the endoplasmic reticulum. Proc Natl Acad Sci U S A 106(46): 19358-19362

Osumi M, Konomi M, Sugawara T, Takagi T, Baba M (2006) High-pressure freezing is a powerful tool for visualization of Schizosaccharomyces pombe cells: ultra-low temperature and low-voltage scanning electron microscopy and immunoelectron microscopy. Journal of Electron Microscopy 55(2): 75-88

Pan X, Roberts P, Chen Y, Kvam E, Shulga N, Huang K, Lemmon S, Goldfarb DS (2000) Nucleus-vacuole junctions in Saccharomyces cerevisiae are formed through the direct interaction of Vac8p with Nvj1p. Mol Biol Cell 11(7): 2445-2457

Parton RG, Hanzal-Bayer M, Hancock JF (2006) Biogenesis of caveolae: a structural model for caveolin-induced domain formation. J Cell Sci 119(Pt 5): 787-796

Parton RG, Simons K (2007) The multiple faces of caveolae. Nat Rev Mol Cell Biol 8(3): 185-194

Paulick MG, Bertozzi CR (2008) The glycosylphosphatidylinositol anchor: a complex membrane-anchoring structure for proteins. Biochemistry 47(27): 6991-7000

Perktold A, Zechmann B, Daum G, Zellnig G (2007) Organelle association visualized by three-dimensional ultrastructural imaging of the yeast cell. FEMS Yeast Res 7(4): 629-638

Pichler H, Gaigg B, Hrastnik C, Achleitner G, Kohlwein SD, Zellnig G, Perktold A, Daum G (2001) A subfraction of the yeast endoplasmic reticulum associates with the plasma membrane and has a high capacity to synthesize lipids. Eur J Biochem 268(8): 2351-2361

Prinz WA, Grzyb L, Veenhuis M, Kahana JA, Silver PA, Rapoport TA (2000) Mutants affecting the structure of the cortical endoplasmic reticulum in Saccharomyces cerevisiae. J Cell Biol 150(3): 461-474

Prosser DC, Drivas TG, Maldonado-Baez L, Wendland B (2011) Existence of a novel clathrin-independent endocytic pathway in yeast that depends on Rho1 and formin. The Journal of Cell Biology 195(4): 657-671

Rapoport TA, Goder V, Heinrich SU, Matlack KE (2004) Membrane-protein integration and the role of the translocation channel. Trends Cell Biol 14(10): 568-575

Reider A, Barker SL, Mishra SK, Im YJ, Maldonado-Baez L, Hurley JH, Traub LM, Wendland B (2009) Syp1 is a conserved endocytic adaptor that contains domains involved in cargo selection and membrane tubulation. EMBO J 28(20): 3103-3116

Reider A, Wendland B (2011) Endocytic adaptors - social networking at the plasma membrane. Journal of Cell Science 124(10): 1613-1622

Reijnst P, Walther A, Wendland J (2011) Dual-colour fluorescence microscopy using yEmCherry-/GFP-tagging of eisosome components Pil1 and Lsp1 in Candida albicans. Yeast 28(4): 331-338

Reinke CA, Kozik P, Glick BS (2004) Golgi inheritance in small buds of Saccharomyces cerevisiae is linked to endoplasmic reticulum inheritance. Proc Natl Acad Sci U S A 101(52): 18018-18023

Resh MD (2006) Trafficking and signaling by fatty-acylated and prenylated proteins. Nat Chem Biol 2(11): 584-590

Robertson A, Smythe E, Ayscough K (2009) Functions of actin in endocytosis. Cellular and Molecular Life Sciences 66(13): 2049-2065

Saffarian S, Cocucci E, Kirchhausen T (2009) Distinct dynamics of endocytic clathrin-coated pits and coated plaques. PLoS Biol 7(9): e1000191

Seger S, Rischatsch R, Philippsen P (2011) Formation and stability of eisosomes in the filamentous fungus Ashbya gossypii. Journal of Cell Science 124(10): 1629-1634

Setty SRG, Strochlic TI, Tong AHY, Boone C, Burd CG (2004) Golgi targeting of ARF-like GTPase Arl3p requires its N[alpha]-acetylation and the integral membrane protein Sys1p. Nat Cell Biol 6(5): 414-419

Shaw AS (2006) Lipid rafts: now you see them, now you don't. Nat Immunol 7(11): 1139-1142

Shevchenko A, Simons K (2010) Lipidomics: coming to grips with lipid diversity. Nat Rev Mol Cell Biol 11(8): 593-598

Shibata Y, Hu J, Kozlov MM, Rapoport TA (2009) Mechanisms shaping the membranes of cellular organelles. Annu Rev Cell Dev Biol 25: 329-354

Shibata Y, Shemesh T, Prinz WA, Palazzo AF, Kozlov MM, Rapoport TA (2010) Mechanisms determining the morphology of the peripheral ER. Cell 143(5): 774-788

Schulz TA, Choi MG, Raychaudhuri S, Mears JA, Ghirlando R, Hinshaw JE, Prinz WA (2009) Lipid-regulated sterol transfer between closely apposed membranes by oxysterol-binding protein homologues. J Cell Biol 187(6): 889-903

Sieber JJ, Willig KI, Kutzner C, Gerding-Reimers C, Harke B, Donnert G, Rammner B, Eggeling C, Hell SW, Grubmuller H, Lang T (2007) Anatomy and Dynamics of a Supramolecular Membrane Protein Cluster. Science 317(5841): 1072-1076

Simons K, Ikonen E (1997) Functional rafts in cell membranes. Nature 387(6633): 569-572

Simons K, van Meer G (1988) Lipid sorting in epithelial cells. Biochemistry 27(17): 6197-6202

Simons K, Vaz WLC (2004) Model systems, lipid rafts, and cell membranes. Annual Review of Biophysics and Biomolecular Structure 33(1): 269-295

Singer SJ, Nicolson GL (1972) The fluid mosaic model of the structure of cell membranes. Science 175(4023): 720-731

Sparkes IA, Frigerio L, Tolley N, Hawes C (2009) The plant endoplasmic reticulum: a cell-wide web. Biochem J 423(2): 145-155

Stimpson HE, Toret CP, Cheng AT, Pauly BS, Drubin DG (2009) Early-arriving Syp1p and Ede1p function in endocytic site placement and formation in budding yeast. Mol Biol Cell 20(22): 4640-4651

Strahl-Bolsinger S, Scheinost A (1999) Transmembrane Topology of Pmt1p, a Member of an Evolutionarily Conserved Family of Protein O-Mannosyltransferases. Journal of Biological Chemistry 274(13): 9068-9075

Studer D, Graber W, Al-Amoudi A, Eggli P (2001) A new approach for cryofixation by high-pressure freezing. J Microsc 203(Pt 3): 285-294

Sud M, Fahy E, Cotter D, Brown A, Dennis EA, Glass CK, Merrill AH, Murphy RC, Raetz CRH, Russell DW, Subramaniam S (2007) LMSD: LIPID MAPS structure database. Nucleic Acids Research 35(suppl 1): D527-D532

Tada T, Simonetta A, Batterton M, Kinoshita M, Edbauer D, Sheng M (2007) Role of Septin Cytoskeleton in Spine Morphogenesis and Dendrite Development in Neurons. Current Biology 17(20): 1752-1758

Takeo K (1985) A Correlation between Mode of Growth and Regional Ultrastructure of the Plasma Membrane of Schizosaccharomyces pombe as Revealed by Freeze-fracturing before and after Filipin Treatment. Journal of General Microbiology 131(2): 309-316

Taylor MJ, Perrais D, Merrifield CJ (2011) A high precision survey of the molecular dynamics of mammalian clathrin-mediated endocytosis. PLoS Biol 9(3): e1000604

Terasaki M (2000) Dynamics of the endoplasmic reticulum and golgi apparatus during early sea urchin development. Mol Biol Cell 11(3): 897-914

Terasaki M, Chen LB, Fujiwara K (1986) Microtubules and the endoplasmic reticulum are highly interdependent structures. J Cell Biol 103(4): 1557-1568

Toret CP, Lee L, Sekiya-Kawasaki M, Drubin DG (2008) Multiple Pathways Regulate Endocytic Coat Disassembly in Saccharomyces cerevisiae for Optimal Downstream Trafficking. Traffic 9(5): 848-859

Toshima JY, Toshima J, Kaksonen M, Martin AC, King DS, Drubin DG (2006) Spatial dynamics of receptor-mediated endocytic trafficking in budding yeast revealed by using fluorescent alpha-factor derivatives. Proc Natl Acad Sci U S A 103(15): 5793-5798

Traub LM (2009) Tickets to ride: selecting cargo for clathrin-regulated internalization. Nat Rev Mol Cell Biol 10(9): 583-596

Valdez-Taubas J, Pelham HRB (2003) Slow Diffusion of Proteins in the Yeast Plasma Membrane Allows Polarity to Be Maintained by Endocytic Cycling. Current Biology 13(18): 1636-1640

van Meer G, Voelker DR, Feigenson GW (2008) Membrane lipids: where they are and how they behave. Nat Rev Mol Cell Biol 9(2): 112-124

Vangelatos I, Roumelioti K, Gournas C, Suarez T, Scazzocchio C, Sophianopoulou V (2010) Eisosome organization in the filamentous ascomycete Aspergillus nidulans. Eukaryot Cell 9(10): 1441-1454

Voeltz GK, Prinz WA, Shibata Y, Rist JM, Rapoport TA (2006) A class of membrane proteins shaping the tubular endoplasmic reticulum. Cell 124(3): 573-586

Walther P, Müller M, Schweingruber ME (1984) The ultrastructure of the cell surface and plasma membrane of exponential and stationary phase cells of Schizosaccharomyces pombe grown in different media. Archives of Microbiology 137(2): 128-134

Walther TC, Aguilar PS, Frohlich F, Chu F, Moreira K, Burlingame AL, Walter P (2007) Pkh-kinases control eisosome assembly and organization. EMBO J 26(24): 4946-4955

Walther TC, Brickner JH, Aguilar PS, Bernales S, Pantoja C, Walter P (2006) Eisosomes mark static sites of endocytosis. Nature 439(7079): 998-1003

Wang HX, Douglas LM, Aimanianda V, Latge J-P, Konopka JB (2011) The Candida albicans Sur7 Protein Is Needed for Proper Synthesis of the Fibrillar Component of the Cell Wall That Confers Strength. Eukaryotic Cell 10(1): 72-80

Weinberg J, Drubin DG (2012) Clathrin-mediated endocytosis in budding yeast. Trends in Cell Biology 22(1): 1-13

West M, Zurek N, Hoenger A, Voeltz GK (2011) A 3D analysis of yeast ER structure reveals how ER domains are organized by membrane curvature. J Cell Biol 193(2): 333-346

Wiederkehr A, Du Y, Pypaert M, Ferro-Novick S, Novick P (2003) Sec3p is needed for the spatial regulation of secretion and for the inheritance of the cortical endoplasmic reticulum. Mol Biol Cell 14(12): 4770-4782

Wu MM, Buchanan J, Luik RM, Lewis RS (2006) Ca2+ store depletion causes STIM1 to accumulate in ER regions closely associated with the plasma membrane. J Cell Biol 174(6): 803-813

Xu T, Shively CA, Jin R, Eckwahl MJ, Dobry CJ, Song Q, Kumar A (2010) A Profile of Differentially Abundant Proteins at the Yeast Cell Periphery during Pseudohyphal Growth. Journal of Biological Chemistry 285(20): 15476-15488

Xu X, Bittman R, Duportail G, Heissler D, Vilcheze C, London E (2001) Effect of the Structure of Natural Sterols and Sphingolipids on the Formation of Ordered Sphingolipid/Sterol Domains (Rafts). Journal of Biological Chemistry 276(36): 33540-33546

Yanez-Mo M, Barreiro O, Gordon-Alonso M, Sala-Valdes M, Sanchez-Madrid F (2009) Tetraspanin-enriched microdomains: a functional unit in cell plasma membranes. Trends Cell Biol 19(9): 434-446

Young ME, Karpova TS, Brugger B, Moschenross DM, Wang GK, Schneiter R, Wieland FT, Cooper JA (2002) The Sur7p Family Defines Novel Cortical Domains in Saccharomyces cerevisiae, Affects Sphingolipid Metabolism, and Is Involved in Sporulation. Molecular and Cellular Biology 22(3): 927-934

Zhang X, Lester RL, Dickson RC (2004) Pil1p and Lsp1p Negatively Regulate the 3-Phosphoinositide-dependent Protein Kinase-like Kinase Pkh1p and Downstream Signaling Pathways Pkc1p and Ypk1p. Journal of Biological Chemistry 279(21): 22030-22038

Ziolkowska NE, Christiano R, Walther TC (2012) Organized living: formation mechanisms and functions of plasma membrane domains in yeast. Trends Cell Biol 22(3): 151-158

Ziolkowska NE, Karotki L, Rehman M, Huiskonen JT, Walther TC (2011) Eisosome-driven plasma membrane organization is mediated by BAR domains. Nat Struct Mol Biol 18(7): 854-856

PUBLICATIONS

RESEARCH PAPER 1

Histochem Cell Biol (2008) 130:1047–1052
DOI 10.1007/s00418-008-0504-x

SHORT COMMUNICATION

Ultrastructural and nuclear antigen preservation after high-pressure freezing/freeze-substitution and low-temperature LR White embedding of HeLa cells

Vendula Strádalová · Katarína Gaplovská-Kyselá · Pavel Hozák

Accepted: 31 August 2008 / Published online: 17 September 2008

Abstract A protocol for high-pressure freezing and LR White embedding of mammalian cells suitable for fine ultrastructural studies in combination with immunogold labelling is presented. HeLa S3 cells enclosed in low-temperature gelling agarose were high-pressure frozen, freeze-substituted in acetone, and embedded in LR White at 0°C. The morphology of such cells and the preservation of nuclear antigens were excellent in comparison with chemically fixed cells embedded in the same resin. The immunolabelling signal for different nuclear antigens was 4-to-13 times higher in high-pressure frozen than in chemically fixed cells. We conclude that one can successfully use high-pressure freezing/freeze-substitution and LR White embedding as an alternative of Lowicryl resins.

Keywords Cryofixation · Freeze substitution · High-pressure freezing · Immunogold labelling · LR White

Introduction

The use of cryofixation methods in transmission electron microscopy proved to be superior to conventional chemical fixation in respect of morphological and antigenic preservation (for example, see: Schwarz et al. 1993; Sawaguchi et al. 2002; Reipert et al. 2004b). Currently, the most powerful method of cryofixation is high-pressure freezing (HPF; reviewed in Dahl and Staehelin 1989; Studer et al. 1989), which physically immobilizes biological material without formation of ice crystals up to 200 μm thickness (Studer et al. 1995). Freeze substitution (FS) then allows to dehydrate the frozen samples and embed them in resin. Unfortunately, there is no universal FS protocol so far and an empirical adjustment is always necessary.

For immunocytochemical studies, Lowicryl resins have been the most widely used acrylic resins because they allow for embedding of the samples at very low temperatures, and they preserve well the ultrastructural details of biological samples (for a few examples, see Roth et al. 1989; Bittermann et al. 1992; Schwarz et al. 1993; Monaghan et al. 1998; McDonald 1999; Bohrmann and Kellenberger 2001; Giddings 2003; Reipert et al. 2004a; Sawaguchi et al. 2004; Mühlfeld and Richter 2006). Despite their disadvantageous toxicity and strong allergenic properties, they are usually the resins of first choice.

Another acrylic resin suitable for immunogold post-embedding detection, LR White, has not been used so widely, in spite of its easy usage and low toxicity. There are only a few reports using LR White for embedding of high-pressure frozen mammalian cells (Landemore et al. 1996; Sawaguchi et al. 2003; von Schack et al. (1993). For instance, Hess (2003) reported LR White embedding of various mammalian culture cell lines (and also plant material) after HPF as a good compromise for immunolabelling signal, morphology and health risk.

We have also shown previously that LR White preserves well the ultrastructure and allows for a sensitive immunodetection on chemically fixed cells, when an optimised protocol is used. The important conditions are the low

V. Strádalová · K. Gaplovská-Kyselá
Institute of Experimental Medicine,
Academy of Sciences of the Czech Republic,
v.v.i., Vídeňská 1083, 142 20 Prague, Czech Republic

P. Hozák (✉)
Institute of Molecular Genetics,
Academy of Sciences of the Czech Republic,
v.v.i., Vídeňská 1083, 142 20 Prague, Czech Republic
e-mail: hozak@img.cas.cz

temperature processing during the dehydration and LR White infiltration steps (Mashadian et al. 1995; Philimonenko et al. 2002). In this paper, we demonstrate fine ultrastructural and nuclear antigen preservation of HeLa cells after a combination of high-pressure freezing, freeze substitution with a complete omitting of chemical fixatives, and low-temperature LR White embedding. This method offers a good alternative to the toxic Lowicryls.

Materials and methods

Cell culture and high-pressure freezing of HeLa cells

HeLa S3 cells were grown in suspension in S-MEM (Sigma, 0.22% $NaHCO_3$) supplemented with 10% foetal bovine serum (Gibco) at 37°C. Before freezing, 10 ml of cell culture was centrifuged at 180*g* for 1 min and the supernatant was removed except for 200–300 µl of medium to prepare a dense cell suspension. This suspension was mixed 3:1 (v:v) with 2% low-temperature gelling agarose at 37°C (type VII, Sigma; diluted in D-MEM without serum). This mixture was transferred to the flat specimen carrier (Leica, 1.2 mm cavity diameter) using a pre-heated (37°C) tip, and the cells were frozen in the Leica EM PACT high-pressure freezer (Studer et al. 2001). The time interval between the removal of the cells from the incubator and the freezing was kept at minimum (always less than 10 min).

Freeze substitution and LR White embedding

Frozen samples in the carriers were transferred under liquid nitrogen to the Leica AFS machine and placed in the substitution solution pre-cooled to −90°C. Freeze substitution protocols were as follows:

(A) Cells were freeze substituted in acetone at −90°C for 3 days. The acetone was dehydrated using dried molecular sieves (Sigma,) and changed three times during the freeze substitution. Thereafter, temperature was elevated at a rate of 2°C per hour to −30°C, and the samples were kept for 12 h at this temperature. Samples were then removed from the metal carriers with a needle and transferred to special plastic capsules (Leica Flo through capsules) which were placed into pre-cooled chamber (Leica FT-chamber) filled with −30°C acetone. The temperature was then raised at a rate of 10°C per hour to 0°C, and the FT-chamber with samples was placed on ice.

(B) The freeze substitution protocol was the same as protocol A with the following modifications: 0.5% uranyl acetate was added to acetone and this was washed out by pure cold acetone after 3 days at −90°C and 12 h at −40°C. The uranyl acetate was dissolved in acetone from a 20% methanolic stock solution.

After transfer to ice, the substituted samples were washed with ice-cold ethanol (96%; 4 times 15 min) to remove the acetone completely since it might interfere with polymerization of the LR White resin. The samples were infiltrated in 2:1 (v:v) and 1:2 (v:v) 96% ethanol/LR White mixtures, 30 min each, and then kept in pure LR White (Sigma; with 2% benzoyl peroxide as initiator) overnight on ice. The resin was exchanged the next day for another 2 h, and the Leica capsules containing the samples were placed into gelatine capsules and covered with fresh resin. The polymerization was done by UV light at 4°C for 48 h.

Sectioning and electron microscopy

Thick sections (70 nm) were cut with an Ultracut S (Leica) equipped with a diamond knife (45°; Diatome) and contrasted with a saturated aqueous solution of uranyl acetate (Agar Scientific) for 4 min, washed, air-dried and examined in a FEI Morgagni 268(D) transmission electron microscope at 80 kV. Images were captured with Megaview II CCD camera.

Immunolabelling and evaluation of immunogold labelling density

For immunogold labelling, sections on gilded copper grids were blocked in 10% normal goat serum in PBTB (PBS + 0.1% Tween 20 + 1% BSA) for 30 min, and incubated for 1 h on droplets of primary antibody diluted in 1% goat serum/PBTB. Afterwards, the grids were washed with PBT (PBS + 0.005% Tween 20) three times 10 min, and incubated with gold-conjugated secondary antibody for 1 h. In controls, the primary antibody was omitted. After three washes in PBT, the grids were finally washed twice in distilled water, air-dried and contrasted as described above.

Immunogold labelling density of nuclear antigens detected on sections of HPF/FS or chemically fixed cells were compared. The comparison was based on evaluating 25–30 random digital images of cell nuclei per each sample at 36,000× (DNA immunolabelling) or 44,000× (lamin A and LAP2α immunolabelling), respectively. Labelling density was expressed as number of gold particles per square micrometer section surface ±STD.

Antibodies

Primary antibodies: mouse monoclonal anti-DNA, clone AC-30-10 (IgM, 1.67 µg/ml; Boehringer Mannheim Biochemica; now sold by Millipore); mouse monoclonal anti-lamin A, clone 133A2 (dilution 1:100; gift from Dr. Y. Raymond); rabbit anti-LAP2α (dilution 1:400; gift from Dr. R. Foisner). Secondary antibodies: 12 nm goat anti-mouse IgM-gold; 6 nm goat anti-mouse IgG/IgM-gold;

12 nm goat anti-rabbit IgG-gold (all from Jackson Immunoresearch Laboratories, diluted 1:30).

Conventional chemical fixation and LR White embedding

HeLa S3 cells grown as described above were washed with Sörensen phosphate buffer (SB; 0.1 M Na/K phosphate buffer, pH 7.3), fixed in a mixture of 3% formaldehyde and 0.1% glutaraldehyde in SB for 20 min at ambient temperature and washed in three changes of SB (5 min each). Cells were then incubated with 0.2 M glycine in SB for 10 min. After two washing steps, the pellet in SB was warmed to 37°C and the same volume of 2% low gelling temperature agarose was quickly added to the cell suspension. This suspension was centrifuged in Eppendorf microtubes and placed on ice.

The hardened agarose blocks were cut under SB into ~1.5 mm pieces, dehydrated in graded ethanol series (30, 50, 70, 90 and 96%; 10 min each), and infiltrated in 2:1 (v:v) and 1:2 (v:v) ethanol/LR White mixtures, 20 min each, on ice. The cells were then infiltrated in pure LR White overnight at 0°C. The resin was exchanged the next day, and after 2 h the samples were placed into gelatine capsules and UV light-polymerized for 48 h at 4°C. Polymerized blocks were sectioned, immunolabelled, contrasted and examined as described above.

Results and discussion

A protocol for high-pressure freezing/freeze-substitution and low-temperature LR White embedding of mammalian cell suspensions for ultrastructural and immunogold studies is presented. Leica flat specimen carriers in combination with agarose were used instead of cellulose capillary tubes (Hohenberg et al. 1994) or copper tube system (Leica) because of the easier manipulation with the samples intended for resin embedding, room temperature sectioning, and immunolabelling. HeLa cells enclosed in 0.5% agarose were high-pressure frozen/freeze-substituted in acetone without additional fixatives (protocol A) and embedded in LR White at 0°C. The cells processed in this way showed highly improved ultrastructure (see Figs. 1 and 2) in comparison with chemically fixed cells.

The use of agarose as a matrix not only prevents cell loss but apparently also serves as an extracellular cryoprotectant also and ensures a better quality of freezing. It has been also successfully used as a cell support for slam-freezing of HeLa cells (Roch et al. 1997), and it appears that the combination of dense cell suspension and agarose in our protocol serves together well.

As reported by others (Studer et al. 2001; Morphew and McIntosh 2003), some microcrystalline ice was present in nuclei of some cells, but the overall cell structure was well preserved. It is known that chromatin is one of the most difficult structures to vitrify (Wild et al. 2001; Morphew and McIntosh 2003). In general, the HPF/FS samples appeared to be less extracted and had a finer structure than the chemically fixed cells as shown in Figs. 1 and 2. In agreement with previous observations (von Schack et al. 1991, 1993), nucleolar components were much finer structured and less discernible than in chemically fixed cells (Fig. 1a). Also the lowered contrast is in agreement with several works mentioning lower contrast after using acrylic resins (Nicolas and Bassot 1993; Roch et al. 1997; von Schack et al. 1991, 1993; Monaghan et al. 1998). This feature, however, can be sometimes an advantage since gold particles become better visible over the cellular structures.

Our experience concerning the visibility of membranes is somewhat different from the literature. Nuclear membranes were generally clearly defined and easy to observe (Fig. 2a, b). As there was no osmium added, they appeared

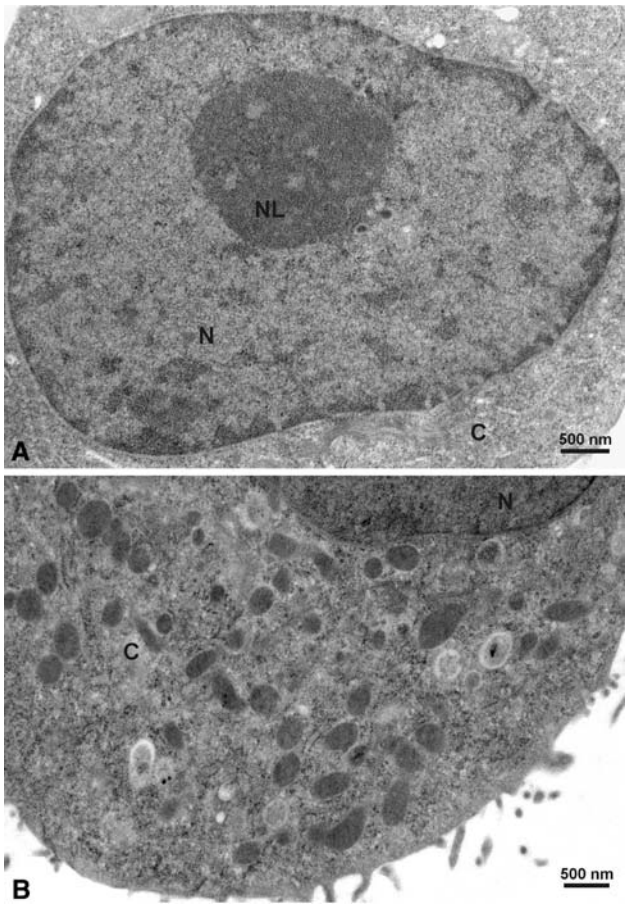

Fig. 1 Improved ultrastructure of HeLa S3 cells in LR White after HPF and FS. The overall ultrastructure of HeLa cells is well preserved. **a** Cell nucleus with nucleolus. The chromatin shows fine granular structure without "wash-out" artefacts known from chemical fixation. **b** Cytoplasm with well defined organelles. *N* nucleus, *NL* nucleolus, *C* cytoplasm

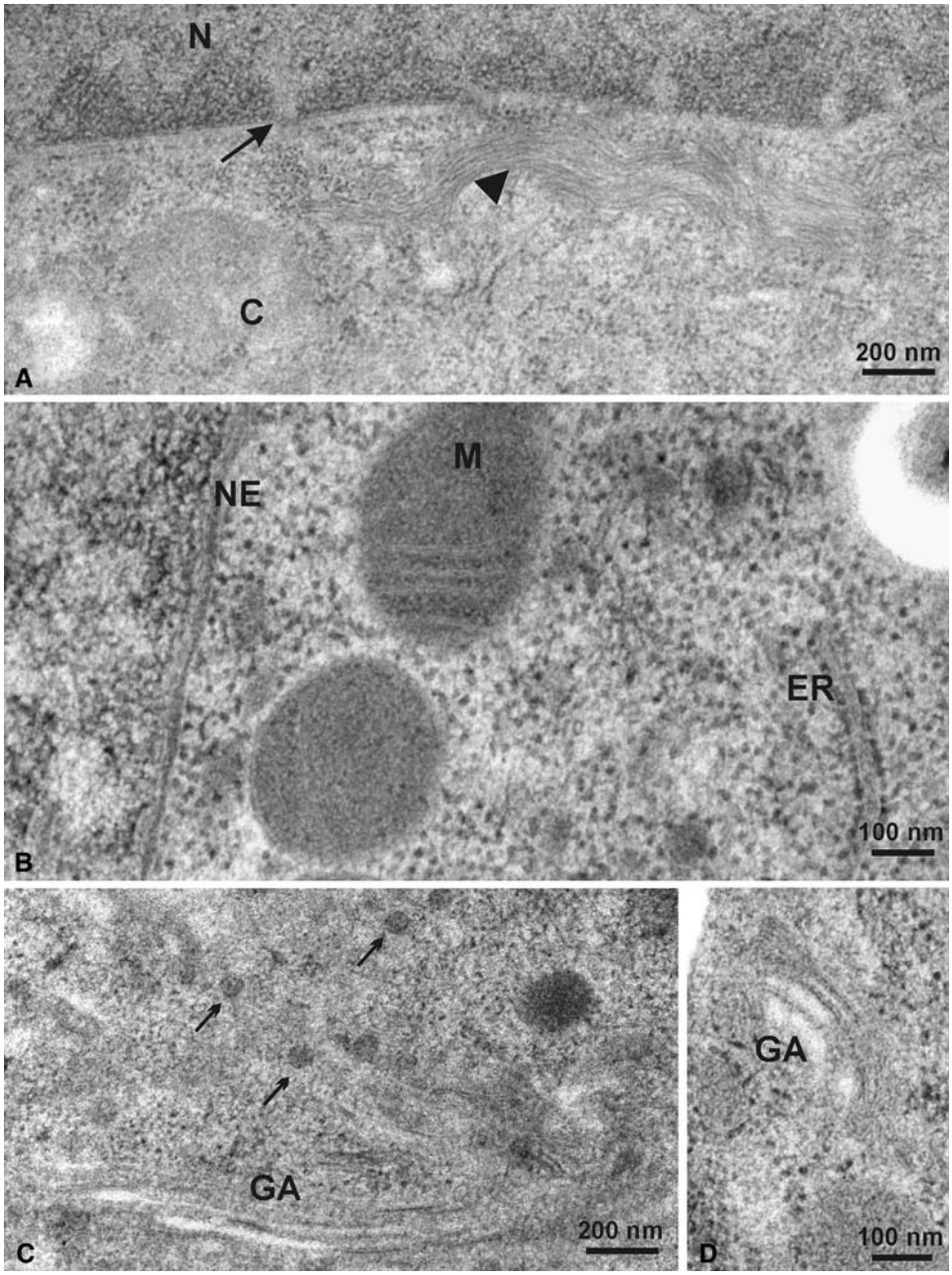

Fig. 2 Details of HeLa S3 cells in LR White after HPF and FS. **a** Detailed view taken from the lower-right part of Fig. 1a. Well preserved nuclear envelope with nuclear pores (*arrow*) and lamina, as well as a neighbouring bundle of cytoplasmic intermediate filaments (*arrowhead*) are visible. *N* nucleus, *C* cytoplasm **b** High-magnification of cytoplasm containing mitochondria (M) with discernible cristae, rough endoplasmic reticulum (ER), and nuclear envelope (NE). **c, d** Details of preserved Golgi apparatus (GA) and vesicles in its vicinity (*arrows*)

in negative contrast. Similar observations were made for the membranes of the endoplasmic reticulum, mitochondria and the Golgi apparatus—typically very difficult to preserve (Fig. 2b–d). Most probably, this good visibility of membranes results from the presence of some water (note that in our protocol, 96% ethanol was used in the last dehydration step). The addition of extra water to the substitution medium possibly might improve membrane contrast even more (Walther and Ziegler 2002).

Addition of uranyl acetate to the freeze substitution medium can increase the contrast of cellular structures (Schwarz et al. 1993; Audit et al. 1996; McDonald 1999; McDonald and Müller-Reichert 2002; Hess 2003; Reipert et al. 2004a). When the uranyl acetate was added to the acetone during freeze-substitution (protocol B), an enhanced contrast mainly of cytoplasmic structures such as mitochondria and ribosomes was observed (Fig. 3a, b). Furthermore, heterochromatin regions in nuclei were also more easily discernible. The membranes still appeared in negative contrast. However, the addition of uranyl acetate should be considered carefully as it can destroy/alter some antigens (Nicolas and Bassot 1993; Hess 2003; Bittermann et al. 1992).

The improved cellular ultrastructure stimulated us to explore the influence of HPF/FS processing (without addition of uranyl acetate) on antigen preservation for immunogold detection. First, we used an anti-DNA antibody which

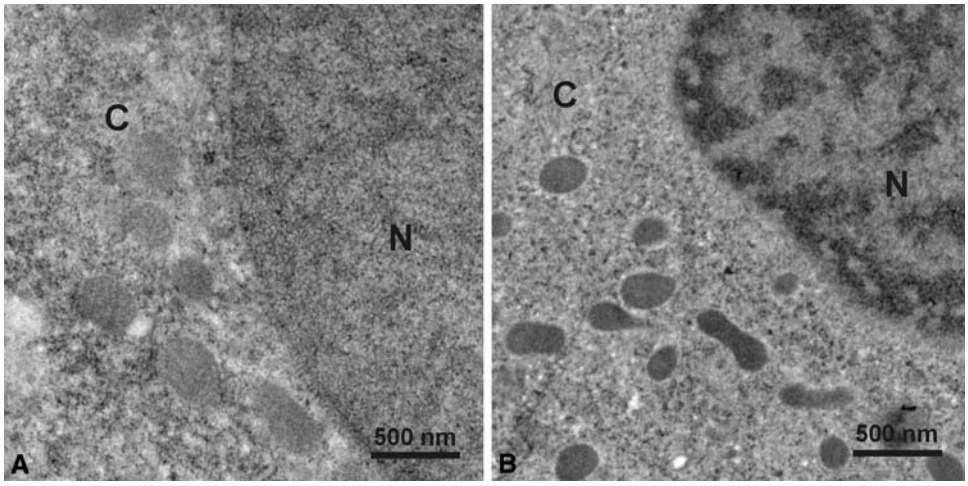

Fig. 3 Addition of uranyl acetate to FS medium enhances contrast of some cellular structures. **a** HeLa cell cryo-substituted in pure acetone. **b** HeLa cell cryo-substituted in acetone with 0.5% uranyl acetate. The most prominent difference was the contrast enhancement of mitochondria, ribosomes and heterochromatin after the addition of uranyl acetate into substitution medium. *N* nucleus, *C* cytoplasm

produced an intense signal after chemical fixation and LR White embedding (labelling density: 7.8 ± 0.8 gold particles/μm^2). An about 13-fold increase in labelling intensity was observed in the HPF/FS samples (102.9 ± 6.6 gold particles/μm^2). For lamin A and LAP2α a fourfold and sevenfold increase, respectively, of immunogold labelling was observed. Lamin A labelling intensity in chemically fixed cells was 0.7 ± 0.1 gold particles/μm^2 and in HPF/FS cells 2.8 ± 0.2 gold particles/μm^2. For LAP2α the corresponding values were 1.1 ± 0.2 gold particles/μm^2 and 7.4 ± 0.5 gold particles/μm^2.

Together, these results indicate the high suitability of HPF/FS in combination with LR White embedding for the detection of nuclear antigens. Certainly, the degree of improvement always depends on the given antigen and an empirical approach to each new sample and antibody is necessary. Thus, our results confirm and extend previous observations (for example, see: Monaghan and Robertson 1990; von Schack et al. 1991, 1993; Bittermann et al. 1992; Nicolas and Bassot 1993; Bohrmann and Kellenberger 2001) that cryofixation and cryosubstitution methods without aldehyde fixatives can permit both the preservation of cellular ultrastructure and efficient immunolabelling.

Acknowledgments We are grateful to Dr. Heinz Schwarz for helpful discussions about freeze substitution, Dr. Yves Raymond and Dr. Roland Foisner for providing the anti-lamin A and anti-LAP2α antibodies, respectively. We thank Dr. Jan Malínský for critical reading of the manuscript and for technical help, and also Věra Lukešová, Ivana Nováková and Iva Jelínková for their excellent technical help. This work was supported by the grant KAN200520704 from the Academy of Sciences of the Czech Republic, grants LC545 and 2B06063 from the MŠMT ČR, and by the institutional grants No. AV0Z50520514 and No. AV0Z50390512. VS was supported by the student program of the Grant Agency of the Czech Republic (reg. no. 204/05/H023).

References

Audit A, Barbier M, Soyer-Gobillard M, Albert M, Geraud M, Nicolas G, Lenaers G (1996) Cyclin B ($p56^{cdc13}$) localization in the yeast Schizosaccharomyces pombe: an ultrastructural and immunocytochemical study. Biol Cell 86:1–10

Bittermann AG, Knoll G, Nemeth A, Plattner H (1992) Quantitative immuno-gold labelling and ultrastructural preservation after cryofixation (combined with different freeze-substitution and embedding protocols) and after chemical fixation and cryosectioning. Histochemistry 97:421–429

Bohrmann B, Kellenberger E (2001) Cryosubstitution of frozen biological specimens in electron microscopy: use and application as an alternative to chemical fixation. Micron 32:11–19

Dahl R, Staehelin LA (1989) High-pressure freezing for the preservation of biological structure: theory and practice. J Electron Microsc Tech 13:165–174

Giddings TH (2003) Freeze-substitution protocols for improved visualization of membranes in high-pressure frozen samples. J Microsc 212:53–61

Hess MW (2003) Of plants and other pets: practical aspects of freeze-substitution and resin embedding. J Microsc 212:44–52

Hohenberg H, Mannweiler K, Müller M (1994) High-pressure freezing of cell suspensions in cellulose capillary tubes. J Microsc 175:34–43

Landemore G, Quillec M, Izard J (1996) Ultrastructure of Kurloff body proteoglycans after high pressure freezing, cryosubstitution and postembedding staining with cuprolinic blue. Glycobiology 6:817–822

Mashadian DY, Grimes GW, Kiss JZ (1995) Improved antigenic preservation of plant tissue by low temperature processing in LR White resin. Microsc Res Tech 31:531–532

McDonald K (1999) High-pressure freezing for preservation of high resolution fine structure and antigenicity for immunolabeling. Methods Mol Biol 117:77–97

McDonald KL, Müller-Reichert T (2002) Cryomethods for thin section electron microscopy. Methods Enzymol 351:96–123

Monaghan P, Robertson D (1990) Freeze-substitution without aldehyde or osmium fixatives: ultrastructure and implications for immunocytochemistry. J Microsc 158:355–363

Monaghan P, Perusinghe N, Müller M (1998) High-pressure freezing for immunocytochemistry. J Microsc 192:248–258

Morphew MK, McIntosh JR (2003) The use of filter membranes for high-pressure freezing of cell monolayers. J Microsc 212:21–25

Mühlfeld Ch, Richter J (2006) High-pressure freezing and freeze substitution of rat myocardium for immunogold labelling of connexin 43. Anat Rec A 288A:1059–1067

Nicolas MT, Bassot JM (1993) Freeze substitution after fast-freeze fixation in preparation for immunocytochemistry. Microsc Res Tech 24:474–487

Philimonenko VV, Janacek J, Hozak P (2002) LR White is preferable to Unicryl for immunogold detection of fixation-sensitive nuclear antigens. Eur J Histochem 46:359–364

Reipert S, Fischer I, Wiche G (2004a) High-pressure freezing of epithelial cells on sapphire coverslips. J Microsc 213:81–85

Reipert S, Fischer I, Wiche G (2004b) High-pressure cryoimmobilization of murine skin reveals novel structural features and prevents extraction artifacts. Exp Dermatol 13:419–425

Roch AM, Nicolas MT, Quash G (1997) Ultrastructural immunolocalization of polyamines in HeLa cells subjected to fast-freezing fixation and freeze substitution. Histochem Cell Biol 107:303–312

Roth J (1989) Postembedding labelling on Lowicryl K4M tissue sections: detection and modification of cellular components. Methods Cell Biol 31:513–551

Sawaguchi A, McDonald KL, Karvar S, Forte JG (2002) A new approach for high-pressure freezing of primary culture cells: the fine structure and stimulation-associated transformation of cultured rabbit gastric parietal cells. J Microsc 208:158–166

Sawaguchi A, Yao X, Forte JG, McDonald K (2003) Direct attachment of cell suspensions to high-pressure freezing specimen planchettes. J Microsc 212:13–20

Sawaguchi A, McDonald KL, Forte JG (2004) High-pressure freezing of isolated gastric glands provides new insight into the fine structure and subcellular localization of H^+/K^+-ATPase in gastric parietal cells. J Histochem Cytochem 52:77–86

Schwarz H, Hohenberg H, Humbel BM (1993) Freeze-substitution in virus research: a preview. In: Hyatt D, Eaton BT (eds) Immunogold electron microscopy in virus diagnostic and research. CRC Press, Boca Raton, pp 349–376

Studer D, Michel M, Muller M (1989) High pressure freezing comes of age. Scanning Microsc Supplement 3:253–269

Studer D, Michel M, Wohlwend M, Hunziker EB, Buschmann MD (1995) Vitrification of articular cartilage by high-pressure freezing. J Microsc 179:321–332

Studer D, Graber W, Al-Amoudi A, Eggli P (2001) A new approach by high-pressure freezing. J Microsc 203:258–294

Von Schack M-L, Fakan S, Villiger W (1991) Some application of cryosubstitution in ultrastructural studies of the cell nucleus. Biol Cell 72:113–119

Von Schack M-L, Fakan S, Villiger W, Muller M (1993) Cryofixation and cryosubstitution: a useful alternative in the analyses of cellular fine structure. Eur J Histochem 37:5–18

Walther P, Ziegler A (2002) Freeze substitution of high-pressure frozen samples: the visibility of biological membranes is improved when the substitution medium contains water. J Microsc 208:3–10

Wild P, Schraner EM, Adler H, Humbel BM (2001) Enhanced resolution of membranes in cultured cells by cryoimmobilization and freeze-substitution. Microsc Res Tech 53:313–321

RESEARCH PAPER 2

Furrow-like invaginations of the yeast plasma membrane correspond to membrane compartment of Can1

Vendula Strádalová[1], Wiebke Stahlschmidt[2], Guido Grossmann[2], Michaela Blažíková[1,3], Reinhard Rachel[4], Widmar Tanner[2] and Jan Malinsky[1,*]

[1]Institute of Experimental Medicine, Academy of Sciences of the Czech Republic, Prague, Czech Republic
[2]Institute of Cell Biology and Plant Physiology, University of Regensburg, Regensburg, Germany
[3]Faculty of Mathematics and Physics, Charles University in Prague, Prague, Czech Republic
[4]Centre for Electron Microscopy–NWF III, University of Regensburg, Regensburg, Germany
*Author for correspondence (malinsky@biomed.cas.cz)

Accepted 21 May 2009
Journal of Cell Science 122, 2887-2894 Published by The Company of Biologists 2009
doi:10.1242/jcs.051227

Summary

Plasma membrane of the yeast *Saccharomyces cerevisiae* contains stable lateral domains. We have investigated the ultrastructure of one type of domain, the membrane compartment of Can1 (MCC). In two yeast strains (*nce102Δ* and *pil1Δ*) that are defective in segregation of MCC-specific proteins, we found the plasma membrane to be devoid of the characteristic furrow-like invaginations. These are highly conserved plasma membrane structures reported in early freeze-fracture studies. Comparison of the results obtained by three different approaches – electron microscopy of freeze-etched cells, confocal microscopy of intact cells and computer simulation – shows that the number of invaginations corresponds to the number of MCC patches in the membrane of wild-type cells. In addition, neither MCC patches nor the furrow-like invaginations colocalized with the cortical ER. In mutants exhibiting elongated MCC patches, there are elongated invaginations of the appropriate size and frequency. Using various approaches of immunoelectron microscopy, the MCC protein Sur7, as well as the eisosome marker Pil1, have been detected at these invaginations. Thus, we identify the MCC patch, which is a lateral membrane domain of specific composition and function, with a specific structure in the yeast plasma membrane – the furrow-like invagination.

Key words: Eisosome, Electron microscopy, MCC, Membrane compartmentalization, Plasma membrane invagination

Supplementary material available online at
http://jcs.biologists.org/cgi/content/full/122/16/2887/DC1

Introduction

The plasma membrane of living cells is considered to be laterally compartmented into domains of specialized composition and function. In the yeast *Saccharomyces cerevisiae*, two such non-overlapping membrane compartments (MCs) have been distinguished. The first, MCC, contains the arginine permease Can1 and the second, MCP, contains the proton ATPase Pma1 (Malinska et al., 2003). MCC consists of evenly distributed isolated patches. Based on confocal localizations of Can1-GFP and Pma1-GFP, the size of the MCC patches was estimated to be ~300 nm. To date, more than 20 cortical proteins have been found to colocalize with the MCC, nine of which are integral to the plasma membrane (Grossmann et al., 2008; Maier et al., 2008; Deng et al., 2009). In addition to Can1, three other permeases with targeting pathways that are dependent on specific lipids, Fur4, Tat2 and heterologous HUP1 (*Chlorella kessleri*), were identified as MCC constituents (Malinska et al., 2004; Grossmann et al., 2006; Grossmann et al., 2007). The compartmentation of the plasma membrane into MCC and MCP is highly stable (Malinska et al., 2004), but the transporters dock within MCC patches in a reversible, membrane-potential-dependent manner. In addition to its specific protein composition, filipin-stained plasma membrane sterols were shown to accumulate in MCC (Grossmann et al., 2007).

The biological function of MCC was unclear until a delayed internalization of MCC-accumulated Can1 was reported recently, suggesting a protective function of MCC patches in protein turnover (Grossmann et al., 2008). Among soluble proteins sharing the MCC distribution, Pil1 and Lsp1, long-chain-base-responsive inhibitors of protein kinases Pkh1 and Pkh2 (Zhang et al., 2004), were postulated to form eisosomes, which are organelles with a proposed role in endocytosis (Walther et al., 2006). MCC markers show a homogenous distribution in the plasma membrane of *pil1Δ* cells, with rare enlarged spotted accumulations. Electron microscopy analysis of these cells suggested that these spots correspond to large aberrant plasma membrane infoldings (Walther et al., 2006).

In wild-type budding yeast, two specialized structures containing invaginated plasma membrane are described: one usually referred to as ‘finger-like’ and the other as ‘furrow-like’. It is believed that the cortical patches of fibrous actin form around finger-like plasma membrane invaginations, 150- to 250-nm-deep tubular structures with a diameter of ~50 nm (Mulholland et al., 1994) that concentrate in areas of polarized growth. The formation of a finger-like invagination in relation to the endocytic event has been explained in molecular detail by fluorescence (Kaksonen et al., 2005) and electron microscopy (Idrissi et al., 2008) studies. Actin patches and/or finger-like invaginations were also suggested to be places of cell wall synthesis (Kopecka and Gabriel, 1995).

By contrast, furrow-like invaginations are rather randomly distributed over the cell surface. On replicas of freeze-fractured cells

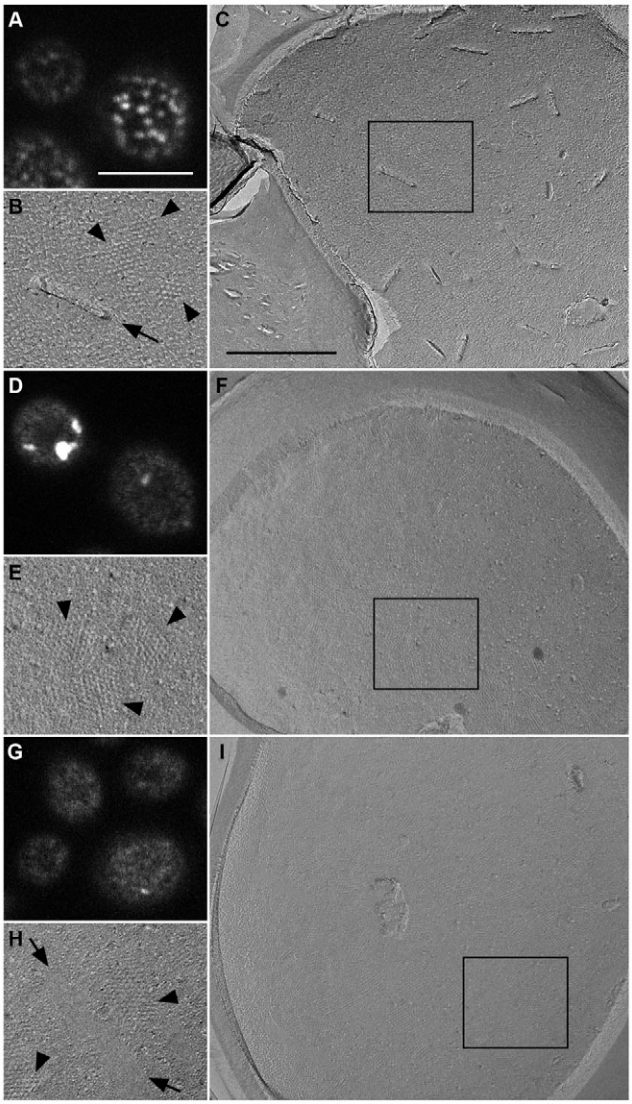

Fig. 1. Plasma membrane in *nce102Δ* and *pil1Δ* strains compared with wild-type cells. Fluorescence patterns of Can1-GFP on tangential confocal sections (A,D,G) and freeze-fracture views of the plasma membrane (P face; details in B,E,H of boxed regions in overviews C,F,I) in BY4741 (A-C), *pil1Δ* (D-F) and *nce102Δ* (G-I) cells. Note the dispersed Can1 pattern in D,G, and the absence of membrane invaginations in E,H. In B,E,H, hexagonally ordered arrays (arrowheads) and smooth elongated areas (arrows) are highlighted. In contrast to the wild type (B), the smooth areas are not invaginated in *nce102Δ* (H). Scale bars: 5 μm (A,D,G), 500 nm (C,F,I).

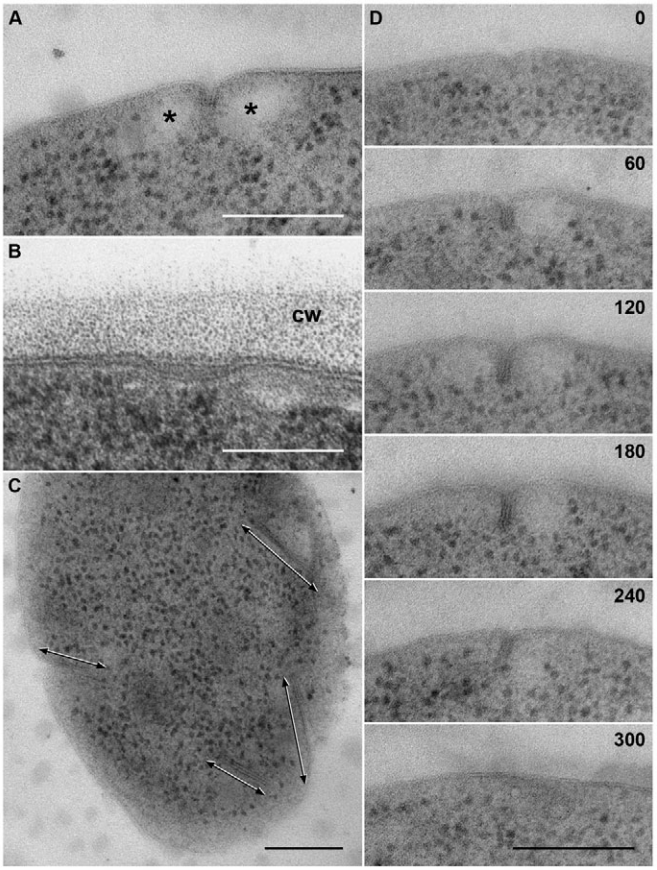

Fig. 2. Fine structure of a furrow-like plasma membrane invagination. Electron micrographs of ultrathin sections of wild-type cells after HPF/FS and HM20 embedding, showing various appearances of furrow-like invaginations: transverse section (A), longitudinal section (B), and almost tangential section, relative to the cell surface (C; invaginations indicated by arrows). The furrow-like character is documented by a series of six consecutive, 60-nm-thin sections of a single invagination (D). The numbers indicate the accumulating sample thickness, reflecting the length of the invagination. In order to maximize the membrane contrast, lead citrate treatment was added in B. Note the electron-lucent granules in A (asterisks) and the contrasted cell wall in B (cw). Scale bars: 200 nm.

they appear as straight linear plasma membrane depressions ~300 nm long (Moor and Mühlethaler, 1963; Gross et al., 1978). Although various examples of similarly shaped plasma membrane structures in other organisms have been reported (see Discussion), the function of furrow-like invaginations remains unclear.

In this study, we present evidence that, in the plasma membrane of *S. cerevisiae*, furrow-like invaginations correspond to MCC patches. A genome-wide screen identified Nce102, a protein of unknown function integral to MCC, and Pil1, a primary component of eisosomes, as the main organizers of MCC composition and structure (Grossmann et al., 2008). Using various electron microscopy approaches, we show the absence of furrow-like invaginations in *nce102Δ* and *pil1Δ* deletion mutants. In addition, we report an altered morphology of MCC patches and the corresponding changes in furrow-like invaginations in two other deletion mutants, *ypr050cΔ* and *mak3Δ*. Finally, using immunolocalization of nanogold probes, Pil1 and an MCC marker Sur7 (Malinska et al., 2004), a protein of unknown function integral to the plasma membrane (Young et al., 2002), were shown to localize to the furrow-like plasma membrane invaginations. For the first time, we assign a lateral plasma membrane domain to a specific membrane structure.

Results

Cells with altered MCC distribution lack furrow-like membrane invaginations

In an attempt to describe the fine structure of the MCC patch, we performed an electron microscopy analysis of yeast mutants showing aberrant MCC distribution (Grossmann et al., 2008). First, we tested plasma membranes of *pil1Δ* and *nce102Δ* cells, exhibiting homogenously distributed MCC markers (Fig. 1D,G; compare with the wild type in Fig. 1A), for possible structural alterations.

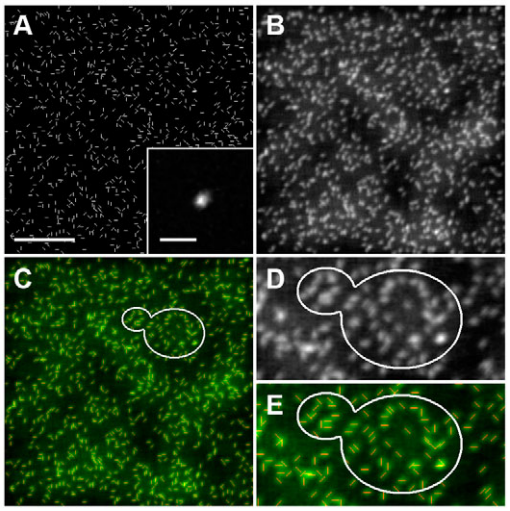

Fig. 3. Computer-simulated plasma membrane invaginations in the optics of a confocal microscope. A field of 1000 randomly distributed model objects (invaginations; A, red in C), and its simulated confocal image (patches; B, green in C) are presented. PSF used for the simulation of the microscope imaging (see Materials and Methods for details) is shown in the inset in A. D and E represent details of B and C, respectively. An outline illustrating the size of a yeast cell is drawn in C-E. Scale bars: 5 μm (A), 1 μm (inset in A).

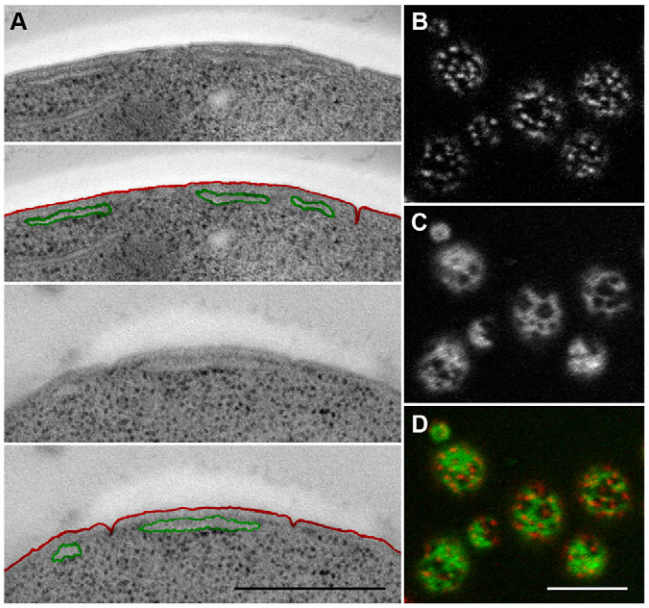

Fig. 4. MCC patches do not colocalize with cortical ER. Ultrathin sections of high-pressure-frozen wild-type cells in HM20 resin (A), and a tangential confocal section of the living cells co-expressing an MCC marker Sur7-mRFP (B, red in D) and ss-GFP-HDEL (C, green in D). Plasma membrane (red) and cisternae of cortical ER (green) are highlighted in A. Scale bars: 500 nm (A), 5 μm (B-D).

Two different approaches were used for visualization of the plasma membrane. First, replicas of freeze-etched *pil1Δ* and *nce102Δ* mutants were prepared and compared with those of the wild type. In accordance with the reports published previously (e.g. Moor and Mühlethaler, 1963; Steere et al., 1980), two types of characteristic structures were recognized on the inner leaflet (P face) (Branton et al., 1975) of the plasma membrane in wild-type cells: (1) areas with a hexagonally ordered repetitive grain pattern, and (2) islets of smooth membrane with straight lines of furrow-like invaginations (Fig. 1B,C). The most striking difference observed in the plasma membrane of mutant cells was the absence (or far lower frequency) of furrow-like membrane invaginations (Fig. 1E,F,H,I). We found 2.5±0.2 invaginations per μm^2 on the surface of wild-type cells. This surface density was decreased to ~20% (0.5±0.2 invaginations per μm^2) in *pil1Δ* cells, and only rare invaginations were detected in the plasma membrane of *nce102Δ* cells.

Similarly, the furrow-like invaginations could not be detected on ultrathin resin sections of *pil1Δ* and *nce102Δ* cells. Curved membrane areas that corresponded to invaginations 200-300 nm long and ~50 nm deep were regularly found in wild-type cells (Fig. 2). As reported previously, these structures were often accompanied by electron-lucent granules of glycogen (Coulary et al., 2001). By contrast, only a planar membrane bilayer without any invaginations was observed in both the mutants (data not shown). The occasional occurrence of large membrane-surrounded structures in *pil1Δ* cells (supplementary material Fig. S1) obviously corresponded to the large aberrant fluorescent patches observed by Walther and co-workers (Walther et al., 2006).

Surface density of furrow-like invaginations corresponds to the number of MCC patches

Next, we determined whether there was a direct relationship between the furrow-like invaginations and MCC patches in the plasma membrane of wild-type cells. Bearing in mind the resolution limit of fluorescence microscopy, we aimed to compare surface densities of these two structures. First, we counted MCC patches. Analysis of 3D stacks of confocal sections revealed a surface density of 1.2±0.2 patches per μm^2 in wild-type cells expressing the MCC marker Sur7-GFP.

Next, we performed a computer simulation of the furrow-like invagination pattern blurred by confocal imaging. We assumed invaginations of a uniform length of 250 nm to be marked by a specific fluorescent marker and spread randomly (Moreira et al., 2009) on a plane (Fig. 3A) with an overall density corresponding to the value measured on freeze-fractured cells (2.5 invaginations per μm^2, see above). The confocal imaging of this model set of microscopic objects was simulated by its convolution with the 2D point spread function (PSF) of the confocal microscope (Fig. 3B; see Materials and Methods for details). Individual foci were counted in the resulting 'confocal image'. In ten images consisting of 1000 model invaginations each, we measured the density of 1.72±0.05 foci per μm^2, which was comparable with the measured surface density of MCC patches.

Cortical ER does not colocalize with MCC patches

We searched for further morphological evidence that the furrow-like invaginations of the plasma membrane represent the ultrastructural correlates of MCC patches. As was apparent from thin sections of high-pressure-frozen cells, cisternae of cortical ER appeared to be next to, but not beneath these invaginations (Fig. 4A). To test the mutual position of cortical ER and MCC patterns, we coexpressed an MCC marker Sur7-mRFP with an ER reporter construct, consisting of GFP fused to a signal sequence for ER localization and the ER retrieval sequence His-Asp-Glu-Leu (ss-GFP-HDEL). A clear separation of both the compartments was detected (Fig. 4B-D). Either the MCC patches were localized in the ER-free zones of the plasma membrane, or a local minimum

of ER-specific signal could be detected underneath, indicating that there are holes in the flat cisternae of cortical ER.

Elongated MCC patches result in elongated furrow-like invaginations

As a consequence of previous findings, we checked the plasma membrane ultrastructure in the yeast strain lacking *YPR050C*, which has been described as a "dubious ORF unlikely to encode a protein" (Fisk et al., 2006). During the evaluation of a visual screen focused on strains with alterations in MCC integrity (Grossmann et al., 2008), we found that *ypr050cΔ* cells show abnormally elongated MCC patches (Fig. 5A,B). Although the appearance of membrane invaginations remained unchanged on transversal ultrathin sections of these cells (data not shown), sections almost parallel to the cell surface (tangential sections), as well as the freeze-fracture cell surface replicas, revealed abnormally elongated furrow-like invaginations (Fig. 5C,D, respectively). Cells lacking *MAK3* (*YPR051W*) showed the same phenotype (data not shown), most probably because of a significant overlap of *MAK3* with *YPR050C* (Murthi and Hopper, 2005). We conclude that individual furrow-like invaginations correspond to the MCC patches.

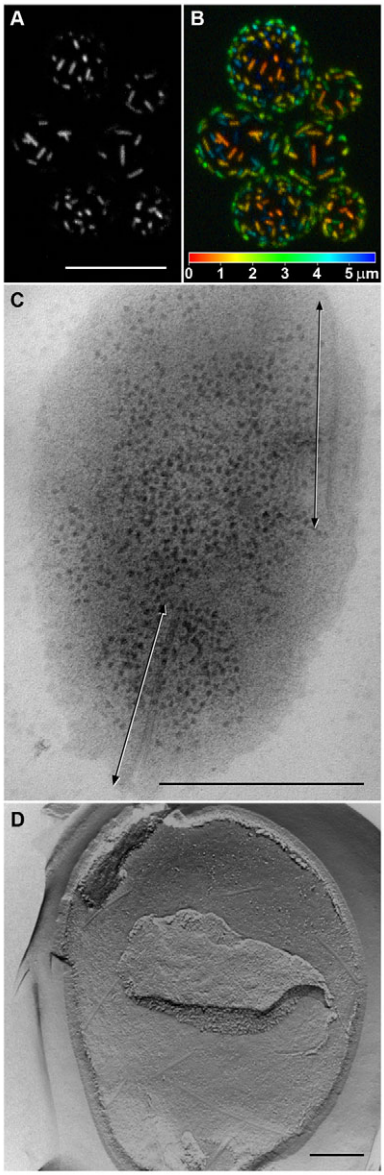

Fig. 5. MCC pattern and furrow-like invaginations in *ypr050cΔ* cells. Comparison of cell surface distributions of MCC patches (labeled with Sur7-GFP; A,B) and the furrow-like invaginations of the plasma membrane (C,D) in *ypr050cΔ* mutant. Superposition of four consecutive confocal sections (A), depth-coded 3D stack covering whole confocally sectioned cells (B), tangential ultrathin section following HM20 embedding (C) and a view of a freeze-fracture face of the inner leaflet of the plasma membrane (P face; D) are presented. The position of two furrow-like invaginations is indicated in C (arrows). Scale bars: 5 µm (A,B), 500 nm (C,D).

MCC and eisosome components localize to furrow-like membrane invaginations

To confirm the above conclusion, we decided to investigate the localization of protein components of MCC patches, as well as cytosolic eisosomes, at the ultrastructural level. Using several labeling protocols, we performed immunogold detection of the MCC and the eisosome markers Sur7 and Pil1.

When tracked by pre-embedding immunogold labeling, including the extractive methanol permeabilization step, Sur7-GFP was localized unequivocally to areas of curved plasma membrane, which corresponded to the furrow-like invaginations (Fig. 6). The labeling signal was specific, confined exclusively to the plasma membrane without a detectable background. Pil1-GFP showed a similar subcellular distribution. In addition, some protein localized to the cell interior, corresponding to a cytoplasmic pool of Pil1 (data not shown).

Post-embedding 'on-section' labeling assuring better fine structure preservation revealed comparable results. In a first attempt using mild chemical fixation and LR White embedding (Mulholland et al., 1994), Sur7-GFP was localized to the plasma membrane

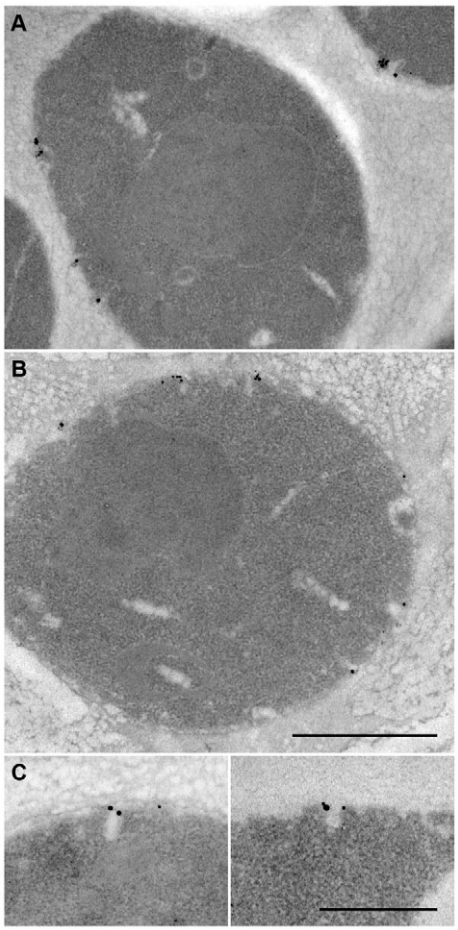

Fig. 6. Pre-embedding immunogold localization of MCC. The MCC marker Sur7-GFP was detected by anti-GFP (A) and anti-Sur7 (B,C) antibodies (epon-durcupan embedding, see the Materials and Methods for details) within areas of invaginated plasma membrane. Scale bars: 500 nm (A,B), 200 nm (C).

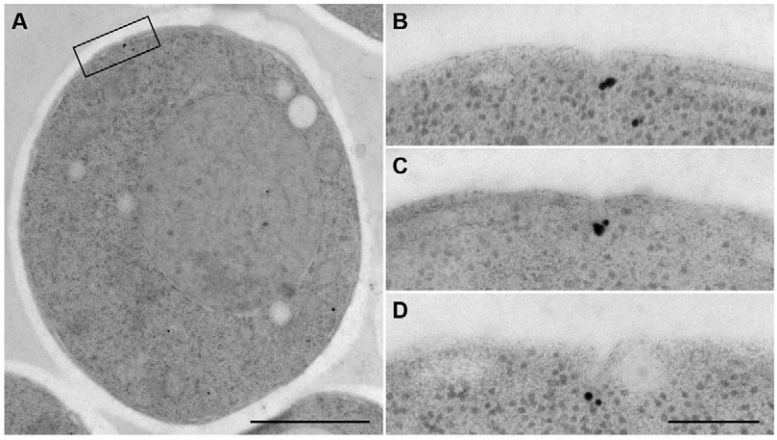

Fig. 7. Post-embedding immunogold localization of Pil1. The eisosome marker Pil1-GFP was localized on ultrathin HM20-embedded sections of high-pressure-frozen cells. Fine structure preservation on the whole cell section (A) and the accurate signal localization upon invagination details (B-D) are shown. The area presented in B is enlargement of the boxed region in A. Scale bars: 1 μm (A), 200 nm (B-D).

invaginations. However, the fine structure of the plasma membrane was altered in these cells, as judged from the artificially tilted and profound invaginations (data not shown).

For unknown reasons, we did not obtain reproducible results using cryosectioning approach (Tokuyasu, 1980). The most reliable method for ultrastructural characterization of the protein composition of plasma membrane invaginations thus seems to be the approach combining high-pressure freezing (HPF), cryosubstitution (freeze substitution or FS) and low-temperature embedding. The use of modified substitution medium (see Materials and Methods for details) led to a poor membrane contrast in these samples. Nevertheless, using the HPF-FS approach, we were able to confirm the Sur7-GFP and Pil1-GFP localization observed on chemically fixed cells, but in the context of a well-preserved ultrastructure (Fig. 7A). In addition, a slight difference could be distinguished between localization of the two proteins; although Pil1 regularly localized along deeper parts of the furrow-like invagination, mainly at its negatively curved bottom (Fig. 7B-D), similar distribution of Sur7 was rare (Fig. 8A, top panel). Sur7 was rather detected at the most superficial parts of the invaginated plasma membrane, at the positively curved rim of this labeled structure (Fig. 8A, mid and bottom panels). Decoration of individual furrows could be followed on superficial, nearly tangential sections (Fig. 8B).

Discussion

Phylogenetically, furrow-like plasma membrane invaginations represent a highly conserved structure. Grooves that are almost identical to those observed in the plasma membrane of *S. cerevisiae* have been found in several other yeast species, such as *Candida albicans* (Barug and de Groot, 1985) and *Schizosaccharomyces pombe* (Takeo, 1984), in other fungi, such as *Lichinella stipatula* (Büdel and Rhiel, 1987) and *Spotothrix schenckii* (Svoboda and Trujillo-Gonzalez, 1990), in bacteria, such as *Micrococcus* (Sleytr and Kocur, 1971; Sleytr et al., 1976) and in green algae, including several *Chlamydomonas* species (Clarke and Leeson, 1985). Similar structures were also observed in higher plants, such as *Plumbago zeylanica* (Southworth et al., 1997). We identify these plasma membrane invaginations with the patches of MCC observed in *S. cerevisiae* by fluorescence microscopy (Malinska et al., 2003). Several pieces of evidence are presented, which allow us to draw this conclusion.

First, furrow-like invaginations are absent in the mutants defective in MCC patch integrity. Drastically reduced numbers of invaginations were observed in the freeze-fractured plasma membrane of *pil1Δ* cells, which show only few aberrant accumulations of fluorescent MCC markers. In the membrane of *nce102Δ* cells with homogenous distribution of MCC transporters, but patchy appearance of Sur7 and Pil1 (Grossmann et al., 2008), flat, smooth, elongated lateral domains, but no invaginations were detected (Fig. 1H,I).

Next, the distribution and surface density of both structures were comparable. Similarly to the MCC patches (Moreira et al., 2009), furrow-like invaginations also seem to be randomly distributed in the membrane (Moor and Mühlethaller, 1963; Gross et al., 1978) and are most abundant in old mother cells (Takeo, 1984). In accordance with the MCC appearance on buds (Grossmann et al., 2008), few invaginations were found on dynamically developing membranes, such as young buds of *S. cerevisiae* and the central division ring in *S. pombe* (Takeo, 1984) or the germ tube of *C. albicans* (Miragall et al., 1986). MCC patches also do not colocalize with the cortical ER (Fig. 4). Direct counting revealed a ~twofold higher density of

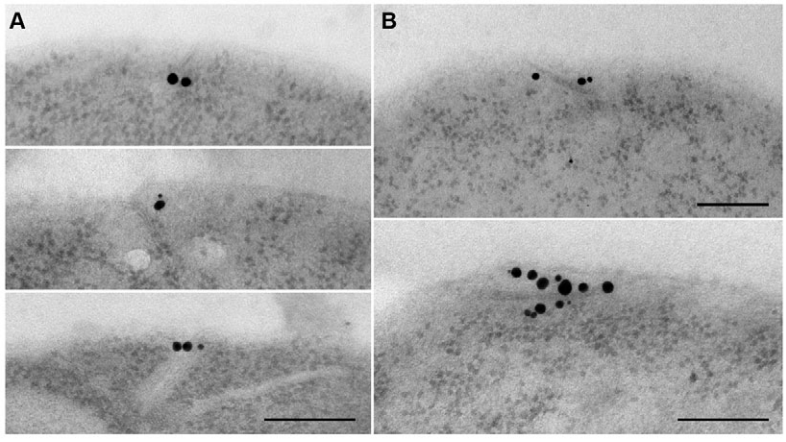

Fig. 8. Post-embedding immunogold localization of Sur7. The MCC marker Sur7-GFP was localized on ultrathin HM20-embedded sections of high-pressure-frozen cells. Three cross sections (A) and two nearly tangential sections (B) are presented. Note the different localization in the upper compared to the mid and lower panels in A (see text for details). Scale bars: 200 nm.

invaginations compared with MCC patches. As a number of cortical proteins (Young et al., 2002; Malinska et al., 2004; Walther et al., 2006; Grossmann et al., 2008) and ergosterol (Grossmann et al., 2007) were colocalized with Sur7 in MCC patches by fluorescence microscopy, it is not likely that only some invaginations contain Sur7 and thus correspond to MCC patches. The Sur7-negative invaginations would then be structurally indistinguishable from MCC patches, but would have completely different protein and lipid composition. Instead, we show by computer simulation, that the observed discrepancy between the two densities can be entirely ascribed to the resolution limit of fluorescence microscopy: even if distributed in a plane perpendicular to the optical axis of the microscope, the neighboring invaginations were often fused in the simulated fluorescence microscopy image (Fig. 3). On a round cell surface, this effect is further increased owing to the poor axial resolution of the microscope.

Abnormally elongated invaginations were observed in protoplasts (Necas et al., 1969). Freeze-fracture data suggested that grooves 1-2 μm long or even longer arose by longitudinal fusion of short invaginations during the protoplast formation (Miragall et al., 1986). Accordingly, elongated, negatively stained MCC patches could be recognized in the plasma membrane pattern of fluorescing H^+-ATPase Pma1-GFP on protoplasts prepared by zymolyase digestion (Malinska et al., 2004). We present here another example of morphologically altered plasma membrane: the membrane of intact *ypr050cΔ* cells with elongated MCC patches and/or invaginations (Fig. 5). As mentioned in the Results, the *ypr050cΔ* phenotype could in fact be caused by the absence of Mak3, the catalytic subunit of N-terminal acetyltransferase C (NatC) complex. NatC-mediated acetylation was shown to be required for the targeting of the small GTPase Arl3 to Golgi membranes (Behnia et al., 2004; Setty et al., 2004). None of the 12 soluble proteins known to colocalize with MCC (Grossmann et al., 2008) seems, however, to be itself a subject of NatC-mediated acetylation. Any role of the NatC complex in MCC patch fission would thus be an indirect one. For example, the impaired recruitment of vesicle-tethering factors to the Golgi in *mak3Δ* cells could lower the rate of vesicle trafficking. Elongated MCC patches in these cells would then appear as a consequence of decreased plasma membrane dynamics.

Finally, the identification of MCC patches with furrow-like plasma membrane invaginations was confirmed by the immunogold localizations of MCC- and eisosome-specific proteins, Sur7 and Pil1, respectively (Figs 6-8). In the well-preserved ultrastructure of high-pressure-frozen cells, a possible spatial separation of Sur7-containing MCC from Pil1-marked eisosomes was indicated. This observation could not be verified on double-labeled specimens because the signal intensity dropped substantially upon usage of antibodies conjugated with bulky gold particles.

Based on these results, we propose the following model of the formation of furrow-like invaginations: (1) Sur7-enriched, elongated, planar domains devoid of hexagonal arrays are assembled by Pil1 in the plasma membrane. Direct involvement of the Sur7-Pil1 interaction in this assembly is unlikely, however, because cortical patches of *C. albicans* Lsp1, a homologue of *S. cerevisiae* Pil1, were detected in a mutant strain of *C. albicans* lacking Sur7 (Alvarez et al., 2008), which is the only member of the Sur7 protein family in this yeast. The formation of Pil1 patches thus seems to be Sur7 independent. (2) Into the preformed patches, specific transporters are recruited by Nce102 (Grossmann et al., 2008). Specific lipids, such as ergosterol, are recruited with these transporters (Grossmann et al., 2007). (3) Although the participation of membrane proteins in the final step of the furrow formation cannot be excluded so far, this local sterol accumulation is already enough to promote the membrane deformation and could form the furrow-like invagination. It is worth mentioning that another lipid preferring curved membrane localization, phosphatidylethanolamine, is essential for targeting an original constituent of the MCC, Can1, to the plasma membrane (Opekarova et al., 2002).

In the past decade, the view of the plasma membrane as a highly dynamic, laterally compartmented cellular organelle, rather than a fluid, homogenous mosaic, has become generally accepted. In light of our findings, partitioning of the plasma membrane into lateral domains is now finally resolvable by direct observation of intact cells. In the freeze-fractured flat plasma membrane of the *nce102Δ* mutant, which is devoid of any invaginations, MCC patches appear to be smooth, elongated areas within an otherwise particle-rich surface. Without any obvious relationship to the cytoskeleton (Malinska et al., 2004), they represent autonomous membrane domains with a specific composition and function.

Materials and Methods

Yeast strains and growth conditions

Yeast strains used in this study are listed in supplementary material Table S1. If not stated otherwise, cells were grown in a rich medium (YPD; 2% peptone, 1% yeast extract, 2% glucose) at 30°C on a shaker. Cells expressing *CAN1-GFP* and *ss-GFP-HDEL* were cultured in arginine- and leucine-free synthetic medium (0.67% Difco yeast nitrogen base without amino acids, 2% glucose and essential amino acids), respectively.

Confocal microscopy and computer simulations

Living yeast cells (Figs 1 and 4: exponentially growing culture, OD_{600} 0.5-1.0; Fig. 5: overnight culture) were washed briefly in 50 mM potassium phosphate buffer (pH 6.3; KPi), immobilized by a thin film of 1% agarose in KPi and observed at 30°C. Specimens were viewed using LSM510-META confocal microscope (Zeiss) with a ×100 PlanApochromat oil-immersion objective (NA=1.4). Fluorescence signals of GFP and mRFP (excitation 488 nm/Ar laser, and 543 nm/HeNe laser) were detected using band-pass 505-550 nm, and long-pass 580 nm emission filters, respectively.

For the computer simulations, the sets of model objects were generated in Matlab software (The MathWorks). Invaginations were simulated as randomly positioned, randomly oriented, 250-nm-long rods. The only distribution constraint applied was the zero overlap of neighboring objects; 1000 objects per image were generated. We used the confocal image of fluorescent latex bead (175 nm in diameter; Molecular Probes) as a 2D point spread function (PSF) of the microscope. All the microscope settings, the objective, pinhole, image sampling, and the excitation and emission wavelengths were set identically to those for the real images. Model objects were convolved with PSF using Matlab.

Pre-embedding immunogold labeling and Epon embedding

Exponentially growing cells (OD 0.5-1.0) were pre-incubated with 30 mM final concentrations EGTA and 10 μg/ml pepstatin A (Sigma) for 5 minutes on a shaker at room temperature. The cells were fixed in 3.7% formaldehyde in PEM buffer (0.1M PIPES, 5 mM EGTA, 5 mM $MgCl_2$; pH 6.9) for 45 minutes at room temperature and washed twice with PEMI (PEM + 10 μg/ml pepstatin A; all centrifugation steps were performed at 200 ***g***). The cell walls were digested using 20 μg/ml zymolyase (zymolyase-20T, Seikagaku) with 40 μg/ml pepstatin A in KCP buffer (0.1 M K_2HPO_4 + 0.1M citric acid, pH 5.9) for 20-40 minutes at room temperature. The cells were washed twice in PEMI, permeabilized with methanol (30%, 50%, 70% and 90% in water, for 2 minutes each) and rehydrated through a methanol series again. After two washing steps in PEMI, the cells were incubated with primary antibody (in PEMI) for 1 hour at room temperature, washed three times in PEMI and incubated in the secondary antibody conjugated with ultra small gold for 1 hour. Post-fixation (4% glutaraldehyde in PEM, 15 minutes) was used to prevent the loss of signal during the subsequent intensification (silver enhancement kit, Aurion). The labeled cells were pelleted in 10% gelatine, fixed again in 4% glutaraldehyde (in water, 1 hour at 4°C), washed and cut into small pieces. The samples were dehydrated at room temperature through a graded ethanol series (30%, 50%, 70%, 90% and 96%), infiltrated subsequently in 1:1 (v:v) ethanol:epon/durcupan mixture (2 hours at room temperature), 2:1 mixture (overnight, 4°C), and the pure resin (1 hour, and then for 2 hours at room temperature). Infiltrated samples were placed in epon/durcupan-filled molds and polymerized at 60°C for 3 days.

High-pressure freezing, freeze substitution and plastic embedding

Living yeast cells (overnight culture) were concentrated by suction filtration (McDonald and Müller-Reichert, 2002) onto a filter and this was then placed onto a YPD agar plate. The yeast paste was scraped from the filter, put on a flat specimen carrier (Leica, 1.2 mm cavity diameter) and quickly frozen in a Leica EM PACT high-pressure freezer (Studer et al., 2001).

Frozen samples in the carriers were transferred under liquid nitrogen to freeze substitution medium (different for each purpose – see below) in cryovials and placed in a Leica AFS machine. Cells were freeze substituted at –90°C for 3 days. Thereafter, the temperature was elevated to –50°C (5°C per hour) and samples were kept for about 12 hours at this temperature. After this period, the specimens were washed four times with fresh pre-cooled acetone at –50°C and then infiltrated with Lowicryl HM20, following one of the following protocols.

For the best structure preservation, the FS medium consisted of 3% glutaraldehyde (70% stock; Sigma), 0.1% uranyl acetate (20% methanolic stock; Polysciences) and 1.3% H_2O in acetone (glass distilled; Polysciences) (O'Toole et al., 2002). For immunolabeling detection, the FS medium was modified to contain 0.1% uranyl acetate and 1% H_2O in acetone. After the acetone wash at –50°C, the samples were infiltrated subsequently in 3:1, 1:1, 1:3 (v:v) acetone:HM20 mixtures for 2 hours each at –50°C; then incubated for 2 hours at –50°C in 100% HM20 and finally placed in fresh resin and polymerized with UV for 48 hours at –40°C and ~3days at 20°C.

Post-embedding immunogold labeling

For immunogold labeling, sections on formvar-coated gilded copper grids were blocked in 5% bovine serum albumin (BSA) in phosphate-buffered saline (PBS) for 30 minutes, and incubated for 1 hour on droplets of primary antibody diluted in 1% BSA-PBS. Afterwards, the grids were washed on droplets of PBS for 15 minutes, and incubated with ultra small gold-conjugated secondary antibody for 2 hours. In controls, the primary antibody was omitted. After three washes in PBS, the grids were post-fixed in 8% glutaraldehyde for 15 minutes, washed on droplets of distilled water, silver-enhanced (Aurion), air-dried and contrasted.

Antibodies for immunogold labeling

Primary antibodies: rabbit anti-Sur7 (Pineda Antikörper-Service, Germany; diluted 1:1000 for pre-embedding detection) was designed to recognize C-terminal (cytoplasmic) epitope of the Sur7 molecule; rabbit anti-GFP (Fitzgerald; diluted 1:100 for pre-embedding detection and 1:50 for post-embedding detection) was used to localize C-terminally tagged Sur7-GFP and Pil1-GFP. In post-embedding procedures, this antibody was pretreated with 0.5 mg/ml purified yeast mannan for 30 minutes to suppress the non-specific cell wall binding (Rossanese et al., 1999). Secondary antibody used was ultra small goat anti-rabbit IgG-gold (Aurion; diluted 1:100).

Freeze fracture and freeze etching

Cells from overnight culture were harvested by centrifugation (1 minute at 1500 ***g***) and washed in KPi buffer (pH 5.5). A 2 µl aliquot of the concentrated cell suspension was loaded onto a gold carrier and frozen rapidly in liquid nitrogen. The sample was cut with a cold knife (≤–185°C), etched for 4 minutes (–97°C; pressure $\leq 1.3\times10^{-5}$ Pa) in a CFE-50 freeze-etch unit (Cressington, Watford, UK), shadowed (1 nm Pt/C, 45°; 10 nm C, 90°), and cleaned in fresh 70% H_2SO_4 for 16 hours (Rachel et al., 2002).

Sectioning and electron microscopy

Ultrathin sections (70 nm; 60 nm for serial sections) were cut with a Leica EM UC6 or Ultracut S ultramicrotome equipped with a diamond knife (35°; 45° for Epon; Diatome) and placed on formvar-coated grids (copper; gilded copper for immunolabeling). Sections were contrasted with a saturated aqueous solution of UA for 1 hour, washed, air-dried and examined in a FEI Morgagni 268(D) transmission electron microscope at 80 kV. Images were captured with Megaview II CCD camera. Some of the freeze-fracture micrographs (Fig. 1) were acquired on Philips CM 12 (FEI, The Netherlands) operated at 120 kV and equipped with a slow CCD camera (TVIPS, Tietz, Gauting/Munchen).

We are grateful to Dusan Cmarko (Charles University, Prague) and Jürgen Stolz (TU Munich) for stimulating discussions, and to Andreas Klingl for skillful assistance with freeze etching. We also thank to Yves Barral (ETH-Hönggerberg, Zürich) for the kind gift of ss-GFP-HDEL plasmid. V.S., M.B. and J.M. were financially supported by the Grant Agency of the Czech Republic (projects 204/07/0133 and 204/08/J024), the Grant Agency of the Academy of Sciences of the CR (KAN200520801), the Grant Agency of the Charles University in Prague (79508) and by the institutional grant (AVOZ50390703). G.G., W.S. and W.T. were supported by the Deutsche Forschungsgemeinschaft (DFG-Priority Program 1108 and TA 36/18-1).

References

Alvarez, F. J., Douglas, L. M. and Konopka, J. B. (2008). Sterol-rich plasma membrane domains in fungi. *Eukaryot. Cell* **6**, 755-763.

Barug, D. and de Groot, K. (1985). Effect of the imidazole derivative lombazole on the ultrastructure of Staphylococcus epidermidis and Candida albicans. *Antimicrob. Agents Chemother.* **28**, 643-647.

Behnia, R., Panic, B., Whyte, J. R. C. and Munro, S. (2004). Targeting of the Arf-like GTPase Arl3p to the Golgi requires N-terminal acetylation and the membrane protein Sys1p. *Nat. Cell Biol.* **6**, 405-413.

Branton, D., Bullivant, S., Gilula, N. B., Karnovsky, M. J., Moor, H., Mühlethaler, K., Northcote, D. H., Packer, L., Satir, B., Satir, P. et al. (1975). Freeze-etching nomenclature. *Science* **190**, 54-56.

Büdel, B. and Rhiel, E. (1987). Studies on the ultrastructure of some Cyanolichen haustoria. *Protoplasma* **139**, 145-152.

Clarke, K. J. and Leeson, E. A. (1985). Plasmalemma structure in freezing tolerant unicellular algae. *Protoplasma* **129**, 120-126.

Coulary, B., Aigle, M. and Schaeffer, J. (2001). Evidence for glycogen structures associated with plasma membrane invaginations as visualized by freeze-substitution and the Thiery reaction in Saccharomyces cerevisiae. *J. Electron Microsc. (Tokyo)* **50**, 133-137.

Deng, C., Xiong, X. and Krutchinsky, A. N. (2009). Unifying fluorescence microscopy and mass spectrometry for studying protein complexes in cells. *Mol. Cell Proteomics* **8**, 1413-1423..

Fisk, D. G., Ball, C. A., Dolinski, K., Engel, S. R., Hong, E. L., Issel-Tarver, L., Schwartz, K., Sethuraman, A., Botstein, D., Cherry, J. M. et al. (2006). Saccharomyces cerevisiae S288C genome annotation: a working hypothesis. *Yeast* **23**, 857-865.

Gross, H., Kuebler, O., Bas, E. and Moor, H. (1978). Decoration of specific sites on freeze-fractured membranes. *J. Cell Biol.* **79**, 646-656.

Grossmann, G., Opekarová, M., Novakova, L., Stolz, J. and Tanner, W. (2006). Lipid raft-based membrane compartmentation of a plant transport protein expressed in Saccharomyces cerevisiae. *Eukaryot. Cell* **5**, 945-953.

Grossmann, G., Opekarová, M., Malinsky, J., Weig-Meckl, I. and Tanner, W. (2007). Membrane potential governs lateral segregation of plasma membrane proteins and lipids in yeast. *EMBO J.* **26**, 1-8.

Grossmann, G., Malinsky, J., Stahlschmidt, W., Loibl, M., Weig-Meckl, I., Frommer, W. B., Opekarová, M. and Tanner, W. (2008). Plasma membrane microdomains regulate turnover of transport proteins in yeast. *J. Cell Biol.* **183**, 1075-1088.

Idrissi, F.-Z., Grötsch, H., Fernández-Golbano, I. M., Presciatto-Baschong, C., Riezman, H. and Geli, M. I. (2008). Distinct acto/myosin-I structures associate with endocytic profiles at the plasma membrane. *J. Cell Biol.* **180**, 1219-1232.

Kaksonen, M., Toret, C. P. and Drubin, D. G. (2005). A modular design for the clathrin- and actin-mediated endocytosis machinery. *Cell* **123**, 305-320.

Kopecka, M. and Gabriel, M. (1995). Actin cortical cytoskeleton and cell wall synthesis in regenerating protoplasts of the Saccharomyces cerevisiae actin mutant DBY 1693. *Microbiology* **141**, 1289-1299.

Maier, P., Rathfelder, N., Maeder, C. I., Colombelli, J., Stelzer, E. H. K. and Knop, M. (2008). The SpoMBe pathway drives membrane bending necessary for cytokinesis and spore formation in yeast meiosis. *EMBO J.* **27**, 2363-2374.

Malínská, K., Malinsky, J., Opekarová, M. and Tanner, W. (2003). Visualization of protein compartmentation within the plasma membrane of living yeast cells. *Mol. Biol. Cell* **14**, 4427-4436.

Malínská, K., Malinsky, J., Opekarová, M. and Tanner, W. (2004). Distribution of Can1p into stable domains reflects lateral protein segregation within the plasma membrane of living S. cerevisiae cells. *J. Cell Sci.* **117**, 6031-6041.

McDonald, K. L. and Müller-Reichert, T. (2002). Cryomethods for thin section electron microscopy. *Methods Enzymol.* **351**, 96-123.

Miragall, F., Rico, H. and Santadreu, R. (1986). Changes in the plasma membrane of regenerating protoplasts of *Candida albicans* as revealed by freeze-fracture electron microscopy. *J. Gen. Microbiol.* **132**, 2845-2853.

Moor, H. and Mühlethaler, K. (1963). Fine structure in frozen-etched yeast cells. *J. Cell Biol.* **17**, 609-628.

Moreira, K. E., Walther, T. C., Aguilar, P. S. and Walter, P. (2009). Pil1 controls eisosome biogenesis. *Mol. Biol. Cell* **20**, 809-818.

Mulholland, J., Preuss, D., Moon, A., Wong, A., Drubin, D. and Botstein, D. (1994). Ultrastructure of the yeast actin cytoskeleton and its association with the plasma membrane. *J. Cell Biol.* **125**, 381-391.

Murthi, A. and Hopper, A. K. (2005). Genome-wide screen for inner nuclear membrane protein targeting in *Saccharomyces cerevisiae*: roles for N-Acetylation and an integral membrane protein. *Genetics* **170**, 1553-1560.

Necas, O., Kopecka, M. and Brichta, J. (1969). Interpretation of surface structures in frozen-etched protoplasts of yeasts. *Exp. Cell Res.* **58**, 411-419.

Opekarová, M., Robl, I. and Tanner, W. (2002). Phosphatidyl ethanolamine is essential for targeting the arginine transporter Can1p to the plasma membrane of yeast. *Biochim. Biophys. Acta* **1564**, 9-13.

O'Toole, E. T., Winey, M., McIntosh, J. R. and Mastronarde, D. N. (2002). Electron tomography of yeast cells. *Methods Enzymol.* **351**, 81-95.

Rachel, R., Wyschkony, I., Riehl, S. and Huber, H. (2002). The ultrastructure of *Ignicoccus*: evidence for a novel outer membrane and for intracellular vesicle budding in an archaeon. *Archaea* **1**, 9-18.

Rossanese, O. W., Soderholm, J., Bevis, B. J., Sears, I. B., O'Connor, J., Williamson, E. K. and Glick, B. S. (1999). Golgi structure correlates with transitional endoplasmic

reticulum organization in *Pichia pastoris* and *Saccharomyces cerevisiae*. *J. Cell Biol.* **145**, 69-81.

Setty, S. R. G., Strochlic, T. I., Tong, A. H. Y., Boone, C. and Burd, C. G. (2004). Golgi targeting of ARF-like GTPase Arl3p requires its Nalpha-acetylation and the integral membrane protein Sys1p. *Nat. Cell. Biol.* **6**, 379-380.

Sleytr, U. B. and Kocur, M. (1971). Structure of *Micrococcus cryophilus* after freeze-etching. *Arch. Mikrobiol.* **78**, 353-359.

Sleytr, U. B., Silva, M. T., Kocur, M. and Lewis, N. F. (1976). The fine structure of *Micrococcus radiophilus* and *Micrococcus radioproteolyticus*. *Arch. Microbiol.* **107**, 313-320.

Southworth, D., Strout, G. and Russell, S. D. (1997). Freeze-fracture of sperm of Plumbago zeylanica L. in pollen and in vitro. *Sex Plant Reprod.* **10**, 217-226.

Steere, R. L., Erbe, E. F. and Moseley, J. M. (1980). Prefracture and cold-fracture images of yeast plasma membrane. *J. Cell Biol.* **86**, 113-122.

Studer, D., Graber, W., Al-Amoudi, A. and Eggli, P. (2001). A new approach by high-pressure freezing. *J. Microsc.* **203**, 258-294.

Svoboda, A. and Trujillo-Gonzalez, A. (1990). *Sporothrix schenckii*-a freeze-fracture study. *J. Basic Microbiol.* **30**, 371-378.

Takeo, K. (1984). Lack of invaginations of the plasma membrane during budding and cell division of *Saccharomyces cerevisiae* and *Schizosacharomyces pombe*. *FEMS Microbiol. Lett.* **22**, 94-100.

Tokuyasu, K. T. (1980). Immunochemistry on ultrathin frozen sections. *Histochem. J.* **12**, 381-403.

Walther, T. C., Brickner, J. H., Aguilar, P. S., Bernales, S., Pantoja, C. and Walter, P. (2006). Eisosomes mark static sites of endocytosis. *Nature* **439**, 998-1003.

Young, M. E., Karpova, T. S., Brügger, B., Moschenross, D. M., Wang,G. K., Schneiter, R., Wieland, F. T. and Cooper, J. A. (2002). The Sur7p family defines novel cortical domains in Saccharomyces cerevisiae, affects sphingolipid metabolism, and is involved in sporulation. *Mol. Cell. Biol.* **22**, 927-934.

Zhang, X., Lester, R. L. and Dickson, R. C. (2004). Pil1p and Lsp1p negatively regulate the 3-phosphoinositide-dependent protein kinase-like kinase Pkh1p and downstream signaling pathways Pkc1p and Ypk1p. *J. Biol. Chem.* **279**, 22030-22038.

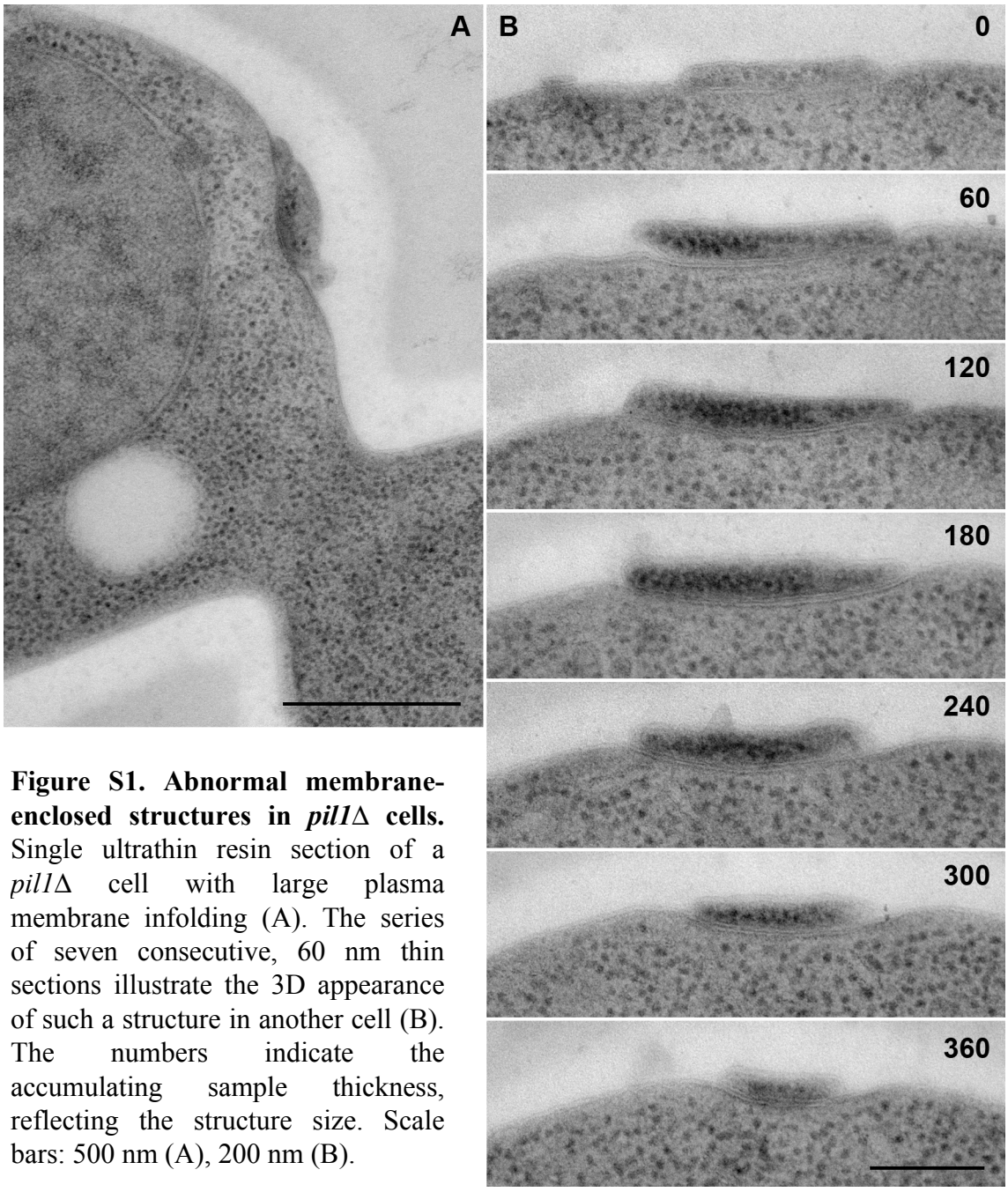

Figure S1. Abnormal membrane-enclosed structures in *pil1*Δ cells. Single ultrathin resin section of a *pil1*Δ cell with large plasma membrane infolding (A). The series of seven consecutive, 60 nm thin sections illustrate the 3D appearance of such a structure in another cell (B). The numbers indicate the accumulating sample thickness, reflecting the structure size. Scale bars: 500 nm (A), 200 nm (B).

Table S1. Strains used in this study

Strain	Genotype	Source
BY4741	*MAT*a *his3_1 leu2_0 met15_0 ura3_0*	Brachmann et al, 1998
BY4742	*MAT_ his3_1 leu2_0 lys2_0 ura3_0*	Brachmann et al, 1998
GYS48	BY4742 ***SUR7::GFP****::URA3* (YIp211)	Grossmann et al, 2007
GYS91	BY4741 ***nce102****::kanMX4*	EUROSCARF
GYS113	BY4742 ***CAN1::GFP****::URA3* (YIp211)	Grossmann et al, 2007
GYS130	BY4741 ***pil1****::kanMX4*	EUROSCARF
GYS206	BY4741 ***SUR7::mRFP****::URA3* (YIp211) 2µp**HDEL::GFP** (*LEU2*)	This study
VSY1	GYS91 ***CAN1::GFP****::LEU2* (YIp 128)	This study
VSY9	BY4741 ***PIL1::GFP****::LEU2* (Yip128)	This study
VSY12	BY4741 ***ypr050c****::kanMX4*	EUROSCARF
VSY13	VSY12 ***SUR7::GFP****::URA3* (YIp211)	This study
VSY14	BY4741 ***mak3****::kanMX4*	EUROSCARF
VSY15	VSY14 ***SUR7::GFP****::URA3* (YIp211)	This study
VSY18	GYS130 ***CAN1::GFP****::LEU2* (YIp128)	This study

RESEARCH PAPER 3

EUKARYOTIC CELL, Aug. 2010, p. 1184–1192 Vol. 9, No. 8
1535-9778/10/$12.00 doi:10.1128/EC.00006-10

C Terminus of Nce102 Determines the Structure and Function of Microdomains in the *Saccharomyces cerevisiae* Plasma Membrane▽

Martin Loibl,[1]† Guido Grossmann,[1]‡ Vendula Stradalova,[2] Andreas Klingl,[3] Reinhard Rachel,[3] Widmar Tanner,[1] Jan Malinsky,[1]* and Miroslava Opekarová[4]

Institute of Cell Biology and Plant Physiology, University of Regensburg, Regensburg, Germany[1]; Institute of Experimental Medicine, Academy of Sciences of the Czech Republic, Prague, Czech Republic[2]; Center for Electron Microscopy—NWF III, University of Regensburg, Regensburg, Germany[3]; and Institute of Microbiology, Academy of Sciences of the Czech Republic, Prague, Czech Republic[4]

Received 8 January 2010/Accepted 21 June 2010

The plasma membrane of the yeast *Saccharomyces cerevisiae* contains stably distributed lateral domains of specific composition and structure, termed MCC (membrane compartment of arginine permease Can1). Accumulation of Can1 and other specific proton symporters within MCC is known to regulate the turnover of these transporters and is controlled by the presence of another MCC protein, Nce102. We show that in an *NCE102* deletion strain the function of Nce102 in directing the specific permeases into MCC can be complemented by overexpression of the *NCE102* close homolog *FHN1* (the previously uncharacterized *YGR131W*) as well as by distant *Schizosaccharomyces pombe* homolog *fhn1* (*SPBC1685.13*). We conclude that this mechanism of plasma membrane organization is conserved through the phylum *Ascomycota*. We used a hemagglutinin (HA)/Suc2/His4C reporter to determine the membrane topology of Nce102. In contrast to predictions, its N and C termini are oriented toward the cytosol. Deletion of the C terminus or even of its last 6 amino acids does not disturb protein trafficking, but it seriously affects the formation of MCC. We show that the C-terminal part of the Nce102 protein is necessary for localization of both Nce102 itself and Can1 to MCC and also for the formation of furrow-like membrane invaginations, the characteristic ultrastructural feature of MCC domains.

Stable lateral domains coexist within the plasma membrane of the yeast *Saccharomyces cerevisiae*. Nce102, a protein originally thought to be involved in nonclassical export (6) and more recently in sensing sphingolipids (10), is the main organizer of one type of these domains, termed MCC (membrane compartment of Can1) (25). MCC consists of evenly distributed, isolated patches enriched in sterols and specific proteins (15, 16, 25, 26). We showed that MCC-specific proton symporters accumulate in these patches in a reversible, membrane potential-dependent manner. This Nce102-mediated transient MCC accumulation plays a key role in the turnover of the transporters (16). Each MCC patch is accompanied by an eisosome, a cytosolic complex located directly beneath the membrane (36).

In an early freeze-etching study, Moor and Mühlethaler (28) demonstrated that the yeast plasma membrane contains numerous furrow-like invaginations. Recently, MCC patches were identified with these plasma membrane structures, and Nce102 was shown to be necessary for furrow formation. On the ultrastructural level, the MCC patches of *nce102*Δ cells appeared as flat, smooth, elongated areas within an otherwise particle-rich plasma membrane (32).

There is now increasing evidence that cytosolic Pil1, a primary component of eisosomes, is a prerequisite for MCC patch formation. It marks the sites where Nce102 and the MCC-specific transporters will subsequently accumulate (16, 23, 29). Data published so far do not indicate a direct involvement of cytoskeletal components in this process (26). Accordingly, markers of classical endocytosis, which are coupled to the cortical patches of actin, were localized outside the MCC (16).

In this paper we examine the contribution of Nce102 to the organization of MCC patches and of furrow-like invaginations. Our results indicate that, in contrast to the prediction of four transmembrane domains (TMDs), the Nce102 molecule might span the plasma membrane only twice, the C and N termini being oriented toward the cytoplasm. We find that the C-terminal 6 amino acids of Nce102 are essential for MCC patch formation as well as for the formation of the furrow-like membrane invaginations. In addition it is shown that this Nce102 function is phylogenetically conserved among *Ascomycota*.

MATERIALS AND METHODS

Yeast strains and growth conditions. Yeast strains used in this study are listed in Table 1 (4, 15, 19, 33). If not stated otherwise, cells were grown in a rich medium (YPD [1% yeast extract, 2% peptone, 2% glucose]) at 30°C on a shaker. Synthetic defined (SD) medium contained 0.67% Difco yeast nitrogen base without amino acids and 2% glucose supplemented with, depending on which marker was used to select for transformed cells, uracil and adenine (both 20 μg/ml) and amino acids (histidine, methionine, and tryptophan, each at 20 μg/ml, and lysine and leucine, each at 30 μg/ml). All yeast transformations were carried out by the high-efficiency method described by Gietz and Woods (14).

Construction of overexpression and tagging plasmids. *S. cerevisiae* genes *NCE102* and *FHN1* (*YGR131W*) and *S. pombe* gene *fhn1* (*SPBC1685.13*) were amplified by PCR from genomic DNA using the following primers (F and R for forward and reverse, respectively): *NCE102*-F (ATATAAGCTTATAATGCTAGC CCTAGC), *NCE102*-R (ATTACTCGAGACTTGGGAAATGGTT), *FHN1*-F (A

* Corresponding author. Mailing address: Institute of Experimental Medicine, Academy of Sciences of the Czech Republic, Videnska 1083, 142 20 Prague, Czech Republic. Phone and fax: 420 241 062 597. E-mail: malinsky@biomed.cas.cz.

† Present address: Heidelberg Institute for Plant Science, Heidelberg University, Heidelberg, Germany.

‡ Present address: Carnegie Institution for Science, Department for Plant Biology, 260 Panama Street, Stanford, CA 94305.

▽ Published ahead of print on 25 June 2010.

TABLE 1. Yeast strains used in this study

Strain	Genotype	Reference or source
BY4741	*MAT***a** *his3Δ1 leu2Δ0 met15Δ0 ura3Δ0*	4
GYS90	BY4741; YIplac211-*CAN1-GFP*	15
GYS91	BY4741; *nce102*::*kanMX4*	EUROSCARF
VSY1	GYS91; *CAN1*::*GFP*::*LEU2* (YIp128)	This study
VSY4	VSY1; pVT100U-*NCE102-mRFP*	This study
VSY5	VSY1; pVT100U-*YGR131W-mRFP*	This study
VSY6	VSY1; pVT100U-*mRFP*	This study
VSY47	VSY1; pVT100U-*SPBC1685.13-mRFP*	This study
STY50	*MAT***a** *his4-401 leu2-3,112 trp1-1 ura3-52 HOL1-1 suc2*::*LEU2*	33
MLY95	STY50 pJK90	18
MLY90	STY50 pJK90-*NCE102*(1-519 bp)	This study
MLY91	STY50 pJK90-*NCE102*(1-438 bp)	This study
MLY92	STY50 pJK90-*NCE102*(1-282 bp)	This study
MLY93	STY50 pJK90-*NCE102*(1-189 bp)	This study
MLY94	STY50 pJK90-*NCE102*(1-84 bp)	This study
MLY100	BY4741; YIplac211-*NCE102*(1-438 bp)-*GFP*	This study
MLY46	BY4741; YIplac211-*NCE102-GFP*	This study
MLY105	GYS90; YIplac128-*NCE102*(1-438 bp)	This study
MLY106	GYS90; YIplac128-*NCE102*(1-501 bp)	This study

GCATCTAGAATAATAAATGCTATCAG), *FHN1*-R (AGTAGGATCCAACC TGGGAAATTGT), *S.pombe-fhn1*-F (CCCAAAGCTTATGGTTGGAATCAG), *S.pombe-fhn1*-R (AAAAGGATCCAACGGCAGACATGAC). Resulting fragments were cloned into plasmid pVT100U-mRFP, which was constructed as follows. The monomeric red fluorescent protein (mRFP) gene including an upstream MluI restriction site, the linker region, the 3′ untranslated region (UTR), and a downstream MfeI site was amplified by PCR from pmRFPkanMX using the primers KM33 (ATATACGCGTTGGAGCAGGGGCGGGTGCCTCCTCCGAGGAC GTC; F) and JST86 (AAAAAACAATTGCAGGCATTTGCTCGGCAT; R). The PCR product was ligated as an MluI-MfeI fragment into pVT100U (2μm *URA3* Amp^R) (35) and transformed into *Escherichia coli* for amplification.

To express 3′-terminally truncated versions of *NCE102*, the genomic sequence was amplified using the primer ML23 (GTGTTTGTTACGCATGCAAGCTTG ATATCGAAATGCTAGCCCTAGCTGATAAC), ML47 (ATATGGATCCTT AAACACCGACTTGGCCAGTTC; $NCE102_{1\text{-}167}$), or ML48 (ATATGGATCC TTAGATCATGTTGAAAACAGACATC; $NCE102_{1\text{-}146}$). The PCR products were inserted as HindIII-BamHI fragments into integrative plasmids YIplac128 and YIplac211-GFP (13, 15). Linearization of these plasmids with BcuI within the *NCE102* gene targets integration in wild-type *S. cerevisiae.* In the case of YIplac128-$NCE102_{1\text{-}167}$ and YIplac128-$NCE102_{1\text{-}146}$, the cells were subsequently transformed using YIplac211-*CAN1-GFP* (15) linearized by BcuI.

Isolation of crude membranes. Early logarithmic cells (100 optical density at 600 nm [OD_{600}] units) were washed twice by 10 mM NaN_3/NaF buffer to block endocytosis and resuspended in ice-cold TNE-I buffer (50 mM Tris-HCl, pH 7.4, 150 mM NaCl, and 5 mM EDTA), supplemented with protease inhibitors (1 mM phenylmethylsulfonyl fluoride [PMSF], 4 μM leupeptin, and 2 μM pepstatin). To isolate crude membranes, the cells were broken with glass beads in a FastPrep instrument (Thermo Fisher Scientific). Unbroken cells and larger cell debris were removed by two-step low-speed centrifugation (500 × *g* and 1,200 × *g*, 5 min each) in an Eppendorf centrifuge at 4°C. Crude membranes were pelleted at 20,000 × *g* for 75 min and resuspended in TNE-I buffer.

Cloning and analysis for topology determination. Topology analysis was performed as described by Kim et al. (18). To amplify and clone 3′-truncated versions of the *NCE102* gene into pJK90 (19), the following PCR primers were used (all primers contain a homologous region for *in vivo* ligation into pJK90): ML23 (F primer, see above) and R primers TGGTCTAGAGGTGTAACCACTTGAGTTC TTAGGGACTTGGGAAATGGTTGGAAC (ML24; amplification of all 519 bp of *NCE102*, excluding the stop codon), TGGTCTAGAGGTGTAACCACTTGAGT TCTTAGGGATCATGTTGAAAACAGACATC (ML25; amplification of 438 bp of *NCE102*), TGGTCTAGAGGTGTAACCACTTGAGTTCTTAGGTCTGATA CCAACGGCCAACAC (ML26; amplification of 282 bp of *NCE102*), TGGTCTA GAGGTGTAACCACTTGAGTTCTTAGGTTCAATGAAGTTGGCAAAGAC (ML27; amplification of 189 bp of *NCE102*), and TGGTCTAGAGGTGTAACCA CTTGAGTTCTTAGGTAACAACGAACTGATTAAACCG (ML28; amplification of 84 bp of *NCE102*). Genomic DNA was used as the template for PCR. For *in vivo* ligation, the vector pJK90 was linearized by digestion with SmaI and treated with calf intestinal alkaline phosphatase to prevent religation. *S. cerevisiae* strain STY50 was transformed with the linearized vector and the full-length *NCE102* or one of the shortened versions of *NCE102* and selected on SD plates lacking uracil (SD −ura plates). Plasmids were isolated, retransformed in *E. coli*, and sequenced. To monitor histidinol dehydrogenase activity, successfully transformed yeast cells were grown on selective media (SD −His −ura supplemented with 6 mM histidinol). For endo-β-*N*-acetylglucosaminidase H (Endo H) assays, 10% SDS and 10% β-mercaptoethanol were added to 20 μl of crude membranes (protein concentration, 8 to 12 μg/μl) to a final concentration of 0.5% each. After incubation at 45°C for 10 min, 88 μl of 100 mM sodium citrate buffer, pH 5.5, and 5.5 μl of 10% octylglucoside were added. The sample was split into two and incubated at 37°C either with 1 μl Endo H (gift from Ludwig Lehle, Regensburg, Germany) or with H_2O as a control. After 2 h of incubation, 1 μl of Endo H or water, respectively, was added again, and the incubation continued for another 2 h. After centrifugation (20,000 × *g* for 5 min), the supernatant was analyzed by SDS-PAGE.

Confocal microscopy. Living yeast cells cultured in SD medium (see Fig. 1 and 3) (log phase; OD_{600} of 0.5 to 1.0) were immobilized by a thin film of 1% agarose in SD medium and observed. Cells cultured in YPD (see Fig. 4) (overnight cultures) were washed briefly in 50 mM potassium phosphate buffer (pH 6.3; KPi), immobilized by a thin film of 1% agarose in KPi, and observed. Specimens were viewed using an LSM510-META confocal microscope (Carl Zeiss) with a 100× PlanApochromat oil immersion objective (numerical aperture [NA] = 1.4). Fluorescence signals of green fluorescent protein (GFP) and mRFP (excitation, 488 nm [Ar laser] and 561 nm [diode-pumped solid-state laser] [see Fig. 1] or 543 nm [He-Ne laser] [see Fig. 4]) were detected using band-pass 505- to 550-nm and long-pass 580-nm emission filters. In double-labeling experiments, sequential scanning was used to avoid any cross talk of fluorescence channels.

Preparation of freeze fracture replicas and electron microscopy. Cells from overnight culture were harvested by mild centrifugation (1,500 × *g* for 1 min) and washed in KPi buffer (pH 5.5). A 2-μl aliquot of the concentrated cell suspension was loaded onto a gold carrier and rapidly frozen in liquid nitrogen. The sample was cut with a cold knife (≤−185°C), etched for 4 min (−97°C; pressure ≤ 1.3×10^{-5} Pa) in a CFE-50 freeze-etch unit (Cressington, Watford, United Kingdom), shadowed (1 nm Pt/C, 45°; 10 nm C, 90°), and cleaned in fresh 70% H_2SO_4 for 16 h (30). Freeze fracture micrographs (see Fig. 5) were acquired using a cooled slow-scan charge-coupled device (CCD) camera (Tvips; Tietz, Gauting, Münich, Germany) mounted on a Philips CM 12 transmission electron microscope (FEI, Netherlands) operated at 120 kV.

RESULTS

Nce102 homologs share Nce102 function in plasma membrane organization. Phylogenetically, furrow-like invaginations of the yeast plasma membrane represent a highly conserved structure (reviewed by Stradalova et al. [32]). Proteins sharing a significant homology with Nce102, a protein shown to be necessary for the final step of the formation of furrows as well as of MCC patches in *S. cerevisiae*, are found in various species of *Ascomycota*. BLAST (Basic Local Alignment Search Tool) analysis (2) reveals more than 40 different Nce102 orthologs. We tested whether the molecular function of promoting the localization of specific transporters in the MCC/furrows is conserved among these Nce102-like proteins.

In the genome of *S. cerevisiae*, open reading frame (ORF) *YGR131W* codes for one of the closest Nce102 homologs (Fig. 1A). Ygr131w shows 55% identity (68% similarity) to Nce102, and its overexpression complements the Nce102 deletion. In the plasma membrane of the *nce102*Δ strain, Can1-GFP is distributed homogenously (16). When overexpressed in *nce102*Δ cells, Ygr131w-mRFP not only accumulates in MCC patches (16) but also induces the accumulation of Can1-GFP in this plasma membrane compartment. Due to the ability of *YGR131W* to replace this *NCE102* function, we named the gene *FHN1* (functional homolog of *NCE102*) (Fig. 1B to D). Since *FHN1* is not able to compensate for the *NCE102* dele-

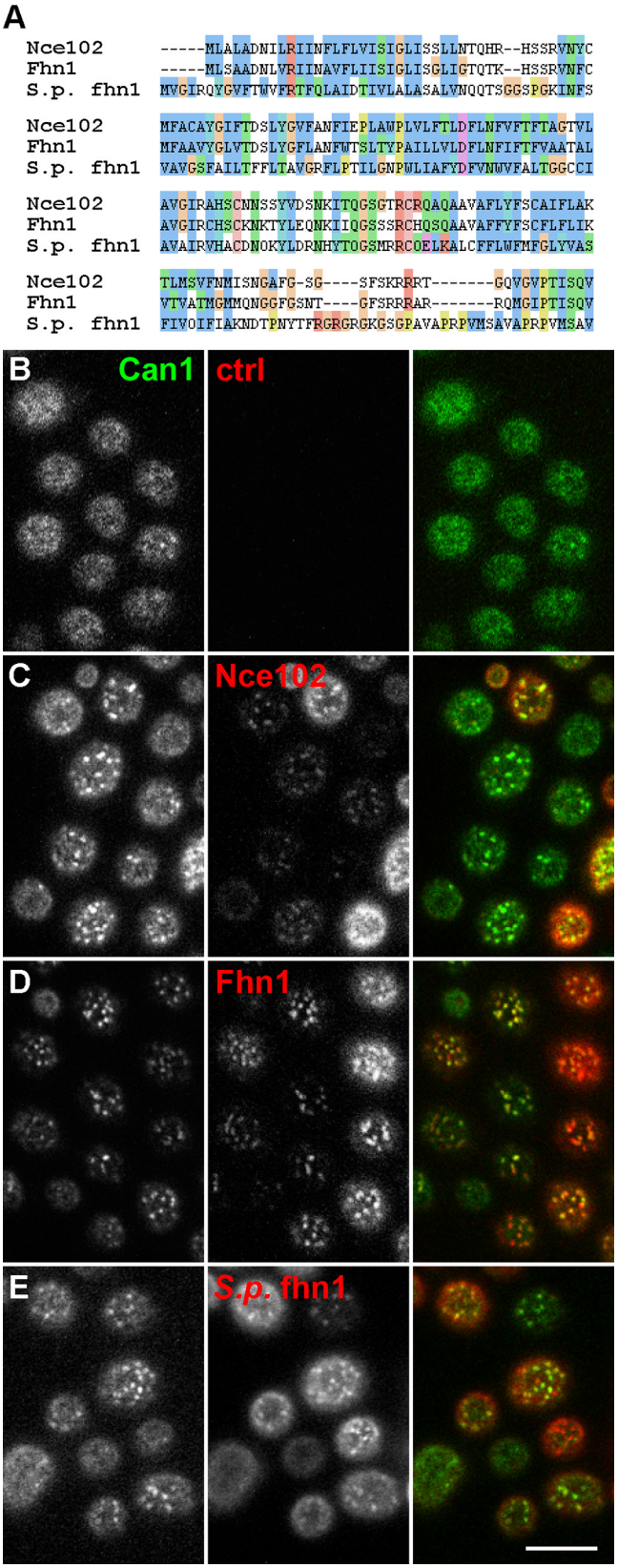

FIG. 1. Nce102-like proteins induce the accumulation of Can1 in MCC patches. (A) *S. cerevisiae* proteins Nce102 and Fhn1 (product of *YGR131W*) and *Schizosaccharomyces pombe* protein fhn1 were aligned using ClustalW 2.0 (22). In the *nce102*Δ mutant of *S. cerevisiae*, Can1-GFP was coexpressed either with an empty plasmid (B) or with vectors coding for *S. cerevisiae* Nce102-mRFP (C) and Fhn1-mRFP (D) and *S. pombe* fhn1-mRFP (E). Note the homogenous distribution of Can1-GFP in panel B and its focal appearance in panels C to E. Bar, 5 μm.

tion when expressed under the control of its own promoter, we conclude that its inherent expression level is not sufficient.

The replacement of Nce102 function in the plasma membrane organization could also be observed when a heterologous *NCE102*-like gene of *Schizosaccharomyces pombe*, the uncharacterized ORF *SPBC1685.13* (31% identity and 52% similarity to *S. cerevisiae NCE102*) (Fig. 1A) was expressed in the *S. cerevisiae nce102*Δ mutant (Fig. 1E). Similarly to Fhn1, the gene product of *SPBC1685.13* was targeted to MCC and induced significant accumulation of Can1-GFP in this compartment. Therefore, we named the gene *fhn1* (functional homolog of *S. cerevisiae NCE102*). Even though the primary structure of Fhn1 shows a relatively low degree of homology with Nce102 (see alignment of *NCE102*, *FHN1*, and *fhn1*), it complements the Nce102 deletion. We concluded therefore that the function of Nce102 in plasma membrane organization is probably widely conserved throughout *Ascomycota*.

Membrane topology of Nce102. Large conserved parts of Nce102 correspond to highly hydrophobic regions of the protein molecule. According to hydropathy analysis tools (e.g., TMHMM2.0; http://www.cbs.dtu.dk/services/TMHMM-2.0/) (21), the protein is predicted to possess 4 transmembrane helices, with N and C termini oriented toward the lumen of the endoplasmic reticulum (ER) during protein synthesis (Fig. 2A, model I) and outside the cell once it reaches the plasma membrane.

To determine the topology of Nce102 experimentally, we employed a technology of a hemagglutinin (HA)/Suc2/His4C chimeric protein tag as a topology reporter (7, 18), a technique widely used for membrane protein topology determination. We constructed vectors coding for Nce102 C-terminally truncated after the 1st, 2nd, 3rd, or 4th predicted transmembrane domain (at amino acid L28, E63, R94, or I146, respectively) (Fig. 2A, model I). The full-length Nce102 and the individual truncated versions described above were C-terminally tagged with HA/Suc2/His4C and expressed in an auxotrophic *his4* strain (7, 9, 18). The ability of the histidinol dehydrogenase (His4C) to convert histidinol to histidine enables a histidine-auxotrophic strain with the reporter located in the cytosol to grow on media lacking histidine but supplemented with histidinol. Invertase (Suc2) and His4C contain eight and four, respectively, consensus acceptor sites for N-linked glycosylation that could be glycosylated only if the reporter is translocated to the lumen of the endoplasmic reticulum. The HA tag is included to allow identification of the expressed fusion proteins by Western blotting.

Anti-HA antibody detected the fusion proteins in crude membranes prepared from all five strains, each expressing one of the truncated versions of *NCE102* or the full-length *NCE102* fused to the reporter. The shift to higher molecular masses of the fusion proteins containing amino acids 1 to 28, 1 to 63, and 1 to 94, which can be abolished by Endo H treatment, proved their glycosylation (Fig. 2C). Therefore, the C termini of these

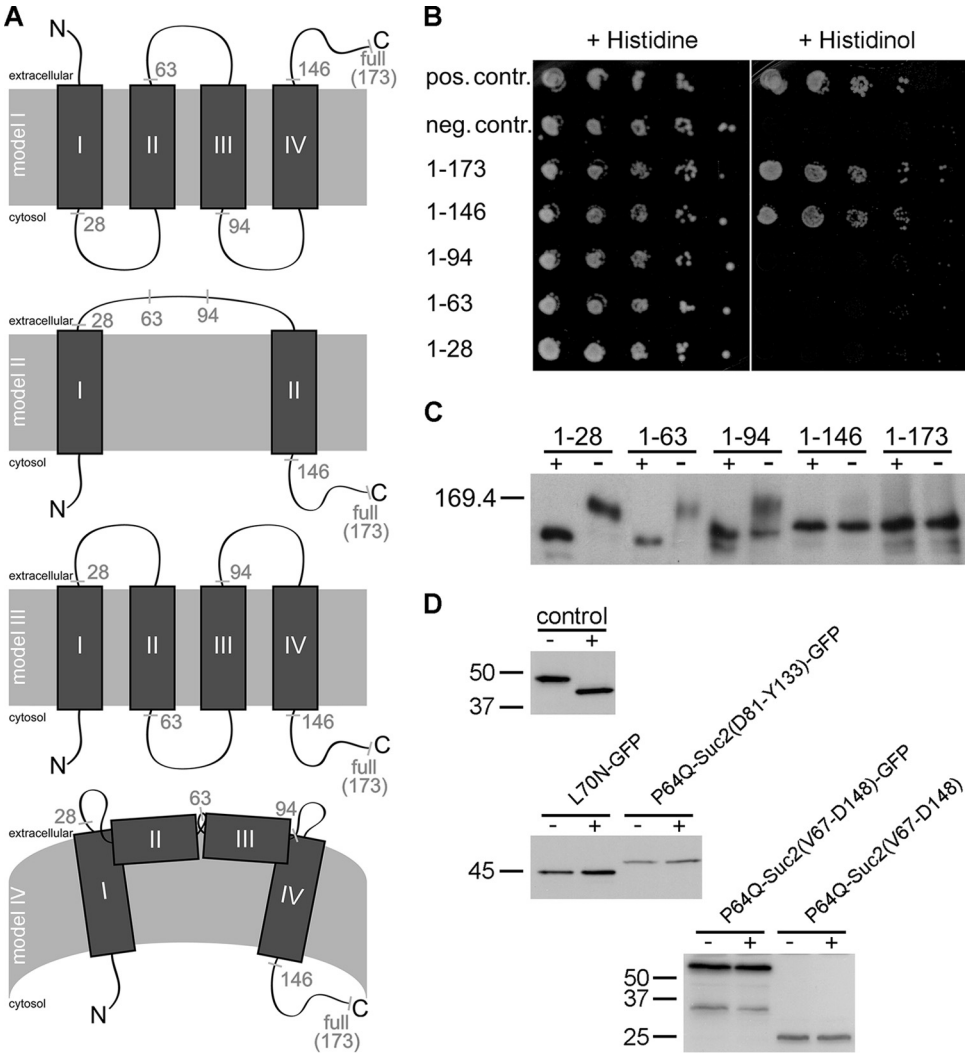

FIG. 2. Nce102 topology. (A) Predicted (I) and experimentally determined (II, III, and IV) topology alternatives for the Nce102 molecule. Sites used for the synthesis of Nce102 truncated versions are depicted. (B) Growth of *his4*Δ cells expressing truncated Nce102s fused to the HA/Suc2/His4C reporter construct was tested on histidine (control; left) and histidinol (His4 substrate; right). Positive control, pJK90-*OST4*-HA-*SUC2-HIS4C* (19); negative control, empty vector. (C) Glycosylation of the reporter can occur only if it faces the ER lumen. Total membrane fractions from strains expressing fusion proteins as described in Materials and Methods were either treated (+) or not treated (−) with Endo H. After SDS-PAGE and Western blotting, the fusion proteins were detected by anti-HA antibody. Cleavage of N-linked glycans was manifested by a shift of the molecular mass. (D) Glycosylation status of Nce102 tested with the use of shortened topology reporters. The positive control (Wbp1, top), L70N Nce102 mutant (middle, left lanes), and Nce102 molecules with shortened Suc2 fragments (middle, right lanes, and bottom) were compared (see text for details).

three constructs were exposed to the ER lumen during their biosynthesis, and consequently, in the plasma membrane, amino acids 28, 63, and 94 should be oriented outside the cell. No molecular mass shift or effect of Endo H treatment was detected in strains bearing the full-length (amino acids 1 to 173) version or the version consisting of amino acids 1 to 146, indicating thus that the stretch of amino acids 146 to 173 was oriented to the cytoplasm (Fig. 2C). This conclusion was also confirmed by the growth on histidinol of the histidine-auxotrophic strains bearing fusion constructs with the full-length or truncated (1 to 146) protein, indicating the cytoplasmic orientation of the C terminus (Fig. 2B).

These results indicate that the Nce102 protein contains only two transmembrane helices (Fig. 2A, model II), corresponding to the first (N-terminal) and last hydrophobic regions in the Nce102 molecule. The middle large hydrophobic region in this interpretation does not span the membrane. A precaution has to be taken is to consider the possibility that the bulky (125-kDa) topology reporter attached to this small (19-kDa) protein and its even smaller fragments could interfere with both their trafficking and folding. However, as shown in Fig. 3, at least the largest Nce102-derived chimeras are targeted properly to the plasma membrane. To minimize the danger of artificial misfolding, we further checked the Nce102 topology by inserting a shortened Suc2 fragment, D81 to Y133 or V67 to D148, into the intact protein. They were inserted after P64Q; including short additional amino acid stretches was thought to possibly prevent potential interference with the putative TMD 2. In

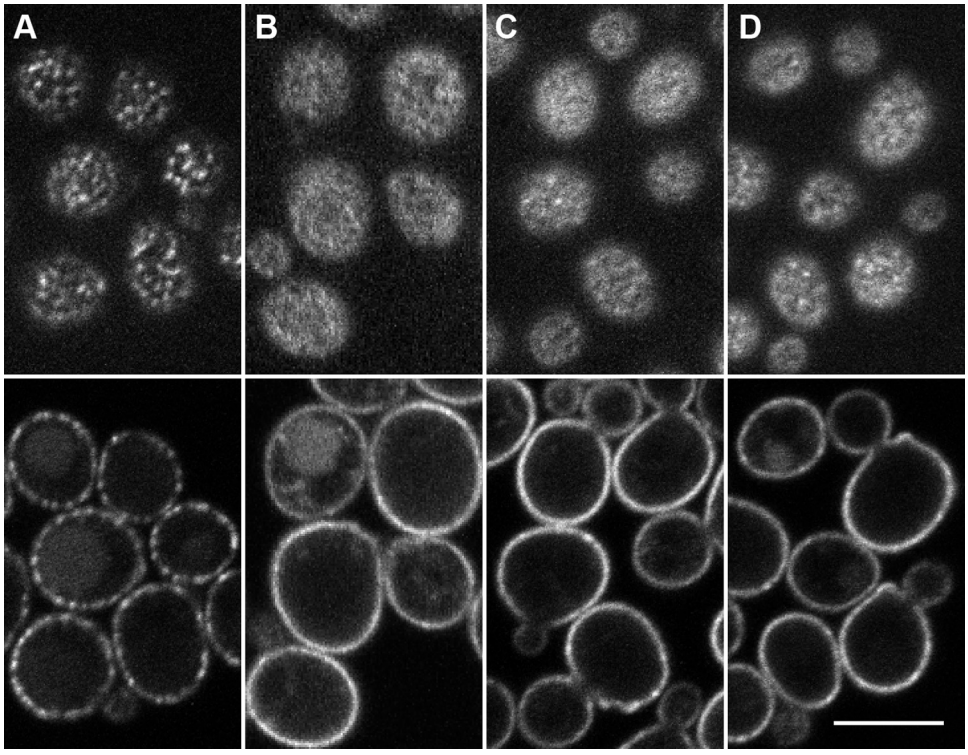

FIG. 3. The C-terminally truncated version of Nce102 is unable to sequester Can1 into MCC. Plasma membrane distributions of Can1-GFP in the wild type (A) and *NCE102* deletion mutant (B) were compared to that in the cells expressing the C-terminally truncated versions of Nce102, $Nce102_{1-146}$ (C) and $Nce102_{1-167}$ (D), under the control of the natural promoter. Surface confocal sections and central confocal cross sections are presented. Bar, 5 μm.

another construct, L70 in Nce102 was exchanged for N to generate a glycosylation site within the loop exposed to the ER lumen in both the computer-predicted topology (model I) and the Suc2/His4C-based experimentally assessed topology above (model II; in this case, however, the orientation of the whole molecule is inverted [Fig. 2A]). The proteins were immunodetected with specific anti-Nce102 antibody. ER protein Wbp1 was used as a positive control for Endo H digestion. As shown in Fig. 2D, the Endo H digestion was not accompanied by a shift in molecular weight with either of the tested proteins, while a clear shift was detected in the control (Wbp1). These results show that the Suc2 reporter was not glycosylated in the ER lumen. The putative model of 4 TMDs with N and C termini inside the cell has, therefore, not definitely been excluded, and model III of Fig. 2A has still to be considered as possibly correct.

The C terminus of Nce102 is necessary to target MCC-specific transporters into MCC. Besides the hydrophobic regions, also the C terminus is highly conserved among the Nce102 homologs. We tested the physiological significance of this highly conserved C terminus in targeting Nce102 to MCC and/or in the gathering (concentrating) of other MCC residents.

The total C-terminal part following the last predicted transmembrane helix, consisting of 27 amino acids, was removed from Nce102, and this truncated version ($Nce102_{1-146}$) was expressed in a wild-type background under the control of an endogenous promoter. In the resulting strain, Can1-GFP was

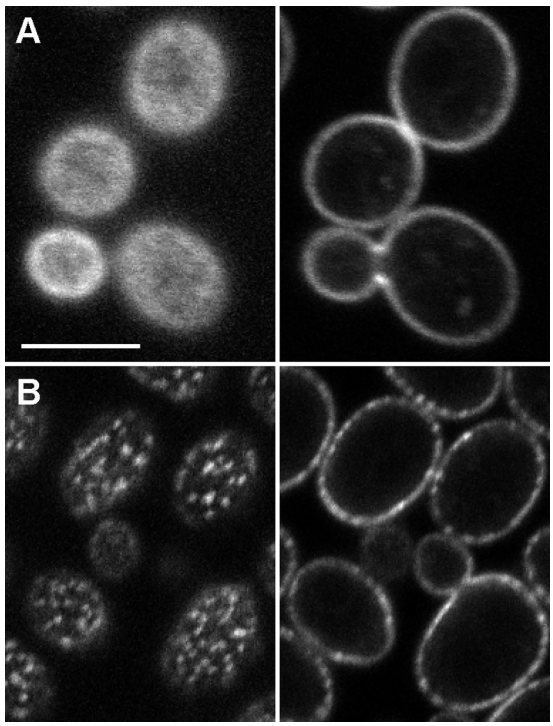

FIG. 4. The C-terminally truncated Nce102 does not localize to MCC. The plasma membrane distribution of C-terminally truncated $Nce102_{1-146}$ (A) tagged with GFP and that of the full-length Nce102-GFP (B) are shown on surface confocal sections (left) and central confocal cross sections (right). Note the absence of a characteristic MCC pattern in panel A. Bar, 5 μm.

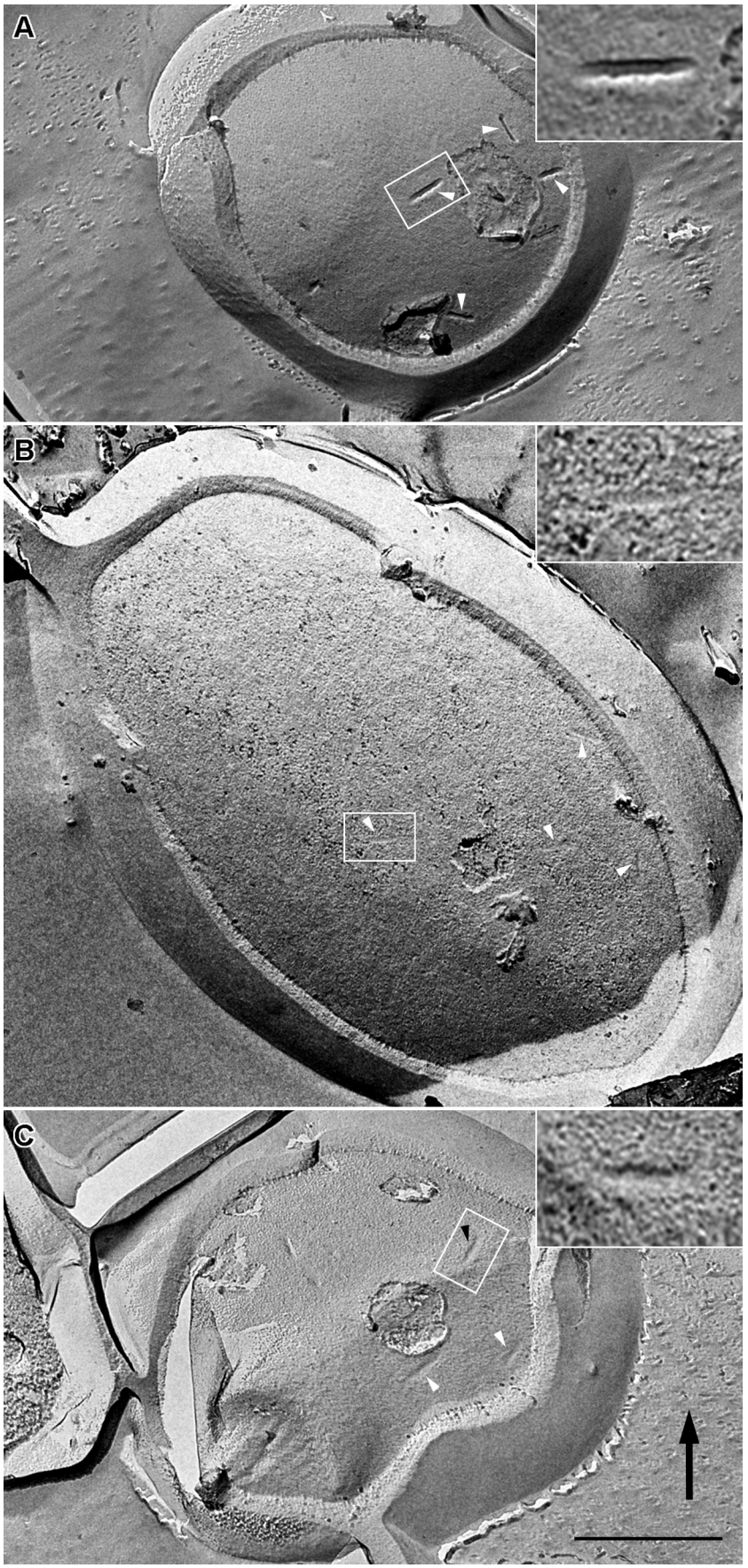
A
B
C

distributed homogenously as in the *nce102*Δ background, which means that Nce102$_{1–146}$ did not substitute for the Can1 accumulation-related function of Nce102 (Fig. 3A to C). A deletion of the 6 terminal amino acids only (Nce102$_{1–167}$) resulted in an identical effect (Fig. 3D). Expression levels of the full-length protein and its C-terminally truncated proteins were mutually comparable (data not shown). As shown by localization of GFP fusion proteins, the two truncated Nce102 versions reached the plasma membrane but, in contrast to the full-length molecule, were distributed homogenously (Fig. 4). These results document that the stretch of the very last 6 amino acids of Nce102 is responsible for directing this protein to MCC patches.

The C terminus of Nce102 is necessary for the formation of the plasma membrane invaginations. As previously observed in freeze-etch preparations of plasma membrane replicas, the full deletion of *NCE102* results in a lack of furrow-like invaginations (32). We therefore tested whether the C-terminal truncation of the Nce102 protein has a similar effect. For direct comparability with the results obtained by confocal microscopy we used the strains expressing *NCE102*-GFP and *NCE102*$_{1–146}$-GFP for replica preparation. In total, 111 cells expressing full-length *NCE102*-GFP and 33 cells expressing *NCE102*$_{1–146}$-GFP were analyzed. While all cells expressing the full-length *NCE102* gene formed furrows, only in 3 out of 33 analyzed Nce102$_{1–146}$-containing cells could shallow, premature furrow-like invaginations be identified. The remaining 90% of cells exhibited flat plasma membranes devoid of the typical furrow-like invagination pattern. Flat, smooth, elongated areas with surface densities comparable to that observed in furrows of wild-type cells were detected instead (Fig. 5). This remarkable change in the plasma membrane morphology was virtually identical to the phenotype previously observed for the *nce102*Δ strain (32). We conclude that, after its C-terminal part had been deleted, Nce102 lost its function in formation of furrows.

DISCUSSION

So far, we have documented nine proteins sharing the MCC localization: four members of the Sur7 family (Sur7, Ynl149c, Fmp45, and Ylr414c), three proton symporters (Can1, Fur4, and Tat2), and Nce102, with its close homolog Fhn1 (15, 16, 25, 26). Among those, no general MCC targeting sequence was revealed. Our findings rather support a step-by-step mechanism for MCC formation as suggested previously: (i) Pil1-driven assembly of planar membrane domains (primary MCC patches) containing Sur7 family proteins; (ii) recruitment of specific lipids, Nce102, and transporters into these domains; and (iii) lipid- and/or protein-mediated invagination of the MCC membrane (for details see references 27 and 32). Previously we showed that Nce102 directs the proton transporters into MCC patches, where they are protected against untimely turnover (16). In this study we document that the mechanism of plasma membrane domain formation and this MCC function is probably conserved through the largest phylum of fungi, the *Ascomycota*. This conclusion is based on the observation that, by expressing one of the most distant Nce102 homologs coded by *S. pombe fhn1*, we were able to reconstitute the Can1-enriched MCC patches in the *nce102*Δ strain of *S. cerevisiae*.

The hydropathy plot of Nce102 revealed four potential membrane-spanning domains. This prediction of the membrane topology, however, does not seem to be correct, at least in the sense of the protein orientation. Using a combination of glycosylation and growth assays, we determined that the C terminus of Nce102 is oriented toward the cytoplasm, while in the predicted protein structure it is exposed to the cell exterior. Taking this observation into account, we consider three putative models of Nce102 accommodation in the plasma membrane (Fig. 2A, models II to IV). The first one (model II), assuming that the protein crosses the membrane only twice, is based on a set of experiments where the topology was determined using the entire HA/Suc2/His4C reporter. However, this tag is quite bulky (125 kDa) compared to the tested Nce102 fragments, and thus it is possible that, during the membrane insertion, the fusion proteins do not fold correctly. On the other hand, it is worthwhile mentioning that, using the same strategy as that described above, we confirmed unambiguously the tetraspan topology of another protein residing in MCC, Sur7 (20; V. Stradalova, unpublished results). To obviate the interference of the bulky HA/Suc2/His4C reporter with the membrane insertion of Nce102-derived peptides, much smaller Suc2 fragments (6 and 9.3 kDa) were tested as glycosylation reporters. As evident from Fig. 2D, in this case the C-terminal reporter on fragment Nce102$_{1-63}$ is not glycosylated, which indicates that the hydrophilic loop following amino acid 63 is not exposed to the ER lumen and therefore probably faces the cytoplasm when the Nce102 protein is incorporated into the plasma membrane. The same holds for a newly created glycosylation site generated at amino acid 70. Conclusions from these results are summarized in topology model III in Fig. 2A. Neither of the two models, however, might be fully fitting. It is noteworthy that the first predicted TMD in Nce102 consists of 18 amino acids only. Usually, at least 23 amino acid residues are required for spanning the yeast plasma membrane (31, 37). However, 7 of 10 amino acid residues of the cytoplasmic N terminus are of positive hydropathy index, and the possibility that they might be involved in protein embedding cannot be excluded. The first extracellular stretch in model III consists of 12 highly polar amino acids, while the second loop, the internal one, contains only 9 amino acids, 7 of which are nonpolar. The other two amino acids are prolines, which are well documented to influence the conformation of, e.g., helical regions (1, 24, 39). Helices containing proline have a pronounced kink, with

FIG. 5. The C-terminally truncated version of Nce102 is unable to form furrow-like invaginations of the plasma membrane. The fine structures of the plasma membrane in wild-type (A)- and C-terminally truncated Nce102$_{1–146}$-expressing cells (B and C) were compared on freeze-etched replicas. MCC domains were marked (arrowheads). Instead of invaginations (A), a flat membrane was found in cells containing the incomplete Nce102 protein (B). Frequently, smooth, elongated areas could be detected in the membrane surface (insert in panel B). Only occasionally could shallow invaginations be recognized, too (C). Regions magnified in inserts are highlighted by frames. Bar, 1 μm.

bending of the helical axis of approximately 30° away from the side with the proline residue (38). Regarding all our results and the specific features of Nce102, we suggest topology model IV, where the proposed TMDs 2 and 3 do not span the plasma membrane but are inserted into the outer leaflet of the membrane. Due to its high hydrophobicity, the short 9-amino-acid stretch located between potential TMDs 2 and 3 might be incorporated into the lipid bilayer as well. In this case, the whole stretch of amino acids 40 to 95 could be embedded in the plasma membrane and the presence of the prolines might be involved in bending this helix.

It is plausible to speculate that these specific features of the Nce102 primary structure endow Nce102 with a certain topological flexibility, which might be of physiological relevance. In this context it is interesting to refer to the recent studies of Fröhlich et al. (10), where Nce102 has been proposed to act as a sensor for sphingolipids, regulating the appearance of the MCC pattern via phosphorylation of Pil1, a cytosolic protein accumulated beneath the MCC patches. Indeed, the involvement of Nce102 in processes including changes of the plasma membrane lipid composition is indicated by its increased expression reported in several screening studies looking for responses to environmental changes, like heat stress, oxidative and osmotic shocks, nitrogen source depletion, diauxic shift, transition to invasive growth, and introduction of various toxic substances (8, 11, 12, 34). The monitoring and transferring of signals from the environment may be due to changes in Nce102 topology, e.g., in the positioning of originally proposed TMDs 2 and 3. Our results document that the N and C termini of Nce102 face the cytosol, and we favor the possibility that the middle part of the molecule is incorporated in or tightly attached to the outer leaflet of the plasma membrane.

We identified a short C-terminal motif (PTISQV), the absence of which resulted in a loss of Nce102 function in the formation of MCC patches as well as of the plasma membrane invaginations (Fig. 3 to 5). Among the Nce102-like proteins resulting from our BLAST search, the motif is strongly (proline, 100% of 42 sequences analyzed; glutamine and valine, >95%) conserved in *Ascomycota* (data not shown). Our data show that even one of the most distant variants of this motif (PvmSaV [lowercase letters refer to amino acids not conserved in the *S. cerevisiae* version of the Nce102 protein]) in *S. pombe* Fhn1 is sufficient to accomplish the Nce102 function. Apparently, the C-terminal part of Nce102 is required for the local accumulation of the protein within Pil1-assembled domains (Fig. 4). In principle, two different mechanisms of membrane bending following this accumulation can be suggested. (i) The consequent transporter/sterol accumulation in MCC patches (15) promotes positive membrane curvature (32). Plasma membrane curvature caused by intercalation of ergosterol into the plane would play a key role in this case. However, lipids with high spontaneous curvature (like sterols) were shown to exhibit rather weak curvature preferences when inserted into membranes (17). (ii) It is possible that the central hydrophobic region of the Nce102 molecule is embedded into the outer layer of the plasma membrane (Fig. 2A, model IV). It is known that a shallow insertion of small hydrophobic inclusions effectively induces membrane curvatures (5). A critical amount of Nce102 at the patches could, in this case, induce the membrane bending. Many other proteins involved in the organization of membrane microdomains, for example, caveolins, reticulons, and flotillins (reggies), contain at least one membrane-integrated, but not membrane-spanning domain, which, it has been suggested, adopts a hairpin structure (3).

Based on our ultrastructural studies, we suggest that Nce102 operates also as a structural protein in bending the plasma membrane, which, of course, involves also the effects of specific lipids in the plasma membrane region. The role of Nce102 in specific structure formation does not exclude the possibility that Nce102 has additional functions.

ACKNOWLEDGMENTS

We are very grateful to Ingrid Fuchs for technical assistance. We also thank Katerina Malinska from the Institute of Experimental Botany, Academy of Sciences of the Czech Republic (Prague), for the construction of the pVTU100-mRFP plasmid and Sabine Strahl, University of Heidelberg, for technical advice.

V.S., M.O., and J.M. were financially supported by the Grant Agency of the Czech Republic (projects 204/07/0133, 204/08/J024, and 204/09/1924), the Grant Agency of the Academy of Sciences of the CR (KAN200520801), and by institutional grants (AVOZ50390703 and AV0Z50200510). M.L., G.G., W.T., A.K., and R.R. were supported by the Deutsche Forschungsgemeinschaft (DFG projects TA 36/18–1, TH, and SFB699 Z2). This work was also financially supported by the German Fonds der chemischen Industrie.

REFERENCES

1. **Altmann, K.-H., J. Wojcik, M. Vasquez, and H. A. Scheraga.** 1990. Helix-coil stability constants for the naturally occurring amino acids in water. XXIII. Proline parameters from random poly (hydroxybutylglutamine-co-L-proline). Biopolymers **30:**107–120.
2. **Altschul, S. F., W. Gish, W. Miller, E. W. Myers, and D. J. Lipman.** 1990. Basic local alignment search tool. J. Mol. Biol. **215:**403–410.
3. **Bauer, M., and L. Pelkmans.** 2006. A new paradigm for membrane-organizing and -shaping scaffolds. FEBS Lett. **580:**5559–5564.
4. **Brachmann, C. B., A. Davies, G. J. Cost, E. Caputo, J. Li, P. Hieter, and J. D. Boeke.** 1998. Designer deletion strains derived from Saccharomyces cerevisiae S288C: a useful set of strains and plasmids for PCR-mediated gene disruption and other applications. Yeast **14:**115–132.
5. **Campelo, F., H. T. McMahon, and M. M. Kozlov.** 2008. The hydrophobic insertion mechanism of membrane curvature generation by proteins. Biophys. J. **95:**2325–2339.
6. **Cleves, A. E., D. N. Cooper, S. H. Barondes, and R. B. Kelly.** 1996. A new pathway for protein export in *Saccharomyces cerevisiae*. J. Cell Biol. **133:** 1017–1026.
7. **Deak, P. M., and D. H. Wolf.** 2001. Membrane topology and function of Der3/Hrd1p as a ubiquitin-protein ligase (E3) involved in endoplasmic reticulum degradation. J. Biol. Chem. **276:**10663–10669.
8. **DeRisi, J. L., V. R. Iyer, and P.O. Brown.** 1997. Exploring the metabolic and genetic control of gene expression on a genomic scale. Science. **278:**680–686.
9. **Deshaies, R. J., and R. Schekman.** 1987. A yeast mutant defective at an early stage in import of secretory protein precursors into the endoplasmic reticulum. J. Cell Biol. **105:**633–645.
10. **Fröhlich, F., K. Moreira, P. S. Aguilar, N. C. Hubner, M. Mann, P. Walter, and T. C. Walther.** 2009. A genome-wide screen for genes affecting eisosomes reveals Nce102 function in sphingolipid signaling. J. Cell Biol. **185:** 1227–1242.
11. **Gasch, A. P., P. T. Spellnam, C. M. Kao, O. Carmel-Harel, M. B. Eisen, G. Storz, D. Botstein, and P. O. Brown.** 2000. Genomic expression programs in the response of yeast cells to environmental changes. Mol. Biol. Cell **11:** 4241–4257.
12. **Gasch, A. P., M. Huang, S. Metzner, D. Botstein, S. J. Elledge, and P. O. Brown.** 2001. Genomic expression responses to DNA-damaging agents and the regulatory role of the yeast ATR homolog Mec1p. Mol. Biol. Cell **12:**2987–3003.
13. **Gietz, R. D., and A. Sugino.** 1988. New yeast-Escherichia coli shuttle vectors constructed with in vitro mutagenized yeast genes lacking six-base pair restriction sites. Gene **74:**527–534.
14. **Gietz, R. D. and R. A. Woods.** 2002. Transformation of yeast by lithium acetate/single-stranded carrier DNA/polyethylene glycol method. Methods Enzymol. **350:**87–96.
15. **Grossmann, G., M. Opekarová, J. Malinsky, I. Weig-Meckl, and W. Tanner.** 2007. Membrane potential governs lateral segregation of plasma membrane proteins and lipids in yeast. EMBO J. **26:**1–8.
16. **Grossmann, G., J. Malinsky, W. Stahlschmidt, M. Loibl, I. Weig-Meckl,**

W. B. Frommer, M. Opekarová, and W. Tanner. 2008. Plasma membrane microdomains regulate turnover of transport proteins in yeast. J. Cell Biol. **183:**1075–1088.
17. **Kamal, M. M., D. Mills, M. Grzybek, and J. Howard.** 2009. Coupling between membrane curvature and lipid shape: measurement of the curvature preference of fluorescently labeled phospholipids. Proc. Natl. Acad. Sci. U. S. A. **106:**22245–22250.
18. **Kim, H., K. Melén, and G. von Heijne.** 2003. Topology models for 37 *Saccharomyces cerevisiae* membrane proteins based on C-terminal reporter fusions and predictions. J. Biol. Chem. **278:**10208–10213.
19. **Kim, H., Q. Yan, G. von Heijne, G. A. Caputo, and W. J. Lennarz.** 2003. Determination of the membrane topology of Ost4p and its subunit interactions in the oligosaccharyltransferase complex in *Saccharomyces cerevisiae*. Proc. Natl. Acad. Sci. U. S. A. **100:**7460–7464.
20. **Kim, H., K. Melén, M. Österberg, and G. von Heijne.** 2006. A global topology map of the *Saccharomyces cerevisiae* membrane proteome. Proc. Natl. Acad. Sci. U. S. A. **103:**11142–11147.
21. **Krogh, A., B. Larsson, G. von Heijne, and E. L. Sonnhammer.** 2001. Predicting transmembrane protein topology with a hidden Markov model: application to complete genomes. J. Mol. Biol. **305:**567–580.
22. **Larkin, M. A., G. Blackshields, N. P. Brown, R. Chenna, P. A. McGettigan, H. McWilliam, F. Valentin, I. M. Wallace, A. Wilm, R. Lopez, J. D. Thompson, T. J. Gibson, and D. G. Higgins.** 2007. Clustal W and Clustal X version 2.0. Bioinformatics **23:**2947–2948.
23. **Luo, G., A. Gruhler, Y. Liu, O. N. Jensen, and R. C. Dickson.** 2008. The sphingolipid long-chain base-Pkh1/2-Ypk1/2 signaling pathway regulates eisosome assembly and turnover. J. Biol. Chem. **283:**10433–10444.
24. **MacArthur, M. W., and J. M. Thornton.** 1991. Influence of proline residues on protein conformation. J. Mol. Biol. **218:**397–412.
25. **Malínská, K., J. Malinsky, M. Opekarová, and W. Tanner.** 2003. Visualization of protein compartmentation within the plasma membrane of living yeast cells. Mol. Biol. Cell **14:**4427–4436.
26. **Malínská, K., J. Malinsky, M. Opekarová, and W. Tanner.** 2004. Distribution of Can1p into stable domains reflects lateral protein segregation within the plasma membrane of living S. cerevisiae cells. J. Cell Sci. **117:**6031–6041.
27. **Malinsky, J., M. Opekarová, and W. Tanner.** 14 April 2010. The lateral compartmentation of the yeast plasma membrane. Yeast doi:10.1002/yea.1772.
28. **Moor, H., and K. Mühlethaler.** 1963. Fine structure in frozen-etched yeast cells. J. Cell Biol. **17:**609–628.
29. **Moreira, K. E., T. C. Walther, P. S. Aguilar, and P. Walter.** 2009. Pil1 controls eisosome biogenesis. Mol. Biol. Cell **20:**809–818.
30. **Rachel, R., I. Wyschkony, S. Riehl, and H. Huber.** 2002. The ultrastructure of *Ignicoccus*: evidence for a novel outer membrane and for intracellular vesicle budding in an archaeon. Archaea **1:**9–18.
31. **Rayner, J. C. and H. R. B. Pelham.** 1997. Transmembrane domain-dependent sorting of proteins to the ER and plasma membrane in yeast. EMBO J. **16:**1832–1841.
32. **Stradalova, V., W. Stahlschmidt, G. Grossmann, M. Blažíková, R. Rachel, W. Tanner, and J. Malinsky.** 2009. Furrow-like invaginations of the yeast plasma membrane correspond to membrane compartment of Can1 (MCC). J. Cell Sci. **122:**2887–2894.
33. **Strahl-Bolsinger, S., and A. Scheinost.** 1999. Transmembrane topology of Pmt1p, a member of an evolutionary conserved family of protein O-mannosyltransferases. J. Biol. Chem. **274:**9068–9075.
34. **Suzuki, C., Y. Hori, and Y. Kashiwagi.** 2003. Screening and characterization of transposon-insertion mutants in a pseudohyphal strain of Saccharomyces cerevisiae. Yeast **20:**407–415.
35. **Vernet, T., D. Dignard, and D.Y. Thomas.** 1987. A family of yeast expression vectors containing the phage f1 intergenic region. Gene **52:**225–233.
36. **Walther, T. C., J. H. Brickner, P. S. Aguilar, S. Bernales, C. Pantoja, and P. Walter.** 2006. Eisosomes mark static sites of endocytosis. Nature **439:**998–1003.
37. **Watson, R. T., and J. E. Pessin.** 2001. Transmembrane domain length determines intracellular membrane compartment localization of syntaxins 3, 4, and 5. Am. J. Physiol. Cell Physiol. **281:**C215–C223.
38. **Woolfson, D. N., and D. H. Williams.** 1990. The influence of proline residues on alpha-helical structure. FEBS Lett. **277:**185–188.
39. **Yun, R. H., A. Anderson, and J. Hermans.** 1991. Proline in alpha-helix: stability and conformation studied by dynamics simulation. Proteins **10:**219–228.

RESEARCH PAPER 4

OPEN ACCESS Freely available online

PLoS one

Distribution of Cortical Endoplasmic Reticulum Determines Positioning of Endocytic Events in Yeast Plasma Membrane

Vendula Stradalova[1], Michaela Blazikova[1,2], Guido Grossmann[3], Miroslava Opekarová[4], Widmar Tanner[5], Jan Malinsky[1]*

1 Institute of Experimental Medicine, Academy of Sciences of the Czech Republic, Prague, Czech Republic, **2** Faculty of Mathematics and Physics, Charles University in Prague, Prague, Czech Republic, **3** Department for Plant Biology, Carnegie Institution for Science, Stanford, California, United States of America, **4** Institute of Microbiology, Academy of Sciences of the Czech Republic, Prague, Czech Republic, **5** Institute of Cell Biology and Plant Physiology, University of Regensburg, Regensburg, Germany

Abstract

In many eukaryotes, a significant part of the plasma membrane is closely associated with the dynamic meshwork of cortical endoplasmic reticulum (cortical ER). We mapped temporal variations in the local coverage of the yeast plasma membrane with cortical ER pattern and identified micron-sized plasma membrane domains clearly different in cortical ER persistence. We show that clathrin-mediated endocytosis is initiated outside the cortical ER-covered plasma membrane zones. These cortical ER-covered zones are highly dynamic but do not overlap with the immobile and also endocytosis-inactive membrane compartment of Can1 (MCC) and the subjacent eisosomes. The eisosomal component Pil1 is shown to regulate the distribution of cortical ER and thus the accessibility of the plasma membrane for endocytosis.

Citation: Stradalova V, Blazikova M, Grossmann G, Opekarová M, Tanner W, et al. (2012) Distribution of Cortical Endoplasmic Reticulum Determines Positioning of Endocytic Events in Yeast Plasma Membrane. PLoS ONE 7(4): e35132. doi:10.1371/journal.pone.0035132

Editor: Martine Bassilana, Université de Nice-CNRS, France

Received November 18, 2011; **Accepted** March 10, 2012; **Published** April 9, 2012

Funding: This work was financially supported by the Grant Agency of the Czech Republic (projects 204/07/0133, P302/11/0146 and 204/09/1924), the Grant Agency of the Academy of Sciences of the Czech Republic (KAN200520801), by the institutional grants (AV0Z50390703 and AV0Z50200510), and by the Deutsche Forschungsgemeinschaft (DFG projects TA 36/18-1; TH; SFB699 Z2). GG was supported by a EMBO long-term fellowship. The funders had no role in study design, data collection and analysis, decision to publish, or preparation of the manuscript.

Competing Interests: The authors have declared that no competing interests exist.

* E-mail: malinsky@biomed.cas.cz

Introduction

Besides its basic function as a selective diffusion barrier, the plasma membrane (PM) hosts a variety of cellular functions including nutrient sensing and transport, sensing of various types of stress, endo- and exocytosis and signaling, and mediates the communication of the cell with its environment. To coordinate these processes and to ensure constant material and information exchange, the plasma membrane has to be precisely organized. Independent lines of evidence show that the membrane is compartmentalized into domains of specific structure and function [1].

Two stable membrane compartments were described in the plasma membrane of the yeast *S. cerevisiae* [2,3]. The Membrane Compartment of arginine permease Can1 (MCC), corresponding to furrow-like plasma membrane invaginations [4], is organized by a cytosolic complex called eisosome [5]. Several possible biological functions of this specialized membrane compartment have been suggested to date, including a role in sphingolipid sensing and signaling [6] and regulation of protein turnover [7], the latter still being a matter of scientific debate [8]. The originally proposed involvement of eisosome in canonical endocytosis [5] has been ruled out [7,8]. The PM area surrounding MCC was named MCP, referring to its first identified constituent, the major H^+/ATPase Pma1 [2]. Dynamic processes apparently take place outside the highly stable MCC domains: endocytic and exocytic sites, for example, do not overlap with MCC [7,8], and the formation of TORC2 signaling complexes occurs in the PM areas that contain neither MCC markers nor the MCP marker Pma1 [9]. The temporal order, in which the specific factors bind the sites of canonical endocytosis, has been described [10,11,12]. The above conclusion concerning the distribution of endocytic events in respect to MCC [7] was based on localization of Ede1, one of the first coat proteins arriving at the endocytic spot [13,14], and thus reflected the process of endocytic site selection at the PM surface. However, the mechanism by which the sites of endo- and exocytosis are selected remains unclear.

In fungi, plants and also animals, a significant part of the cytosolic side of the plasma membrane is associated with the cortical endoplasmic reticulum (cortical ER) [15,16,17]. The cortical ER forms a dynamic meshwork in the close vicinity underneath the PM; sheets and tubules of the endoplasmic reticulum (ER) are continuously rearranged [16,18,19,20]. Apart from its role in the secretory pathway, the ER establishes numerous membrane contact sites (MCS), connecting it with other membranous organelles in a cell, including the plasma membrane. In yeast, the best characterized MCS so far are nucleus-vacuole junctions [21,22], whereas less is known about the composition and function of the others, including ER-PM contact sites. The upper distance limit defining ER-PM contact sites in yeast was set by Pichler and coworkers at about 30 nm. More than a thousand ER-PM MCS per yeast cell were identified by this set-up [19]. Only recently, the ER-PM spacing was measured more

exactly to vary from 16 to 59 nm with a mean value of about 33 nm [20]. This indicates that the majority of the PM-associated cortical ER may be at a distance suitable for MCS formation.

Here we address the question whether close association of cortical ER and PM could locally affect endo- and exocytosis. The formation of an endocytic vesicle about 50 nm in diameter [23] may require accessibility to cytosolic components. For a substantial part of the PM inner surface [20], the cortical ER could represent a spatial hindrance for vesicular formation and/or delivery. It is known that cytoplasmic factors can modulate the PM organization. In yeast, actin filaments, for example [24], deliver various cargoes to the plasma membrane, and eisosomes, sub-membrane protein clusters organize protein and lipid distribution therein [25,26,27]. In the case of cortical ER, however, it would be the shape of a membranous cytoplasmic organelle that influences the local functional properties of the plasma membrane. We show that the endocytic machinery is positioned and functional only at PM sites free of cortical ER. The cortical ER pattern, on the other hand, is influenced by the association of eisosomes with MCC.

Results

Distribution of cortical ER with respect to endocytosis and MCC

To test whether endocytosis occurs at sites equally distributed throughout MCP of the yeast plasma membrane or whether the close apposition of the cortical ER network to the PM results in a non-random appearance of endocytic events, we monitored endocytic events with respect to the presence of cortical ER in the cortex of isotropically growing mother cells. We chose Ede1-GFP as an endocytic marker because it is one of the first proteins arriving at the endocytic spot [13,14], and the ER luminal marker ss-dsRed-HDEL [28]. By observation of exponentially growing living yeast cells expressing both the markers we were able to visualize endocytic events and cortical ER simultaneously. As is evident from tangential confocal sections, the initiation of endocytosis occurred almost exclusively in PM zones not occupied by cortical ER (Fig. 1A). As a control, we included MCC into this mutual localization analysis and colocalized mCherry- and GFP-tagged versions of the MCC constituent Sur7 [29] with the above markers for ER and endocytic sites. In agreement with previous findings [4,7,8], we observed MCC domains not colocalized with either of these markers (Fig. 1B, C). Quantification of the entire dataset of acquired images revealed that markers of all three studied cortical structures (MCC, endocytic sites, and cortical ER) occupied three separate domains in the PM (Table 1). This PM partitioning seems to be independent on the yeast strain background as BY4741 and W303-1A cells yielded identical results (Table 1, compare also Fig. 1 and Fig. S1).

Then we attempted to describe the distribution of endocytic events in more detail. We measured the minimal distance of endocytic spots in areas not covered by the cortical ER (holes) to the ER network. We defined the ER boundary as a line connecting points that exhibited half of the local intensity drop between the signal of the ER marker ss-dsRed-HDEL and the hole. Adaptive character of this border definition makes it independent on signal intensity and thus more reliable than any threshold-based definition. The method could lead to an overestimation of the real ER size in the range of $\sim$100 nm in any direction, since defining the ER border in this way possibly includes the blur of the fluorescence signal of the ER marker. We measured the distance between this cortical ER border and maxima of the Ede1 signal. As a control, we generated a set of images containing foci randomly distributed in the plasma membrane over the cortical ER pattern (see Methods for details). We selected about 30% of these foci, which localized into the holes in the ER pattern, and again measured their distance from cortical ER. Comparison of the two distributions revealed that endocytic events are randomly positioned within the free-of-ER plasma membrane, with a weak preference of places lying further apart from cortical ER border (Fig. 2, note the asymmetry of the endocytic foci distribution). Nonetheless, this means that most of the endocytic sites are selected at the plasma membrane not further than 200 nm from the ER border (Fig. 2). Similar analysis of MCC foci distribution revealed that MCC is also randomly distributed in areas devoid of cortical ER coverage. But, in contrast to Ede1 and random foci, the fluorescence signal of Sur7 remains some minimal distance from the ER border (see the symmetric distribution of Sur7 foci in Fig. S2).

Local variations in spatio-temporal distribution of cortical ER

The network of cortical endoplasmic reticulum represents a highly dynamic organelle undergoing continuous rearrangement that may further contribute to the dynamic accessibility of the plasma membrane for membrane trafficking. To track the dynamics of cortical ER, we measured the movement of GFP-HDEL stained ER (Fig. 3A) in Sur7-mCherry expressing cells. The immobile, Sur7-mCherry-labeled MCC domains were used for alignment of 20 consecutive frames (increment: 10 s/frame) in a time-lapse series. Consistent with earlier observations reporting 57–77% of the cell periphery to be covered by cortical ER [18,19,30], we observed a GFP-HDEL signal over 65$\pm$8% of the PM surface (n = 30 series; 20 frames each). The binarized cortical ER patterns (Fig. 3B) were superimposed in order to visualize the local durations of plasma membrane coverage with cortical ER during the monitored time window. Within 3 minutes, almost the entire area of PM (98.7$\pm$1.3%) was covered at least once by cortical ER. 9.3$\pm$3.8% of the PM surface was covered with cortical ER permanently (dark red areas in Figs. 3C–E). This visualization allowed for identification of micron-scale PM zones with strikingly diverse relative cortical ER coverage. While domains that are almost permanently covered by cortical ER exist on the inner surface of PM (red and orange zones in Fig. 3), other zones barely came in contact with cortical ER (blue in Fig. 3).

We propose that the cortical ER is involved in functional compartmentalization of the PM as it confines the immediate communication between the PM and cytosol to distinct (ER-free) zones. This becomes clearly visible when the Ede1-GFP signal is accumulated in time. In cells exhibiting low cortical ER dynamics, Ede1-GFP appears in isolated domains within the plasma membrane surrounded by ER. During the same time period, cells with higher ER dynamics become evenly covered with Ede1-marked sites (Fig. 4).

The only stable parts of the PM in our study are the MCC areas, which are not accessible either for interaction with ER or for initiation of endocytosis. Our analysis showed that both cortical ER and endocytic sites can extend to the rest of the plasma membrane, although their immediate plasma membrane distributions at any given time do not overlap (Figs. 3, 4).

Pil1 influences the cortical ER network spreading

Previously, we have shown that the cortical ER does not overlap with the stable, invaginated MCC/eisosome domains (Fig. 1B and Fig. S2A) [4]. The invaginations stretch into the cytosol with a depth of about 50 nm and may possibly cause a hindrance for lateral cortical ER spreading. We tested whether mutants being

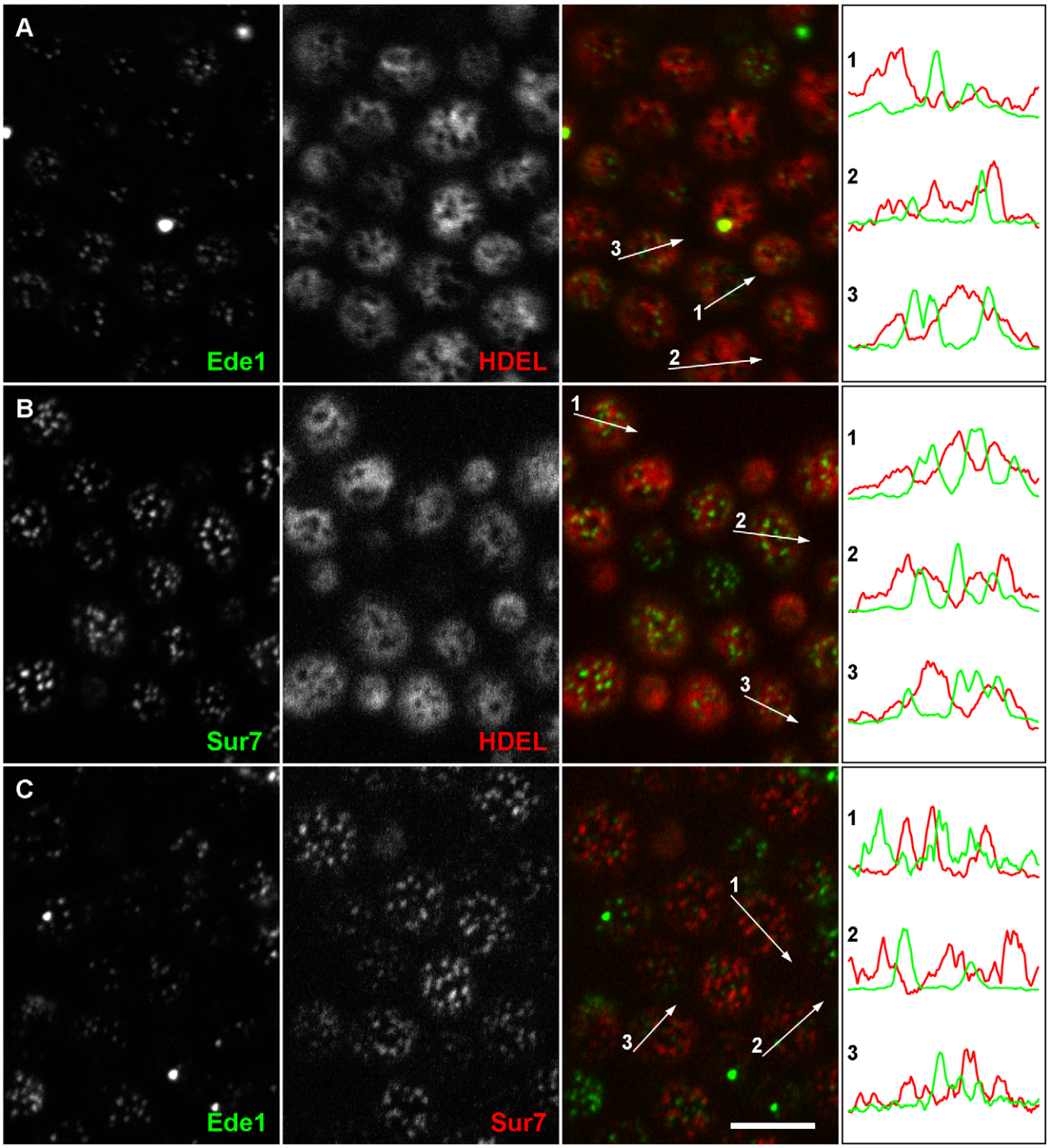

Figure 1. Endocytosis is initiated in the ER-free zones of the plasma membrane. Mutual localization was performed for Ede1-GFP, a marker of early stages of endocytosis, and cortical ER visualized by ss-dsRed-HDEL. Only rare colocalization events were detected (**A**). Similarly, the cortical ER network (**B**) and the initiation sites of endocytosis (**C**) were not colocalized with MCC domains marked with Sur7-GFP and Sur7-mRFP, respectively. Tangential confocal sections of BY4741 cells expressing fluorescently labeled proteins are presented. The fluorescence intensity profiles along the numbered arrows were scaled to the same range in the red and green channels. Bar: 5 μm.
doi:10.1371/journal.pone.0035132.g001

affected in MCC/eisosome distribution or invagination show an altered cortical ER arrangement beneath the PM.

First, we explored the cortical ER pattern in strains *pil1Δ* [5] and *nce102Δ* [7] which were shown to be defective in MCC appearance. The fluorescence pattern of cortical ER resembles a network: the compact labeled areas appear fragmented by circular or irregularly shaped holes (perforations) into a system of more or less fibrous (tubular) structures and sheets (cisternae). We detected morphological changes of this network in selected mutants. In *pil1Δ* cells, in which both MCC and the eisosome structure are

Table 1. Quantification of mutual localization of MCC, Ede1 sites and cortical ER.

Analyzed structures	BY4741	W303-1A
Ede1/cortical ER	93±10% (n = 144 cells)*	94±8% (n = 148)*
Sur7/cortical ER	98±3% (n = 139)**	98±4% (n = 142)**
Ede1/Sur7	99±4% (n = 150)*	99±5% (n = 160)*

*fraction of Ede1 sites non-colocalizing with cortical ER or the Sur7 signal.
**fraction of Sur7 domains non-colocalizing with the cortical ER signal.
doi:10.1371/journal.pone.0035132.t001

disrupted [5], the cortical ER network was generally more compact and indiscrete (Fig. 5A). Quantitative analyses revealed a cortical ER with fewer but larger perforations as compared to the wild type (Fig. 5B, C, Fig. S3 and Movies S1,S2,S3). Accordingly, less fragmented, unequally distributed tubuli and cisternae of cortical ER were also clearly discernible beneath the plasma membrane of ultrathin-sectioned *pil1Δ* cells (Fig. 6) observed by the transmission electron microscope. On the other hand, cells over-expressing Pil1, which were reported to contain more eisosomes than the wild type [31], exhibited cortical ER with a high number of smaller holes (Fig. S4). In *nce102Δ* mutant cells eisosomes correctly localize beneath MCC domains [6,32], but membrane invaginations are lacking [4]. Testing the distribution of cortical ER in *nce102Δ* cells did not reveal any significant alteration in the cortical ER morphology (Figs. 5, 6), indicating that the invagination of MCC domains is not required to restrain the cortical ER from spreading over MCC areas.

To test whether the distinct localization of MCC and cortical ER is preserved in the two MCC defective strains, we analyzed the localization of ss-dsRed-HDEL and Sur7-GFP in *pil1Δ* and *nce102Δ* cells. In agreement with previously published data [6], we found a lower surface density of Sur7 domains in *nce102Δ* cells ($0.75\pm0.19\ \mu m^{-2}$) as compared to the wild type ($1.21\pm0.27\ \mu m^{-2}$). In *pil1Δ* cells, the Sur7 protein was originally reported to be clustered only into occasional big "eisosome remnants" and otherwise homogenously distributed in the membrane [5]. In agreement with our earlier observations [7], we show on tangential confocal sections of *pil1Δ* cells that aside the eisosome remnants Sur7-GFP was also not completely evenly distributed, but rather concentrated into smaller, less distinct domains (Fig. S5). We analyzed the percentage of overlap between Sur7 domains and cortical ER in *nce102Δ*and *pil1Δ* cells, including all discernible Sur7 domains in *pil1Δ*, and found no significant difference between the tested strains (Fig. 7). Thus we demonstrate that, even under the conditions when Sur7 is not concentrated in large, easily distinguishable domains, the protein localizes preferentially to PM areas devoid of cortical ER coverage. We also examined and quantified the positioning of endocytic Ede1-GFP sites in respect to the cortical ER area in the two mutant strains. Again, endocytosis occurred solely outside the ER-covered PM areas, as about 94% of endocytic sites did not colocalize with cortical ER network in either of *nce102Δ* or *pil1Δ* cells (data not shown).

Finally, to check whether the dynamics of ER rearrangement is affected upon MCC disintegration, we explored the rate of ER network movement in GFP-HDEL/Sur7-mCherry expressing strains. The Sur7-mCherry domains were again used to align the frames in the time-lapse series. We used a relative displacement, i.e. proportion of the area covered by cortical ER at a given time but not covered after a selected time interval, as a measure of the ER mobility. Mainly due to cell-to-cell variations in ER mobility, no significant difference in the dynamics of cortical ER rearrangements between the wild type and *nce102Δ* or *pil1Δ* cells was detected (Fig. S6A). Similar to WT, we were also able to detect the micron-scale plasma membrane zones exhibiting different cortical ER coverage in both the mutant strains. Consistent with the above-mentioned observation of altered cortical ER distribution in *pil1Δ* cells (Fig. 5 and Fig. S3), the

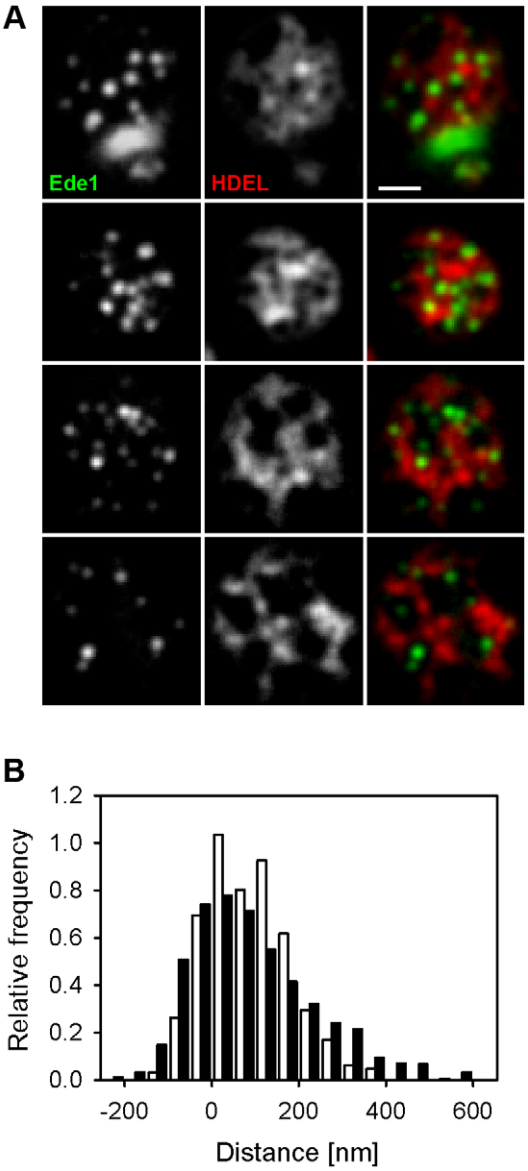

Figure 2. Endocytic events are randomly distributed within ER-free PM areas. In tangential confocal sections of individual W303 cells expressing Ede1-GFP and ss-dsRed-HDEL (**A**), the minimal distance of endocytic sites from the cortical ER boundary was measured. The histogram of the measured distances (full bars in **B**; 906 sites in 200 cells were analyzed) was compared to the distribution of the distances of model foci randomly positioned in the plasma membrane (empty bars in B; 320 foci in 100 cells; see Methods for details). In order to maximize the accuracy of the distance measurements, for all the measurements we chose only the foci located to easily discernible ER holes positioned in central parts of the tangential confocal sections, so that the entire borders of the holes could be traced. Bar: 1 μm.
doi:10.1371/journal.pone.0035132.g002

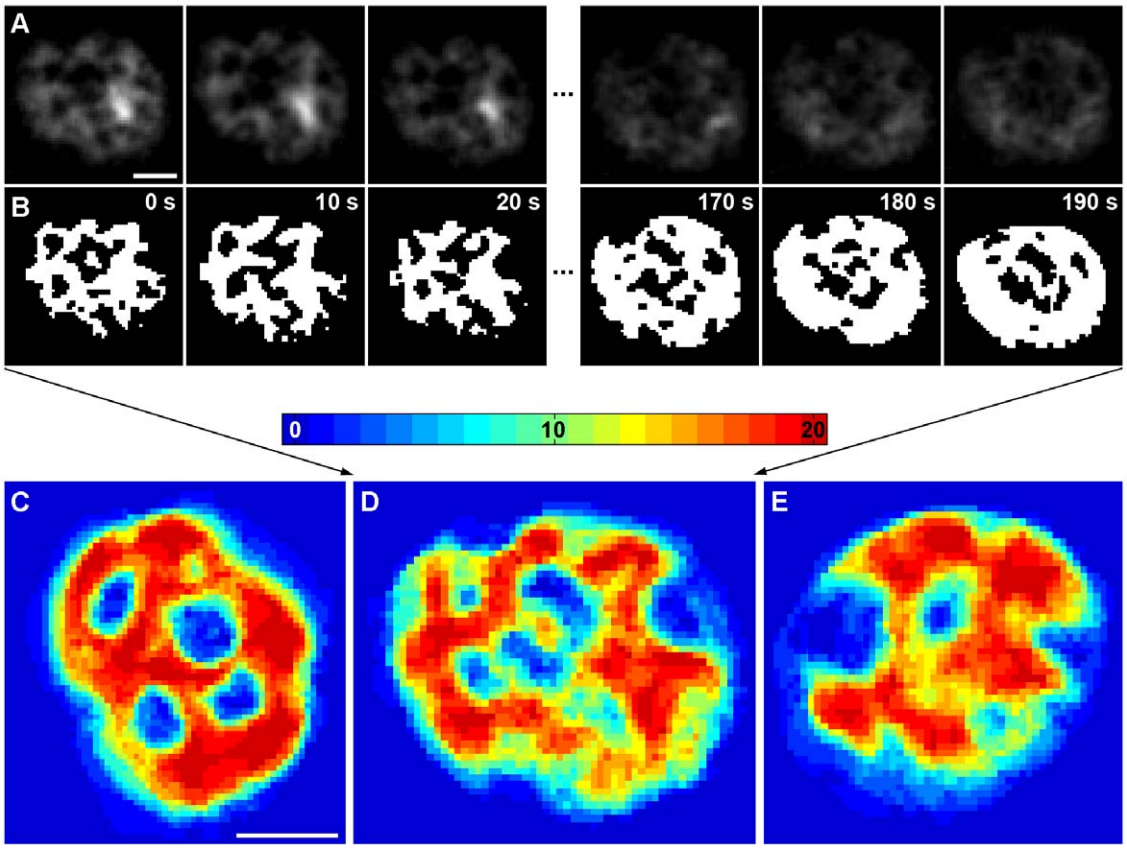

Figure 3. Differential cortical ER coverage defines micron-scale PM domains. The dynamics of cortical ER was followed in time-lapse series of 20 tangential confocal sections of BY4741 cells expressing ss-GFP-HDEL together with Sur7-mCherry (rate: 10 s/frame). Raw data after a 3×3 mean filtration (**A**) and binarized cortical ER pattern (**B**) of the first and the last three frames in the series are presented. For better lucidity, the red fluorescence channel (MCC/Sur7-mCherry) is not shown. In order to visualize the local dynamics of cortical ER, all twenty binarized frames were superimposed. Three out of 33 cells analyzed are presented in false colors denoting the number of frames in the series in which cortical ER was detected (**C–E**). Bar: 1 μm.
doi:10.1371/journal.pone.0035132.g003

pattern of these domains was changed accordingly (Fig. S6B; compare with Fig. 3).

We conclude that the eisosome core protein Pil1 influences the distribution of the cortical ER network. Pil1 is not required for normal cortical ER mobility or PM binding but Pil1-driven eisosome formation rather contributes to cortical ER fragmentation.

Discussion

Directional targeting of material exchange-related processes like endo- and exocytosis is one of the basic processes enabling a living cell to exist. For clathrin-mediated endocytosis, a detailed picture of the order and timing has been acquired by Drubin and coworkers [11]. The regulation and spatial distribution of sites of endocytosis, however, remain elusive. In our study, we used baker's yeast for mapping endocytic events in relation to cortical ER and the known, immobile domains of MCC, which are regulated by the subjacent eisosomes. We found sites of endocytosis to be non-randomly distributed and restricted to sites free of cortical ER and free of MCC. Cortical ER distribution itself also appears to be dependent on normal MCC-eisosome formation.

Specific re-positioning of the ER during the process of budding was described in detail in a recent study [20]. We report that apart from this polar organization of the cellular cortex, the uneven and variable distribution of cortical ER can be followed within the plasma membrane of *S. cerevisiae*. We found micrometer-sized domains preferentially covered by the cortical ER network and domains preferentially free of this coverage coexisting within the PM in a time scale of minutes (Fig. 3).

As evident from the Ede1-cortical ER co-labeling experiments (Fig. 1), plasma membrane areas devoid of cortical ER coverage determine the emergence of endocytic vesicles. Being a soluble, cytosolic protein, Ede1 is one of the first proteins marking the future site of endocytosis by clustering at the plasma membrane [13,14]. Even if its movement in cytoplasm was driven solely by diffusion, it is likely that its interaction with PM would occur preferentially in the membrane domains that are not covered with cortical ER. Our quantifications show that this preference is very strong (93±10%). Recently, a similar mechanism of indirect soluble protein routing in the cell cortex has been observed in *S. pombe*: the actomyosin ring organizing protein Mid1 is directed to a cortical ER-determined "permissive zone" in the plasma membrane, in which the plane of cell division (cytokinesis) is consequentially established [33]. The distribution of Ede1 foci in plasma membrane domains not covered with cortical ER is rather random (Fig. 2), thus indicating that initiation of endocytosis is independent from the lateral distance to cortical ER as long as the plasma membrane is not covered with ER.

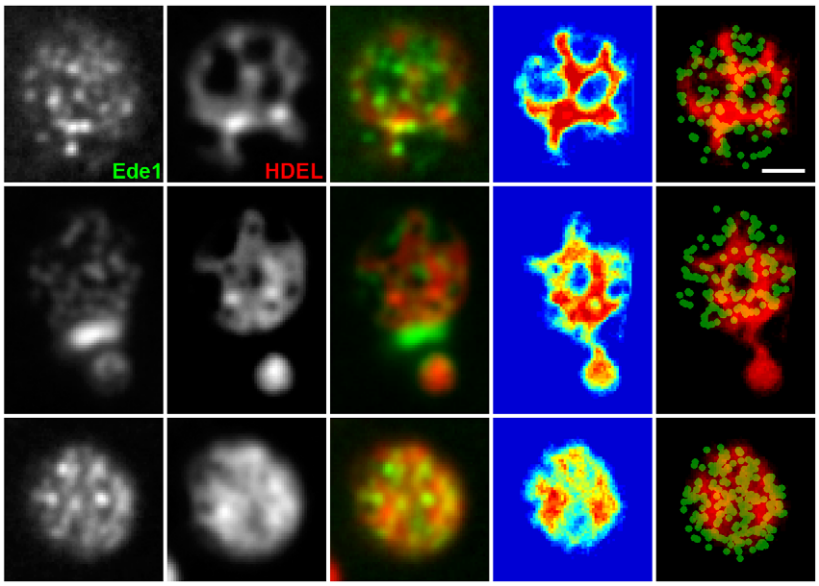

Figure 4. Lateral mobility of cortical ER determines the positioning of endocytic events. Initiation of endocytic events in cells co-expressing Ede1-GFP and ss-dsRed-HDEL was monitored in a time-lapse experiment (20 frames, 30 s/frame). Superposition of all the frames is presented. The 4th column represents the superimposed binarized ER signals from 20 consecutive frames in a false-color blue-to-red scale to highlight the dynamics of the cortical ER network (see Fig. 3 legend for an explanation). The column on the far right shows this superposition of binarized ER signals in red overlaid by the green channel, in which the positions of the maxima of the Ede1 sites in the 20 frames were marked by round spots. Bar: 1 μm.
doi:10.1371/journal.pone.0035132.g004

Plasma membrane invaginations (MCC domains) and eisosomes seem to modulate the ratio of cortical ER tubules to extended cisternae. Contrary to our expectations, we found that the depth of furrow-like PM invaginations/eisosome has no, or only a minor influence on the cortical ER morphology. Rather the presence or absence of MCC/eisosomes, independent of the local PM topology, determines the local perforation of the cortical ER network. Several lines of evidence allow for this conclusion. First, these two structures localize in distinct parts of the plasma membrane (Fig. 1, Fig. S1) as we also reported previously [4]. More significantly, a lack of the eisosomal Pil1p results in fewer MCC/eisosome domains and fewer holes in the pattern of cortical ER (Figs. 5, 6). Pil1 overexpression, however, increases the number of MCC/eisosome domains and perforations of cortical ER network (Fig. S4). Even in the absence of specific MCC-ER interactions, it can be difficult for the ER sheet or tubulus to enter between adjacent eisosomes, which are as frequent as 2.5 ± 0.2 um^{-2} in the plasma membrane surface and about 300 nm long each (parameters reported by a freeze-etching study in Stradalova et al., 2009), simply because of mechanical obstacles. The surface tension in the ER membrane and the fact that the formation of curved areas in the ER membrane anticipates the assistance of specific lipids will contribute here. In any case, we do observe high ER dynamics beneath the plasma membrane. Thus, one can assume that these obstacles are not impossible to overcome and that ER still can enter most of inter-MCC gates visible at the resolution of fluorescence microscopy.

In contrast to stable MCC/MCP partitioning of the plasma membrane, the dynamics of membrane areas with differential cortical ER coverage is much higher. We do not expect, therefore, that discriminative protein or lipid markers of these domains will be found in the PM. One can rather imagine that cortical ER distribution supports more or less stable gradients of the PM constituents as it directs the flows of cytoplasmic soluble factors and vesicles towards certain zones of the PM. Similar steady-state modulation of the PM structure/function was recently suggested in plants: polar accumulation of auxin transporter Pin2 was reported to result from spatially defined exo- and endocytosis in *Arabidopsis* [34]. Based on the present knowledge, we propose a simplified scheme of yeast cell cortex showing its spatial and consequent functional map (Fig. 8).

Materials and Methods

Yeast strains and growth conditions

The yeast strains used in this study are listed in Table S1. The cells were grown in a synthetic complete medium (0.67% Difco yeast nitrogen base without amino acids, 2% glucose, and amino acids; for W303-derived strains supplemented with 2× more adenine) to mid-log phase (OD_{600} about 0.6) at 30°C on a shaker. The cells in Figure S4 were cultivated in synthetic medium lacking uracil. For electron microscopy preparations, the cells were cultured in a rich medium (YPD; 2% peptone, 1% yeast extract, 2% glucose) to the same OD_{600} and under the same conditions as the cells in synthetic medium.

Plasmids

YIp211-Ede1-GFP [7]**; YIp211-Sur7-GFP** [35]**; YIp128-Sur7-mRFP**: The SUR7 gene was inserted as a HindIII-BamHI fragment into YIp128-mRFP plasmid [35]; **YIp211-Sur7-mCherry**: The mCherry gene was cut from pVTU100-HUP1-mCherry (G. Grossmann, unpublished) plasmid using BamHI-BssHII restriction sites and ligated into YIp211-SUR7-GFP plasmid instead of the GFP gene. Before transformation, the plasmid was linearized by digestion with EagI; **YIp204-TKC-dsRed-HDEL** [28]; **YIp128-TRP1-TKC-dsRed-HDEL**: The TRP1-TKC-dsRed-HDEL cassette was amplified by PCR from the YIp204-TKC-dsRed-HDEL plasmid using the primers HDEL_FW (GATTACGCCAAGCTTGCAAATTAAAGC) and HDEL_RV (CTTGGAGCTCGTCTGTTATTAATTTCAC).

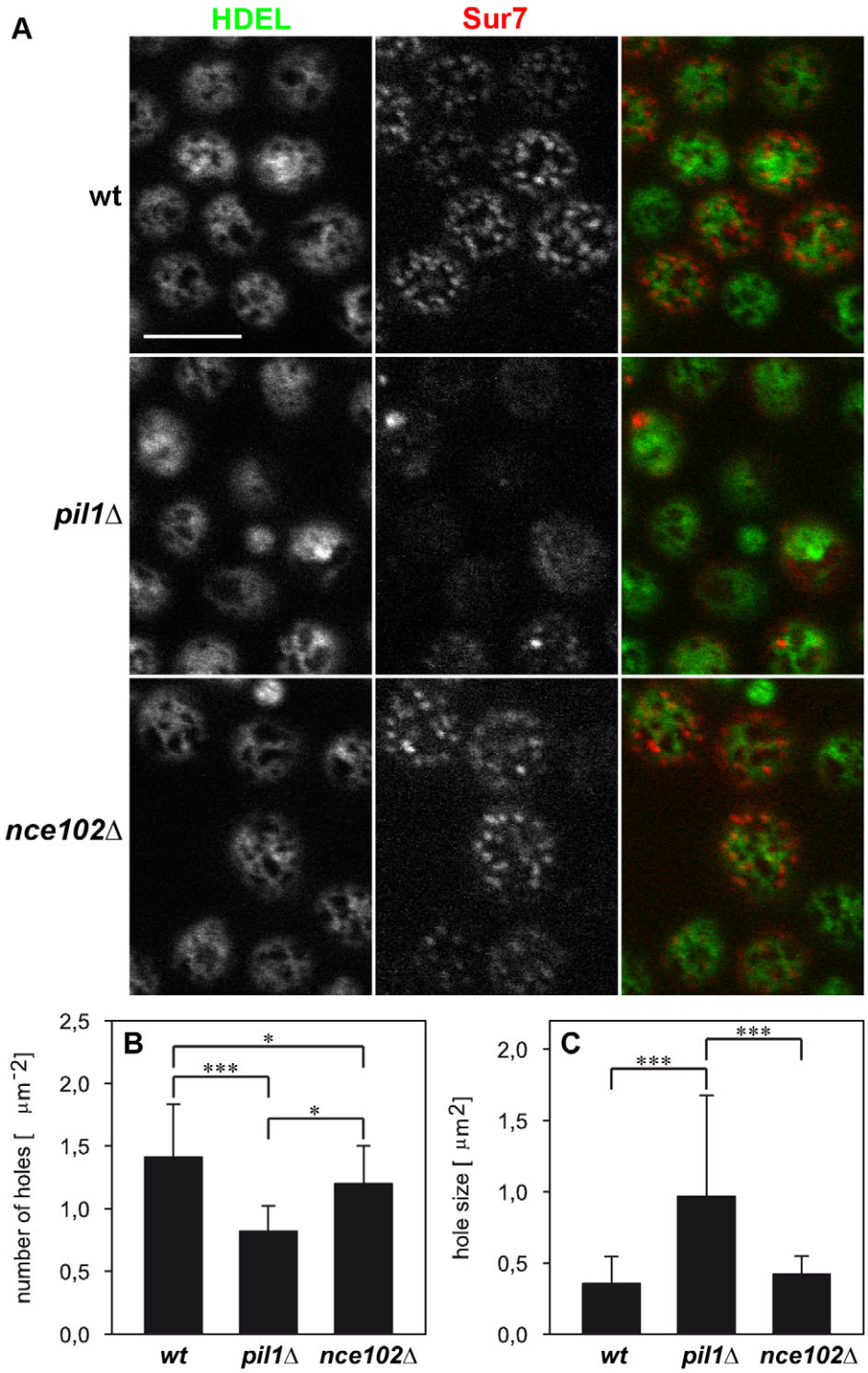

Figure 5. Defect in MCC integrity results in alteration of the cortical ER pattern. Tangential confocal sections of BY4741, *pil1Δ* and *nce102Δ* cells expressing ss-GFP-HDEL and Sur7-mCherry markers are presented (**A**). Statistical analysis of cortical ER pattern in all strains (n>30) revealed that the cortical ER network in *pil1Δ* cells exhibits fewer (**B**) but larger (**C**) holes. Importantly, no difference in total cortical ER area with respect to the individual tested strains was detected. Mean values (± standard deviation) are compared and the significance of detected effects as revealed by Student T test is denoted (* $p<0.05$;***$p<0.001$). Bar: 5 µm.
doi:10.1371/journal.pone.0035132.g005

The obtained fragment was ligated into YIp128 plasmid using the HindIII-SacI restriction sites. The plasmid was linearized before yeast transformation by Bsu36I enzyme and integrated into TRP1 locus; **YIp128-TRP1-TKC-GFP-HDEL**: The GFP gene was amplified by PCR from the YIp211-SUR7-GFP plasmid using the primers VN155_HDEL_F (TATAGGATCCCATGTC-

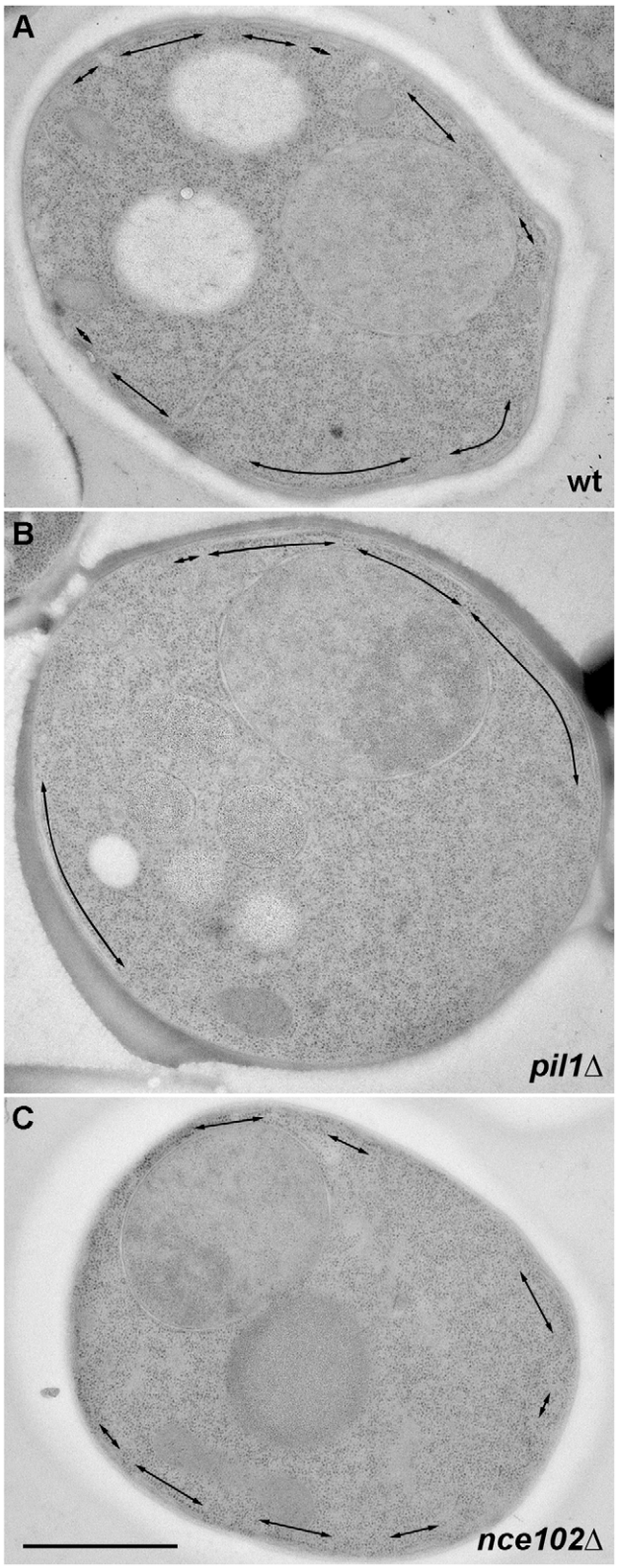

Figure 6. Electron microscopic analysis of the MCC-specific alterations of cortical ER pattern. The length and distribution of cortical ER cisternae (arrows) on thin sections of BY4741 (**A**), *pil1Δ* (**B**) and *nce102Δ* cells (**C**) were compared. No difference in total length of the cortical ER structures with respect to the individual tested strains was detected. Bar: 1 μm.
doi:10.1371/journal.pone.0035132.g006

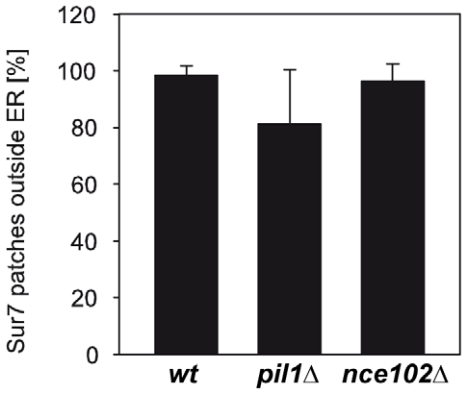

Figure 7. Distinct localization of MCC marker Sur7 and cortical ER distributions is maintained in MCC-defective strains. The mutual position of fluorescence signals in tangential confocal sections of BY4741, *pil1Δ* and *nce102Δ* cells co-expressing Sur7-GFP and ss-dsRed-HDEL (n>140) was analyzed. Relative numbers (mean ± standard deviation) of Sur7-GFP domains localized outside the ss-dsRed-HDEL (cortical ER) pattern are compared.
doi:10.1371/journal.pone.0035132.g007

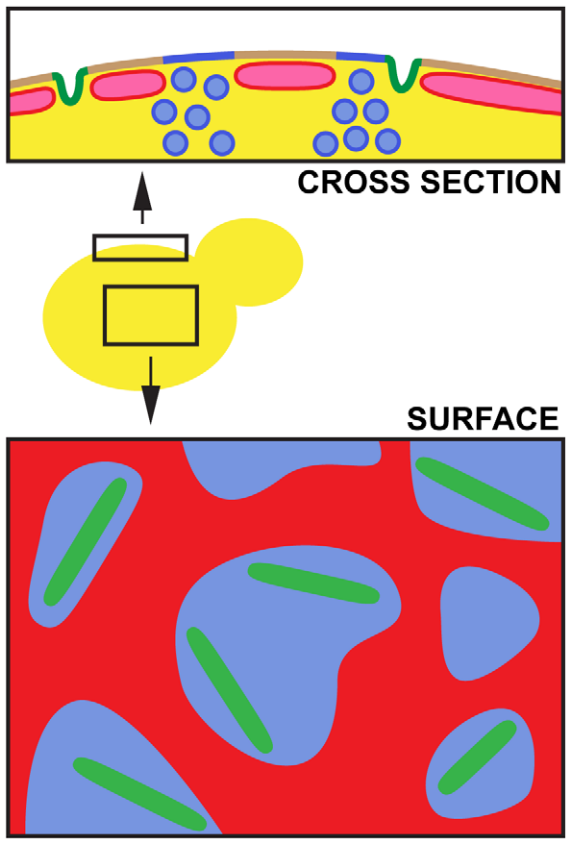

Figure 8. Model of functional plasma membrane compartmentalization in yeast. Three distinct domains can be distinguished in the yeast PM: stable MCC domains (green) surrounded by a membrane covered with a dynamic network of cortical ER (red) and the PM free of cortical ER coverage (blue). Vesicle transport can take place only in the ER-free PM.
doi:10.1371/journal.pone.0035132.g008

TAAAGGTGAAG) and VC155_HDEL_R (TATATCTAGAT-TACAATTCGTCGTGTTTGTACAATTCATC). The obtained GFP-HDEL fragment was inserted into 128-TRP1-TKC-dsRed-HDEL via BamHI-XbaI restriction sites instead of dsRed-HDEL gene. The plasmid was linearized before yeast transformation by Bsu36I enzyme and integrated into TRP1 locus; **pVTU100-Pil1-mRFP**: The PIL1 gene was inserted as a HindIII-BamHI fragment into pVTU100-mRFP plasmid [32] under the ADH1 promoter.

Confocal microscopy

Living yeast cells in synthetic medium were concentrated by brief centrifugation, immobilized on a 0.17 mm coverglass by a thin film of 1% agarose prepared in the synthetic complete medium and observed using LSM510-META confocal microscope (Zeiss) with a 100× PlanApochromat oil-immersion objective (NA = 1.4), with the exceptions listed below. Fluorescence signals of GFP and mRFP/dsRed/mCherry (excitation 488 nm/Ar laser, and 561 nm/solid state laser) were detected using the 505–550 nm band-pass, and 580 nm long-pass emission filters, respectively. Cells for Fig. 3 and Figs. S2, S6 were visualized using Zeiss/Yokogawa Cell Observer spinning disc microscope with a 100× PlanApochromat oil-immersion objective (NA = 1.4); cells for Fig. 2 and Fig. 4 were visualized using Zeiss/Yokogawa Axio Observer.Z1 spinning disc microscope with a 100× PlanApochromat oil-immersion objective (NA = 1.46). The fluorescence signals of GFP and mCherry were detected using band pass emission filters (520/35 and 617/73 nm, respectively) and recorded using a Andor iXon+ 888 back-illuminated EMCCD camera (Fig. 3, S2 and S6) or AxioCamMR3 camera (Fig. 2 and 4).

Electron microscopy

Yeast cells were processed as described previously [4], in brief: cells were filtered, loaded in a flat specimen carrier and frozen in EM PACT (Leica). Frozen samples were freeze-substituted in acetone supplemented with 3% glutaraldehyde (10% stock in acetone; SPI Supplies, USA), 0.1% UA and 1% water in AFS machine (Leica) and then embedded in HM20 resin. Ultrathin sections (70 nm) were cut with Ultracut S ultramicrotome equipped with a diamond knife (35°; Diatome) and placed on copper formvar-coated grids. Sections were contrasted with a saturated aqueous solution of UA for 1 hour, washed, air-dried and examined in a FEI Morgagni 268(D) transmission electron microscope at 80 kV. Images were captured with MegaView G2 CCD camera (Olympus).

Image processing and evaluation

If not stated otherwise, raw microscopic data are presented. Mutual localization of MCC, endocytic sites, and cortical ER was evaluated manually as follows: any overlap between the two fluorescence channels was considered as a colocalization event. The only exception from this rule was the case when focal accumulation of endocytic or MCC marker overlapped with a local minimum in the cortical ER pattern. This particular case was evaluated as non-colocalization (small hole in the ER pattern, partially filled with the blur from the surroundings). Processing of time-lapse image series (Figures 3 and S6) (alignment, [3×3] mean filtering, binarization) was performed in Matlab software (The MathWorks): the positions of the MCC domains were determined as local maxima of the Sur7-mCherry signal. A convex hull using the Delaunay triangulation was constructed to determine the cell shape. Combination of thresholding and morphological operations was used to determine the inner structure of the cortical ER – positions and shapes of the perforations in the cortical ER pattern. Images for Figs. 2, 4 and S2 were filtered as stated above; the alignment for Fig. 4 was treated manually.

In analysis of the distances between the Ede1-GFP (Sur7-mCherry) domains and the cortical ER, images with random population of foci (the control for surface distribution analysis) were obtained as follows: the ER channel in the real images previously analyzed was left untouched. The fluorescence signal in the focal (MCC) channel was replaced by a regular hexagonal lattice of Gaussian foci (frequency: 1.2 μm^{-2}). Only the foci falling inside the convex hull of the ER fluorescence signal were taken into account.

Supporting Information

Figure S1 Endocytosis is initiated in the ER free zones of the plasma membrane in W303-1A cells. Mutual localization of Ede1-GFP, a marker of early stages of endocytosis, and cortical ER visualized by ss-dsRed-HDEL was performed. Only rare colocalization events were detected (**A**). Similarly, cortical ER network and initiation sites of endocytosis were not colocalized with MCC domains marked with Sur7-GFP (**B**) and Sur7-mRFP (**C**), respectively. Tangential confocal sections of W303-1A cells expressing fluorescently labeled proteins are presented. Fluorescence intensity profiles along the numbered arrows were scaled to the same range in the red and green channels. Bar: 5 μm.
(TIF)

Figure S2 Distribution of MCC domains through the holes in the cortical ER pattern. In tangential confocal sections of individual cells expressing Sur7-mCherry and GFP-HDEL (**A**), the minimal distance of the Sur7 labeled MCC domains from the cortical ER boundary was measured. The histogram of the measured distances (full bars in **B**; 399 foci in 64 cells were analyzed) was compared to the distribution of the distances of model foci randomly positioned in the plasma membrane (empty bars in B; 320 foci in 100 cells; see Methods for details). The Gaussian fits of the distributions are also depicted (Sur7 solid, randomly positioned foci dotted). In order to maximize the accuracy of the distance measurements, for all the measurements we chose only the foci located to easily discernible ER holes positioned in central parts of the tangential confocal sections, so that the entire borders of the holes could be traced Bar: 1 μm.
(TIF)

Figure S3 Cortical ER pattern in MCC-defective strains. Transparency projections (LSM Image Browser) of ER patterns in BY4741, *pil1Δ* and *nce102Δ* cells expressing ss-GFP-HDEL and Sur7-mCherry markers are compared. Only the green (ER) fluorescence pattern is presented. More projections of the same cells see also in Movies S1,S2,S3. Bar: 5 μm.
(TIF)

Figure S4 Overexpression of Pil1 leads to increased fragmentation of the cortical ER pattern. Cells co-expressing ss-GFP-HDEL (green) and Pil1-mRFP (red) under a strong promoter (strain VSY177) were observed. Compare the number of MCC/eisosomes and the number of cortical ER holes with those of wild type (Fig. 1) and *pil1Δ* cells (Fig. 5). Superposition of two consecutive confocal sections is presented. Bar: 5 μm.
(TIF)

Figure S5 Distribution of Sur7 in *pil1Δ* cells. Tangential confocal sections of *pil1Δ* cells expressing ss-dsRed-HDEL and Sur7-GFP markers (only green fluorescence channel visible) are presented. Note that, in addition to large and intensive "eisosome

remnants", smaller and less intensive local accumulations of Sur7-GFP are discernible in the surrounding membrane. Bar: 5 μm.
(TIF)

Figure S6 Speed of cortical ER movement is not affected in MCC defective strains. The speed of the cortical ER movement was measured as a decrease in the mutual overlap of the ss-GFP-HDEL patterns detected in living BY4741 (white), *pil1Δ* (grey) and *nce102Δ* (black) cells (n>30) after an increasing interval of time (**A**). The dynamics of cortical ER was followed in a time-lapse series of 20 tangential confocal sections of *pil1Δ* cells expressing ss-GFP-HDEL together with Sur7-mCherry (rate: 10 s/frame). For better lucidity, the red fluorescence channel (MCC/Sur7-mCherry) is not shown. The data were processed and binarized as shown in Fig. 3 and all twenty binarized frames were superimposed to visualize the local dynamics of cortical ER. Three out of 30 cells analyzed are presented in false colors denoting the number of frames in the series in which cortical ER was detected (**B**). Bar: 1 μm.
(TIF)

Table S1 Strains used in this study.
(DOC)

Movie S1 Maximum intensity projections of ER pattern in BY4741cells. Twenty-one MIP (Maximum Intensity Projections) of BY4741 cells from Fig. S1 in 3° angle increment (−30 to +30°) were calculated and joined. Presentation speed: 10 frames/s.
(AVI)

Movie S2 Maximum intensity projections of ER pattern in *pil1Δ*cells. Twenty-one MIP of *pil1Δ* cells from Fig. S1 in 3° angle increment (−30 to +30°) were calculated and joined. Presentation speed: 10 frames/s.
(AVI)

Movie S3 Maximum intensity projections of ER pattern in *nce102Δ* cells. Twenty-one MIP of *nce102Δ* cells from Fig. S1 in 3° angle increment (−30 to +30°) were calculated and joined. Presentation speed: 10 frames/s.
(AVI)

Acknowledgments

The authors are grateful to František Hudeček (Carl Zeiss, spol. s r. o., Prague, Czech Republic) and Sven Laarmann (Carl Zeiss MicroImaging GmbH, Göttingen, Germany) for lending the Cell Observer SD microscope and Lenka Hlavínová (IEM AS CR, Prague, CZ) for careful analysis of the fluorescence images. We would also like to thank Tom Rapoport (Harvard Medical School, Boston, MA) for dsRed-HDEL containing plasmid.

Author Contributions

Conceived and designed the experiments: VS MB GG MO WT JM. Performed the experiments: VS MB. Analyzed the data: VS MB JM. Contributed reagents/materials/analysis tools: JM WT. Wrote the paper: VS JM MO WT GG.

References

1. Lingwood D, Simons K (2010) Lipid rafts as a membrane-organizing principle. Science 327: 46–50.
2. Malinska K, Malinsky J, Opekarova M, Tanner W (2003) Visualization of protein compartmentation within the plasma membrane of living yeast cells. Mol Biol Cell 14: 4427–4436.
3. Malinsky J, Opekarova M, Tanner W (2010) The lateral compartmentation of the yeast plasma membrane. Yeast 27: 473–478.
4. Stradalova V, Stahlschmidt W, Grossmann G, Blazikova M, Rachel R, et al. (2009) Furrow-like invaginations of the yeast plasma membrane correspond to membrane compartment of Can1. J Cell Sci 122: 2887–2894.
5. Walther TC, Brickner JH, Aguilar PS, Bernales S, Pantoja C, et al. (2006) Eisosomes mark static sites of endocytosis. Nature 439: 998–1003.
6. Frohlich F, Moreira K, Aguilar PS, Hubner NC, Mann M, et al. (2009) A genome-wide screen for genes affecting eisosomes reveals Nce102 function in sphingolipid signaling. J Cell Biol 185: 1227–1242.
7. Grossmann G, Malinsky J, Stahlschmidt W, Loibl M, Weig-Meckl I, et al. (2008) Plasma membrane microdomains regulate turnover of transport proteins in yeast. J Cell Biol 183: 1075–1088.
8. Brach T, Specht T, Kaksonen M (2011) Reassessment of the role of plasma membrane domains in the regulation of vesicular traffic in yeast. J Cell Sci 124: 328–337.
9. Berchtold D, Walther TC (2009) TORC2 plasma membrane localization is essential for cell viability and restricted to a distinct domain. Mol Biol Cell 20: 1565–1575.
10. Idrissi FZ, Grotsch H, Fernandez-Golbano IM, Presciatto-Baschong C, Riezman H, et al. (2008) Distinct acto/myosin-I structures associate with endocytic profiles at the plasma membrane. J Cell Biol 180: 1219–1232.
11. Kaksonen M, Toret CP, Drubin DG (2005) A modular design for the clathrin- and actin-mediated endocytosis machinery. Cell 123: 305–320.
12. Toret CP, Drubin DG (2006) The budding yeast endocytic pathway. J Cell Sci 119: 4585–4587.
13. Stimpson HE, Toret CP, Cheng AT, Pauly BS, Drubin DG (2009) Early-arriving Syp1p and Ede1p function in endocytic site placement and formation in budding yeast. Mol Biol Cell 20: 4640–4651.
14. Toshima JY, Toshima J, Kaksonen M, Martin AC, King DS, et al. (2006) Spatial dynamics of receptor-mediated endocytic trafficking in budding yeast revealed by using fluorescent alpha-factor derivatives. Proc Natl Acad Sci U S A 103: 5793–5798.
15. Orci L, Ravazzola M, Le Coadic M, Shen WW, Demaurex N, et al. (2009) From the Cover: STIM1-induced precortical and cortical subdomains of the endoplasmic reticulum. Proc Natl Acad Sci U S A 106: 19358–19362.
16. Prinz WA, Grzyb L, Veenhuis M, Kahana JA, Silver PA, et al. (2000) Mutants affecting the structure of the cortical endoplasmic reticulum in Saccharomyces cerevisiae. J Cell Biol 150: 461–474.
17. Sparkes IA, Frigerio L, Tolley N, Hawes C (2009) The plant endoplasmic reticulum: a cell-wide web. Biochem J 423: 145–155.
18. Perktold A, Zechmann B, Daum G, Zellnig G (2007) Organelle association visualized by three-dimensional ultrastructural imaging of the yeast cell. FEMS Yeast Res 7: 629–638.
19. Pichler H, Gaigg B, Hrastnik C, Achleitner G, Kohlwein SD, et al. (2001) A subfraction of the yeast endoplasmic reticulum associates with the plasma membrane and has a high capacity to synthesize lipids. Eur J Biochem 268: 2351–2361.
20. West M, Zurek N, Hoenger A, Voeltz GK (2011) A 3D analysis of yeast ER structure reveals how ER domains are organized by membrane curvature. J Cell Biol 193: 333–346.
21. Kvam E, Goldfarb DS (2007) Nucleus-vacuole junctions and piecemeal microautophagy of the nucleus in S. cerevisiae. Autophagy 3: 85–92.
22. Pan X, Roberts P, Chen Y, Kvam E, Shulga N, et al. (2000) Nucleus-vacuole junctions in Saccharomyces cerevisiae are formed through the direct interaction of Vac8p with Nvj1p. Mol Biol Cell 11: 2445–2457.
23. Kukulski W, Schorb M, Welsch S, Picco A, Kaksonen M, et al. (2011) Correlated fluorescence and 3D electron microscopy with high sensitivity and spatial precision. J Cell Biol 192: 111–119.
24. Engqvist-Goldstein AE, Drubin DG (2003) Actin assembly and endocytosis: from yeast to mammals. Annu Rev Cell Dev Biol 19: 287–332.
25. Olivera-Couto A, Grana M, Harispe L, Aguilar PS (2011) The eisosome core is composed of BAR domain proteins. Mol Biol Cell 22: 2360–2372.
26. Walther TC, Aguilar PS, Frohlich F, Chu F, Moreira K, et al. (2007) Pkh-kinases control eisosome assembly and organization. EMBO J 26: 4946–4955.
27. Ziolkowska NE, Karotki L, Rehman M, Huiskonen JT, Walther TC (2011) Eisosome-driven plasma membrane organization is mediated by BAR domains. Nat Struct Mol Biol 18: 854–856.
28. Bevis BJ, Hammond AT, Reinke CA, Glick BS (2002) De novo formation of transitional ER sites and Golgi structures in Pichia pastoris. Nat Cell Biol 4: 750–756.
29. Malinska K, Malinsky J, Opekarova M, Tanner W (2004) Distribution of Can1p into stable domains reflects lateral protein segregation within the plasma membrane of living S. cerevisiae cells. J Cell Sci 117: 6031–6041.
30. Loewen CJ, Young BP, Tavassoli S, Levine TP (2007) Inheritance of cortical ER in yeast is required for normal septin organization. J Cell Biol 179: 467–483.
31. Moreira KE, Walther TC, Aguilar PS, Walter P (2009) Pil1 controls eisosome biogenesis. Mol Biol Cell 20: 809–818.
32. Loibl M, Grossmann G, Stradalova V, Klingl A, Rachel R, et al. (2010) C terminus of Nce102 determines the structure and function of microdomains in the Saccharomyces cerevisiae plasma membrane. Eukaryot Cell 9: 1184–1192.
33. Zhang D, Vjestica A, Oliferenko S (2010) The cortical ER network limits the permissive zone for actomyosin ring assembly. Curr Biol 20: 1029–1034.

34. Kleine-Vehn J, Wabnik K, Martiniere A, Langowski L, Willig K, et al. (2011) Recycling, clustering, and endocytosis jointly maintain PIN auxin carrier polarity at the plasma membrane. Mol Syst Biol 7: 540.

35. Grossmann G, Opekarova M, Malinsky J, Weig-Meckl I, Tanner W (2007) Membrane potential governs lateral segregation of plasma membrane proteins and lipids in yeast. EMBO J 26: 1–8.

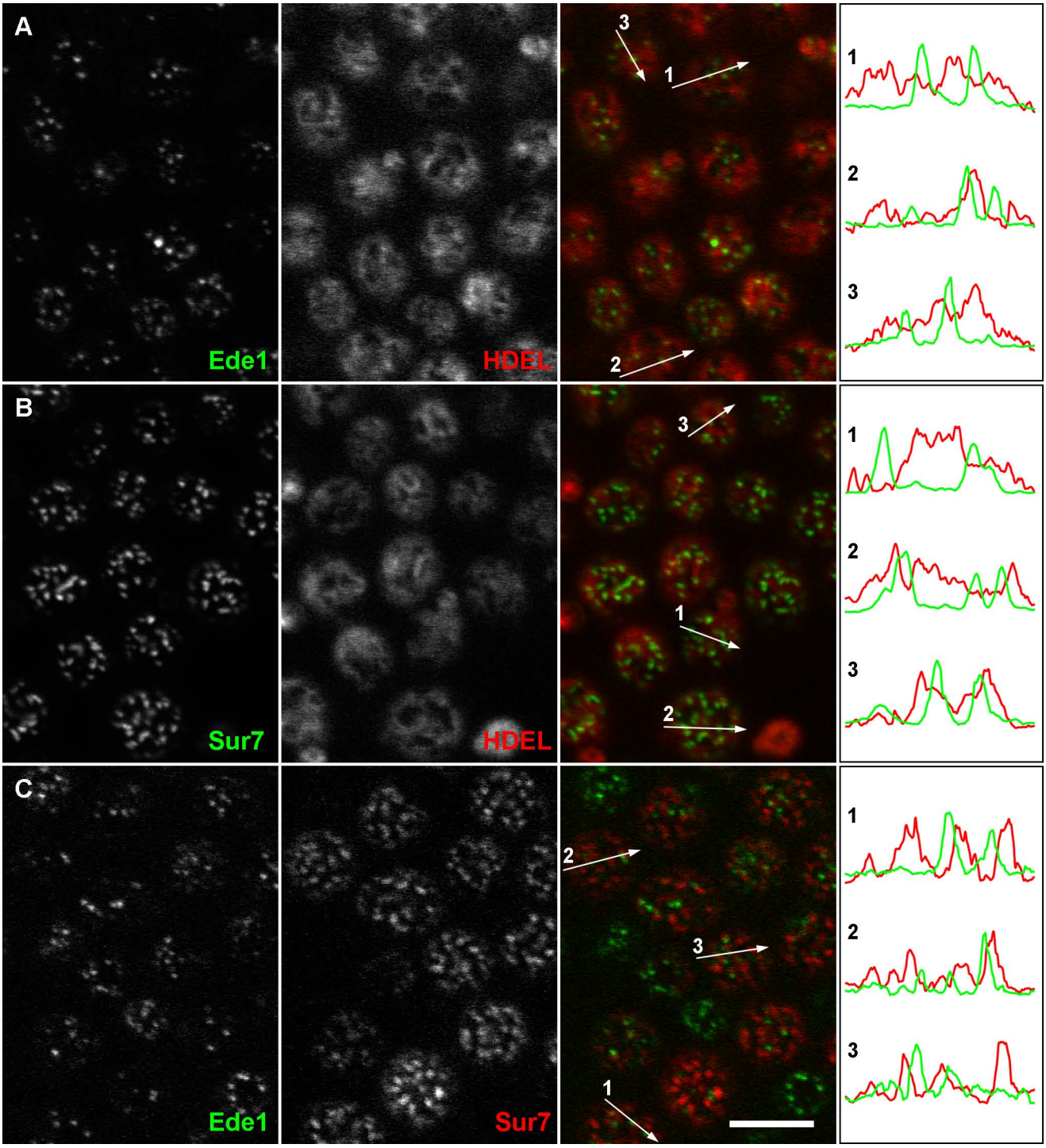

Figure S1. Endocytosis is initiated in the ER free zones of the plasma membrane in W303-1A cells. Mutual localization of Ede1-GFP, a marker of early stages of endocytosis, and cortical ER visualized by ss-dsRed-HDEL was performed. Only rare colocalization events were detected (**A**). Similarly, cortical ER network and initiation sites of endocytosis were not colocalized with MCC domains marked with Sur7-GFP (**B**) and Sur7-mRFP (**C**), respectively. Tangential confocal sections of W303-1A cells expressing fluorescently labeled proteins are presented. Fluorescence intensity profiles along the numbered arrows were scaled to the same range in the red and green channels. Bar: 5 µm.

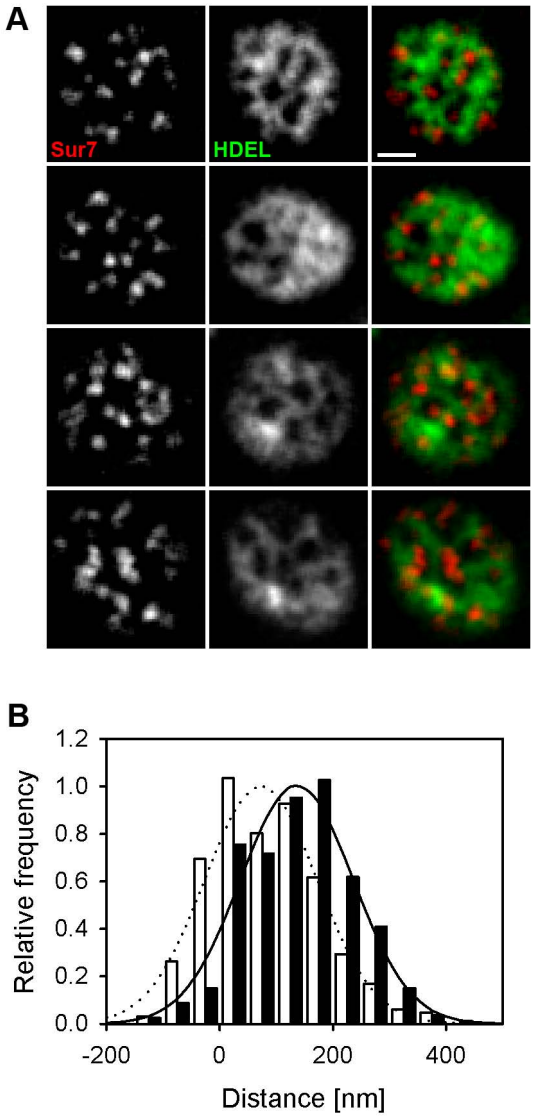

Figure S2. Distribution of MCC domains through the holes in the cortical ER pattern. In tangential confocal sections of individual cells expressing Sur7-mCherry and GFP-HDEL (**A**), the minimal distance of the Sur7 labeled MCC domains from the cortical ER boundary was measured. The histogram of the measured distances (full bars in **B**; 399 foci in 64 cells were analyzed) was compared to the distribution of the distances of model foci randomly positioned in the plasma membrane (empty bars in B; 320 foci in 100 cells; see Methods for details). The Gaussian fits of the distributions are also depicted (Sur7 solid, randomly positioned foci dotted). In order to maximize the accuracy of the distance measurements, for all the measurements we chose only the foci located to easily discernible ER holes positioned in central parts of the tangential confocal sections, so that the entire borders of the holes could be traced. Bar: 1 µm.

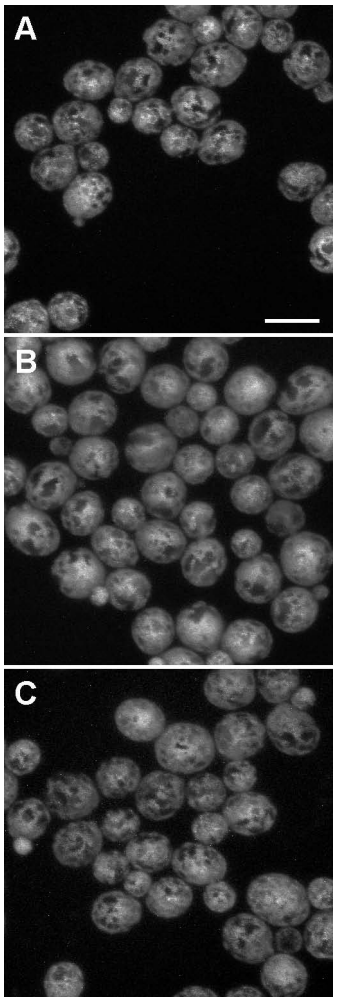

Figure S3. Cortical ER pattern in MCC-defective strains. Transparency projections (LSM Image Browser) of ER patterns in BY4741, *pil1Δ* and *nce102Δ* cells expressing ss-GFP-HDEL and Sur7-mCherry markers are compared. Only the green (ER) fluorescence pattern is presented. More projections of the same cells see also in Movies S1,S2,S3. Bar: 5 µm.

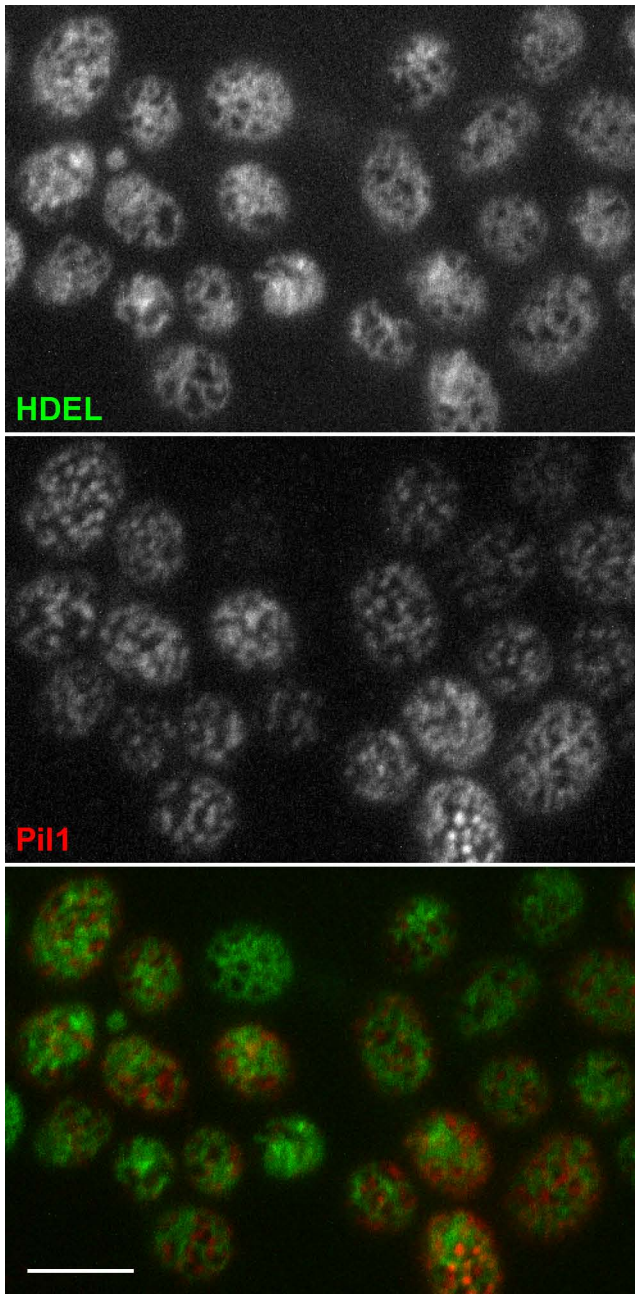

Figure S4. Overexpression of Pil1 leads to increased fragmentation of the cortical ER pattern.

Cells co- expressing ss-GFP-HDEL (green) and Pil1-mRFP (red) under a strong promoter (strain VSY177) were observed. Compare the number of MCC/eisosomes and the number of cortical ER holes with those of wild type (Fig. 1) and *pil1Δ* cells (Fig. 5). Superposition of two consecutive confocal sections is presented. Bar: 5 µm.

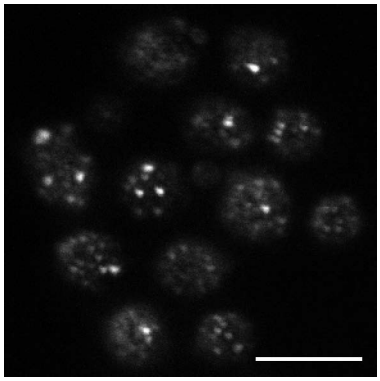

Figure S5. Distribution of Sur7 in *pil1Δ* cells.
Tangential confocal sections of *pil1Δ* cells expressing ss-dsRed-HDEL and Sur7-GFP markers (only green fluorescence channel visible) are presented. Note that, in addition to large and intensive "eisosome remnants", smaller and less intensive local accumulations of Sur7-GFP are discernible in the surrounding membrane. Bar: 5 µm.

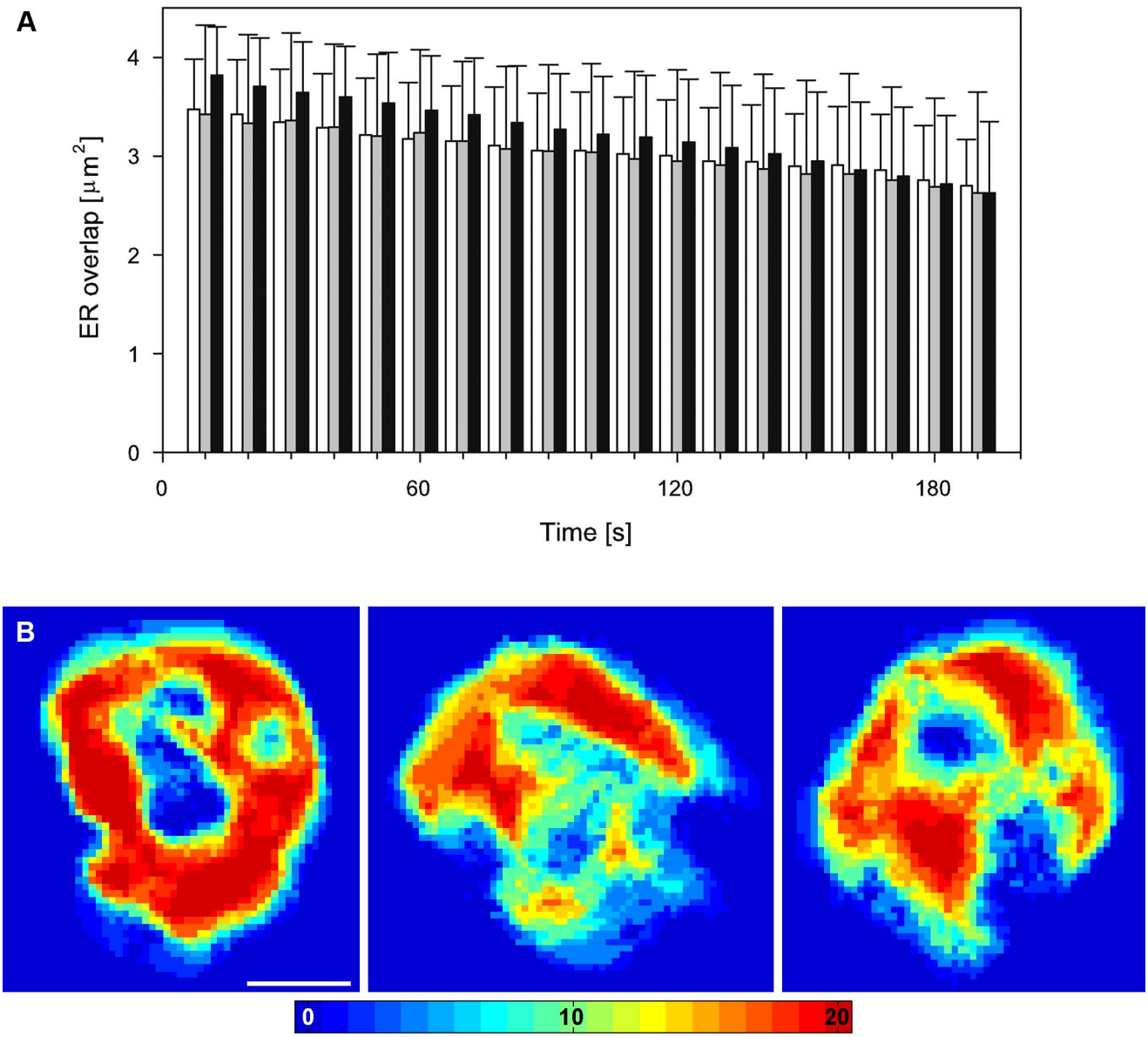

Figure S6. Speed of cortical ER movement is not affected in MCC defective strains. The speed of the cortical ER movement was measured as a decrease in the mutual overlap of the ss-GFP-HDEL patterns detected in living BY4741 (white), *pil1Δ* (grey) and *nce102Δ* (black) cells (n>30) after an increasing interval of time (**A**). The dynamics of cortical ER was followed in a time-lapse series of 20 tangential confocal sections of *pil1Δ* cells expressing ss-GFP-HDEL together with Sur7-mCherry (rate: 10 s/frame). For better lucidity, the red fluorescence channel (MCC/Sur7-mCherry) is not shown. The data were processed and binarized as shown in Fig. 3 and all twenty binarized frames were superimposed to visualize the local dynamics of cortical ER. Three out of 30 cells analyzed are presented in false colors denoting the number of frames in the series in which cortical ER was detected (**B**). Bar: 1 µm.

Table S1. Strains used in this study.

Strain	Genotype	Source
BY4741	*MAT*a *his3Δ1 leu2Δ0 met15Δ0 ura3Δ0*	Brachmann et al, 1998*
W303-1A	*MATa leu2-3,112 trp1-1 can1-100 ura3-1 ade2-1 his3-11,15*	Thomas and Rothstein, 1989**
GYS91	BY4741 *nce102::kanMX4*	EUROSCARF
GYS130	BY4741 *pil1::kanMX4*	EUROSCARF
VSY 182	W 303-1A Ede1::GFP::URA3 (YIp211); ss-dsRed-HDEL::TRP1 (YIp204)	This study
VSY 24	W303-1A Sur7::GFP::URA3 (YIp211); ss-dsRed-HDEL::TRP1(YIp204)	This study
VSY 40	W303-1A Sur7::mRFP::LEU2 (YIp128); Ede1::GFP::URA3 (YIp211)	This study
VSY 26	BY4741 Ede1::GFP::URA3 (YIp211); Sur7::mRFP::LEU2 (YIp128)	This study
VSY103	BY4741 Sur7::mCherry::URA3 (YIp211); TRP1::ss-GFP-HDEL::LEU2 (YIp128)	This study
VSY99	BY4741 Ede1::GFP::URA3 (YIp211); TRP1::ss-dsRed-HDEL::LEU2 (YIp128)	This study
VSY98	BY4741 Sur7::GFP::URA3 (YIp211); TRP1::ss-dsRed-HDEL::LEU2 (YIp128)	This study
VSY 107	GYS91 Sur7::mCherry::URA3 (YIp211); TRP1::ss-GFP-HDEL::LEU2 (YIp128)	This study
VSY 83	GYS91 Sur7::GFP::URA3 (YIp211); TRP1::ss-dsRed-HDEL::LEU2 (YIp128)	This study
VSY 134	GYS91 Ede1::GFP::URA3 (YIp211); TRP1::ss-dsRed-HDEL::LEU2 (YIp128)	This study
VSY 108	GYS130 Sur7::mCherry::URA3 (YIp211); TRP1::ss-GFP-HDEL::LEU2 (YIp128)	This study
VSY 85	GYS130 Sur7::GFP::URA3 (YIp211); TRP1::ss-dsRed-HDEL::LEU2 (YIp128)	This study
VSY 135	GYS130 Ede1::GFP::URA3 (YIp211); TRP1::ss-dsRed-HDEL::LEU2 (YIp128)	This study
VSY 177	BY4741 TRP1::ss-GFP-HDEL::LEU2 (YIp128); pVTU100-Pil1-mRFP	This study

* Brachmann et al. (1998), Yeast 14:115-32
** Thomas & Rothstein (1989), Cell 56:619-630